

**COLLOCATION MODELS FOR  
DISTILLATION UNITS  
AND  
SENSITIVITY ANALYSIS STUDIES IN  
PROCESS OPTIMIZATION**

By

PANAGIOTIS SEFERLIS, Dipl. Chem. Eng.

A Thesis

Submitted to the School of Graduate Studies  
in Partial Fulfillment of the Requirements  
for the Degree  
Doctor of Philosophy

McMaster University

© Copyright by Panagiotis Seferlis, April 1995

**DISTILLATION UNIT MODELS AND  
SENSITIVITY ANALYSIS IN OPTIMIZATION**

To my parents, Caterina and Sophia

**COLLOCATION MODELS FOR  
DISTILLATION UNITS  
AND  
SENSITIVITY ANALYSIS STUDIES IN  
PROCESS OPTIMIZATION**

DOCTOR OF PHILOSOPHY (1995)  
(Chemical Engineering)

McMASTER UNIVERSITY  
Hamilton, Ontario

TITLE: Collocation models for distillation units and sensitivity analysis studies in  
process optimization

AUTHOR: Panagiotis Seferlis, Dipl. Chem. Eng. (Aristotle University of Thessaloniki,  
Greece)

SUPERVISOR: Professor A. N. Hrymak

NUMBER OF PAGES: xiv, 264

## Abstract

This thesis examines problems in two related subject areas.

The first subject area involves the development orthogonal collocation on finite elements (OCFE) models for stagewise distillation processes for use in steady-state optimization. The OCFE model formulation divides the column sections into smaller subdomains (finite elements) in order to track irregularities in the column profiles. Stages that have feed or sidestreams entering or leaving the column are modeled as discrete equilibrium stages in the OCFE model. An adaptive element breakpoint placement procedure determines an element partition for each column section so that a solution of improved accuracy is obtained. The element partition is based on the equidistribution of the material and energy balances residuals around envelopes in the column. OCFE models converge to the same optimal solution as tray-by-tray models in less computational time, but have similar sensitivity at the optimum with respect to major model parameters.

The second area involves the study of parametric sensitivity analysis in process optimization. A sensitivity analysis procedure is developed that calculates the behaviour of the optimal solution for changes in one independent parameter using continuation methods. A procedure is proposed to modify the equation set which allows the study of the effects of multiple simultaneous parameter variations along specified directions in the optimal solution. Special attention is given to the detection and analysis of singularities in the optimal solution path caused by violation of either the strict complementarity, linear independence or second-order optimality conditions. The methodology provides information to determine the range of parameter estimate variation for which the active constraint set or the characteristics of the optimal solution remain unchanged. The adjustment of the independent variables in a multiple unit flowsheet, so that optimality is maintained, is investigated in the presence of model parameter variation.

## Acknowledgements

I would like to express my deepest gratitude to my supervisor Professor A. N. Hrymak for his guidance, stimulating discussions and encouragement during the course of this work.

I would also like to thank the members of my supervisory committee, Dr. J. M. Dickson, Dr. A. Peirce and Dr. T. E. Marlin, for their many useful suggestions and comments that enhanced the quality of this work.

The contribution from Dr. C. Schmid and Professor L. T. Biegler of their r-SQP code is greatly appreciated.

The financial support by an Imperial Oil University Research Grant and by the McMaster Advanced Control Consortium is gratefully acknowledged.

My friends, the students in the Penthouse, shared with me my good and bad moments during all these years. I will always remember Thanassis for being such a great friend all these years, Sridhar for sharing the mixed feelings of frustration and sometimes of success during the after hours simulation runs, Andre and Jean Luc for the intellectual and motivating philosophical and political discussions, Bhupinder the good, supportive friend, Kim for her guidance and assistance during my first steps at McMaster, Stephane the always optimistic and joyful friend, Atsushi for revealing me the secrets of MINOS, Francois for the enjoyable mathematical conversations, Pavlos for sharing all these common memories from the moment our plane took off from Athens and Dave for the great company and the excellent beer we brewed together.

Furthermore, I would like to thank the families of Athena Gegiou, Vina and Pavlos Kanaroglou, Maria and Yoryos Papageorgiou, Patra and Costas Patinioti for their kindness and hospitality during my stay in Canada.

My parents deserve the most, for all their sacrifices and support, both emotional and financial, that gave me hope and will to reach my goals.

Finally, I would like to express my deepest gratitude to Sophia for her love, continuous encouragement and caring that brightened my life.

## Table of Contents

	Page
Abstract	iii
Acknowledgements	iv
List of Figures	viii
List of Tables	xii
1 Introduction	1
1.1 Reduced-Order Models for Optimization of Distillation Units	4
1.2 Sensitivity Analysis of Chemical Processes	6
1.3 Thesis Outline	7
2 Orthogonal Collocation on Finite Elements Models for Distillation Units	10
2.1 EquilibriumStage Distillation Models - An Overview	10
2.2 Full-Order Model	16
2.2.1 Tray-by-tray Model Formulation	16
2.2.2 Solution Methods for the MESH Equations	20
2.3 Orthogonal Collocation on Finite Elements Models	22
2.3.1 Orthogonal Collocation on Column Sections	22
2.3.2 Orthogonal Collocation on Finite Elements of Column Sections	28
2.4 Steady-State Optimization of Distillation Columns	33
2.4.1 Case I: Propylene-propane (C <sub>3</sub> ) Splitter	33
2.4.2 Case II: Deisobutanizer (DIB)	39
2.4.3 Case III: C <sub>3</sub> -C <sub>4</sub> Splitter	48
2.4.4 Case IV: Ethylbenzene-styrene EB/S Column	48
2.4.5 Initial Point Dependence	50
2.4.6 Approximation Error Analysis	54
2.5 Chapter Summary	58
3 Adaptive Collocation on Finite Elements Models for Distillation Units	59
3.1 Introduction	59
3.2 Adaptive OCFE Models for Distillation Units	61

3.2.1	Residual-based Breakpoint Placement	63
3.2.2	Error Equidistribution using Spline Approximation to the Derivatives	68
3.3	Steady-State Optimization with Approximation Error Criteria	74
3.3.1	Deisobutanizer (DIB) Example	74
3.3.2	C <sub>3</sub> -splitter Example	83
3.3.3	EB/S Column Example	85
3.4	Chapter Summary	91
4	Sensitivity Analysis in Chemical Process Optimization	92
4.1	Introduction	92
4.2	Local Sensitivity Analysis in Nonlinear Programming	93
4.2.1	Theoretical Background	93
4.2.2	Computational Considerations	97
4.2.3	Parameter Rank Ordering in Sensitivity Analysis	100
4.3	Nonlinear Parametric Programming	103
4.3.1	Literature Review	103
4.3.2	Parameterized Karush-Kuhn-Tucker Set	104
4.3.3	Simple Variable Bounds	107
4.3.4	Multiple Parameter Perturbations	108
4.4	Continuation Methods for the Pathfollowing of the Optimal Solution	111
4.4.1	Description of PITCON	111
4.5	Singularities in the Optimal Solution Path	115
4.5.1	Violation of the Strict Complementarity (SC) Condition	115
4.5.2	Linear Independence Loss	119
4.5.3	Special Case of LI Loss	121
4.5.4	Singularity of the Reduced Hessian	125
4.6	Algorithm for the Pathfollowing of the Optimal Solution	127
4.7	Chapter Summary	128
5	Parametric Sensitivity Analysis in Chemical Processes	131
5.1	Williams-Otto Plant	131
5.1.1	Parameter Variation along Eigenvector Directions	134

5.1.2	Kinetic Parameter Variations	139
5.2	Multicomponent Distillation Units	141
5.2.1	Deisobutanizer (DIB) with a Tray Efficiency Model	141
5.2.2	Column Train Example	149
5.2.3	Comparison of Parametric Sensitivity Results between Tray-by-tray and OCFE Models	154
5.2.4	Optimal Solution Sensitivity to Element Partition Variations for OCFE Models	160
5.3	Ammonia Synthesis Reactor	169
5.3.1	Parametric Sensitivity Analysis	169
5.4	Chapter Summary	177
6	Conclusions	181
7	Bibliography	186
	Appendix A. Coefficients for the Regressed Equations 2.16, 2.17 and 2.19	198
	Appendix B. Cost Coefficients for Equations 2.45, 2.46 and 5.1	201
	Appendix C. Eigenvector directions for matrix $X^T X$	202
	Appendix D. Conventions for vector differentiation	204

## List of Figures

	Page	
Figure 1.1	Typical schematic of the real-time optimization layer.	3
Figure 1.2	Thesis outline.	8
Figure 2.1	Schematic of a conventional tray distillation column.	19
Figure 2.2	Feed tray formulation in the OCFE model.	27
Figure 2.3	OCFE model formulation for a conventional distillation column.	30
Figure 2.4	Boundary conditions between finite elements.	32
Figure 2.5	Comparison of the temperature profiles at the optimum in the tray-by-tray and OCFE models for the C <sub>3</sub> -splitter.	40
Figure 2.6	Comparison of the liquid composition profiles at the optimum in the tray-by-tray and OCFE models for the C <sub>3</sub> -splitter.	41
Figure 2.7	Comparison of the liquid composition profiles for the key components (at the optimum) in the tray-by-tray and OCFE models for the DIB.	45
Figure 2.8	Comparison of the liquid composition profiles for the nonkey components (at the optimum) in the tray-by-tray and OCFE models for the DIB.	46
Figure 2.9	Comparison of the temperature profiles at the optimum in the tray-by-tray and OCFE models for the DIB.	47
Figure 2.10	Comparison between the initial and optimal iC <sub>4</sub> liquid composition profiles for the DIB.	52
Figure 3.1	Material and energy balance envelopes for a typical adaptive OCFE distillation model.	66
Figure 3.2	Approximation of the (k+1)-th derivative of the state variable profile (de Boor, 1974).	71

Figure 3.3	Maximum absolute error in liquid composition in every element for different element partitions in the DIB. See Tables 3.1 and 3.2.	80
Figure 3.4	Maximum absolute error in temperature in every element for different element partitions in the DIB. See Tables 3.1 and 3.2.	81
Figure 3.5	Maximum absolute error in liquid composition in every element for different element partitions in the C <sub>3</sub> -splitter. See Tables 3.4 and 3.5.	87
Figure 3.6	Maximum absolute error in temperature in every element for different element partitions in the C <sub>3</sub> -splitter. See Tables 3.4 and 3.5.	88
Figure 3.7	Optimal composition and temperature profiles for the EB/S column.	90
Figure 4.1	Relation between the relative changes of parameters for multiple model parameter variations, (a) linear relation (Equation 4.18), (b) nonlinear relation (Equation 4.19).	110
Figure 4.2	Schematic of the predictor-corrector procedure in PITCON.	114
Figure 4.3	Optimal solution path for problem (P4.4).	117
Figure 4.4	Optimal solution path for problem (P4.5).	122
Figure 4.5	Optimal solution path around a point where a special case of LI occurs (solid curves: local minimizers, dashed curves: generalized critical points).	124
Figure 4.6	Optimal solution path for problem (P4.6)	126
Figure 4.7	Flowsheet of the optimal solution pathfollowing algorithm.	129
Figure 5.1	Williams-Otto plant flowsheet.	132
Figure 5.2	Optimal solution path of the (a) objective function value, (b) heat exchanger cooling water flow rate, (c) reactor temperature and (d) flow rate of reactant 'b' for the Williams-Otto plant ( $\epsilon$ perturbation	

	along the first eigenvector direction, $\times$ perturbation along the second eigenvector direction).	137
Figure 5.3	Optimal solution path for changes in the activation energy estimates of the reactions in the Williams-Otto plant (solid curves: local minimizers, dashed curves: saddle points).	140
Figure 5.4	Optimal solution path for changes in the feed composition estimates of the DIB: (a) objective function value, (b) reflux ratio, (c) reboiler heat duty and (d) $iC_4$ molar fraction in bottoms product (solid curves: local minimizers, dashed curves: local maximizers).	145
Figure 5.5	Comparison between the optimal solution path and the trajectory of the solution with the setpoints fixed at the values obtained in the nominal case (point A): (a) objective function value, (b) reflux ratio.	150
Figure 5.6	Schematic of the distillation column train.	151
Figure 5.7	Optimal solution path for changes in the feed composition estimates in the column train: (a) profit, (b) DB bottoms product flow rate, (c) DB reflux to feed flow rate ratio, (d) DIB reflux ratio and (e) $iC_4$ molar fraction in SP overhead product.	159
Figure 5.8	Optimal solution path for an OCFE DIB model for variations in the element partition of the rectifying section: (a) objective function value, (b) reflux ratio.	164
Figure 5.9	Optimal solution path for the reflux ratio for variations in the length of the third element in the stripping section, (o) fourth-order polynomial approximation, ( $\times$ ) third-order polynomial approximation.	168
Figure 5.10	Schematic of the ammonia synthesis reactor.	170
Figure 5.11	Typical optimal heat transfer coefficient profile for the ammonia	

	reactor.	174
Figure 5.12	Comparison of the simulation profiles in the ammonia reactor between an orthogonal collocation solution (o) and a Runge-Kutta integration solution (solid lines).	176
Figure 5.13	Optimal solution path for parametric variation in the $U_{\max}$ for the ammonia reactor (constrained case): (a) profit function, (b) first reactor section length.	178
Figure 5.14	Optimal solution path for parametric variation in the $U_{\max}$ for the ammonia reactor (unconstrained case).	179

## List of Tables

		Page
Table 2.1	Column specifications.	34
Table 2.2	Propylene-propane splitter optimization results with linear objective.	37
Table 2.3	Propylene-propane splitter optimization results with nonlinear objective.	38
Table 2.4	Deisobutanizer (DIB) optimization results with linear objective.	42
Table 2.5	Deisobutanizer (DIB) optimization results with nonlinear objective.	43
Table 2.6	C <sub>3</sub> -C <sub>4</sub> splitter optimization results with linear objective.	49
Table 2.7	EB/S column optimization results with nonlinear objective.	51
Table 2.8	Optimization results for the DIB for different initial variable value sets.	53
Table 2.9	Approximation error in different OCFE schemes for the C <sub>3</sub> -splitter.	57
Table 3.1	Optimization results with adaptive breakpoint placement for the DIB (linear objective).	76
Table 3.2	Error sum of squares of composition and temperature and sum of absolute values of balance residuals for different element partitions (meshes) for the DIB.	79
Table 3.3	Optimization results with adaptive breakpoint placement for the DIB (nonlinear objective).	82
Table 3.4	Optimization results with adaptive breakpoint placement for the C <sub>3</sub> -splitter.	84
Table 3.5	Error sum of squares of composition and temperature and sum of absolute values of balance residuals for different element partitions for the C <sub>3</sub> -splitter.	86

Table 3.6	Optimization results with adaptive breakpoint placement for the EB/S.	89
Table 5.1	Model parameter values and directions of perturbation for the Williams-Otto plant.	133
Table 5.2	Variable bounds for the DIB.	143
Table 5.3	Singularities in the optimal solution path for the DIB.	146
Table 5.4	Variable bounds for the distillation column train.	153
Table 5.5	(a) Singularities in the optimal solution path for the distillation column train. (b) Constraint numbers for Table 5.5a.	155
Table 5.6	Singular points in the optimal solution paths obtained by tray-by-tray and OCFE models for variation in the feed composition estimate.	161
Table 5.7	Singular points in the optimal solution paths obtained by tray-by-tray and OCFE models for variation in the column pressure estimate.	162
Table 5.8	Comparison of the optimal solution of different OCFE models.	167
Table 5.9	Notation and data for the ammonia synthesis reactor.	172

## 1. Introduction

Steady-state optimization of chemical processes aims to determine the operating conditions that provide the optimum value for a specified economic criterion. There are two major categories of methods for the steady-state optimization, direct search and model-based optimization methods.

Direct search methods (Garcia and Morari, 1981, McFarlane and Bacon, 1989) require a number of different plant operating points in order to determine a direction that optimizes the objective function. This implies that plant experimentation should be performed that may upset the plant from its normal operating conditions. Such a situation is undesirable in many cases since the plant may operate under tight specifications that may be violated in the presence of small changes in the operating conditions.

Model-based optimization (Darby and White, 1988), that is considered in this work, requires a process model that describes the underlying material and energy balances and operating constraints in the plant. The process models are usually based on certain assumptions in order to provide an acceptable level of accuracy in predicting the behaviour of the plant with a degree of simplification that will allow their use in an on-line environment. An optimization algorithm uses the information from the process model to determine the optimal operating conditions for the plant. However, the plant-model mismatch inherited from the simplifying assumptions in the model may result in a considerable amount of discrepancy between the optimal solution of the model and the actual plant optimum.

The steady-state optimization is embedded into the more general control framework of on-line real-time optimization (RTO), which attempts to maintain optimality for the plant in an environment of continuous variations of economic factors and production specifications. The RTO layer interacts with the advanced process

control system (Prett and Garcia, 1988). RTO provides a number of setpoints for the independent manipulated variables to the control system that will ensure economic optimality given the existing economic factors, product specifications and input variables to the plant.

A typical schematic of the RTO system is shown in Figure 1.1 (Darby and White, 1988, Forbes, 1993). The different stages of the RTO system are summarized as follows:

- a) *Input data validation.* The measurements obtained from the plant are analyzed to ensure that the plant is at steady-state. Possible erroneous variable measurements due to gross errors (sensor failures, leakage from process units) are eliminated. The measurements are then reconciled so that the material and energy balances are satisfied in an optimal sense.
- b) *Model update.* The reconciled plant data from the input data validation stage are used in order to update the estimates of the model parameters. A nonlinear least squares fit of the model output to the data is the most commonly used method for the model parameter update. The parameter estimates are subject to a level of uncertainty mainly due to random measurement errors.
- c) *Model-based optimizer.* The model parameter estimates are fed into the model-based optimizer, a nonlinear programming solver, in order to obtain the optimal values for the manipulated variables.
- d) *Post-optimality analysis.* The last stage of the RTO system will examine the applicability of the determined optimal set of manipulated variables and check for violations of the feasible operating window of the plant. Post-optimality analysis investigates the level of uncertainty in the calculated optimal solution, due to modeling error and parameter uncertainty, using sensitivity analysis tools. Parametric sensitivity analysis provides useful information about the variation of the optimal solution for a given change in the parameter estimates.

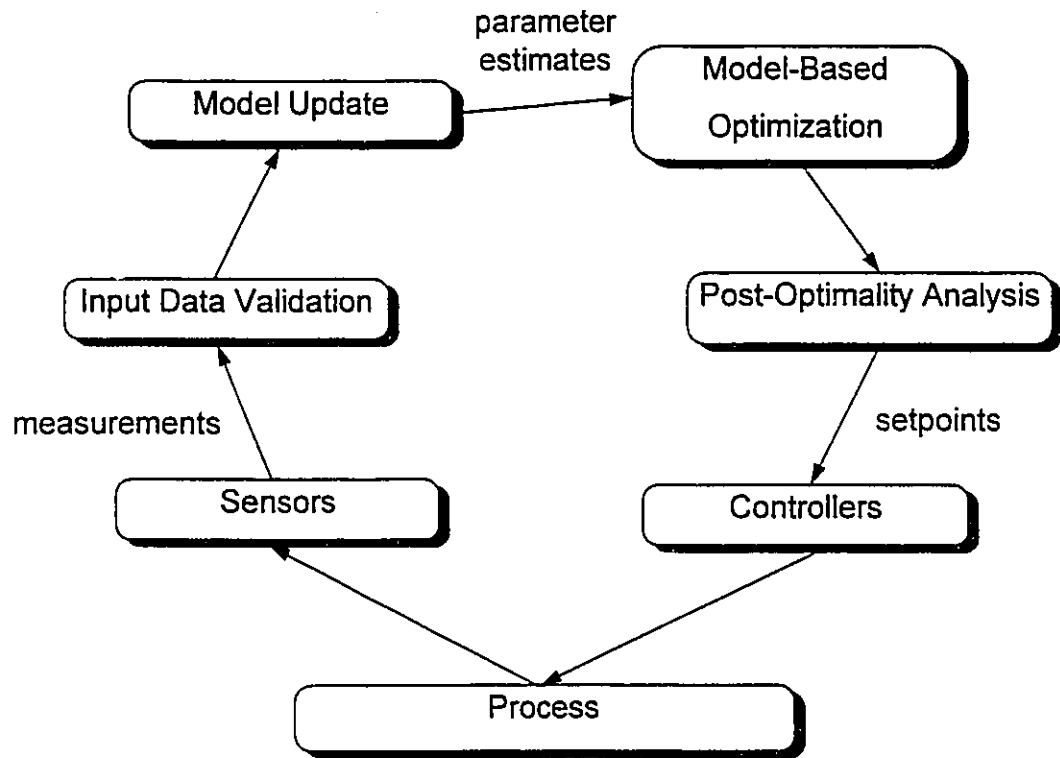


Figure 1.1 Typical schematic of the real-time optimization layer.

This thesis mainly focuses on the process modeling and post-optimality analysis stages of the RTO system. The research involves the development of efficient reduced-order models for use in steady-state optimization for stagewise multicomponent distillation units and the investigation of the behaviour of the optimal solution obtained by a model-based optimizer under model parameter variations.

## 1.1 Reduced-order Models for Optimization of Distillation Units

A large number of fast and efficient algorithms have been developed for the solution of the tray-by-tray model for distillation columns (Holland, 1981). However, the computational effort required for the steady-state optimization of distillation units may increase dramatically when the simultaneous optimization of multiple units is involved. In real-time applications, such as RTO, process monitoring and fault diagnosis, the time frame available to reach a decision is very restrictive. An accurate model prediction must be obtained in a very short time. Furthermore, reliability and robustness of the model to different operating conditions become important factors in the proper selection of a process model.

Thus process model size reduction is useful in many practical applications. A requirement for a reduced-order model to perform steady-state optimization purposes is that it must recognize the optimal solution of the plant. The simplified model should have an optimal solution at the same set of manipulated variables as the actual plant, regardless of the optimal objective function value (Forbes, 1993). In this work it will be assumed that for distillation units the full-order, tray-by-tray, model represents an *adequate* process model as defined by Forbes (1993). Hence the optimal solution of the proposed reduced-order model will be compared to the optimal solution obtained by a tray-by-tray model at the same operating conditions.

The simplifying assumptions in a reduced-order model may lead to significant information loss, particularly gradient information loss, such that the reduced-order model fails to predict the optimal solution determined by the rigorous modeling option.

Biegler et al. (1985) showed that an “inside-out” type of algorithm (Kisala et al., 1987), that uses a simplified model in an inner loop with the rigorous model incorporated in an outer loop, may fail to converge or converges to a different optimum from the rigorous model solution. Biegler and coworkers required that the simplified model gradients match the rigorous model gradients in the operating conditions of interest and has a Karush-Kuhn-Tucker (KKT) point at the rigorous model optimum. However, it is desirable that the simplified model not only converge to the same optimal solution as the rigorous model, but also have the same sensitivity at the optimum with respect to the major model parameters. The reason for maintaining the same sensitivity at the optimum is that the actual values of the model parameters are not known exactly, due to random measurement errors and model mismatch, and hence are subject to variation.

The model size reduction technique that is selected for the development of distillation unit models is based on orthogonal collocation on finite elements (OCFE) methods. An existing collocation model formulation based on the work by Stewart et al. (1985) is modified in order to enhance its accuracy in predicting the tray-by-tray optimal solution. A new approach is proposed for stages that have sidestreams leaving or entering the column in a OCFE model. A finite element formulation within each column section improves the ability of the OCFE model to track irregularities in the composition and temperature profiles. A procedure is incorporated within the economic optimization formulation that allows the OCFE model to adaptively change the finite element partition in the column depending on the optimal operating conditions, so that a solution of increased accuracy is achieved. The desirable element partition distributes an estimate of the approximation error equally within the column. Steady-state optimization and sensitivity analysis results will be used to assess the performance of the OCFE models for stagewise distillation units.

## 1.2 Sensitivity Analysis of Chemical Processes

The optimal solution obtained using a model-based optimization is subject to uncertainty associated with the estimates of the model parameters. Random measurement errors, measured and unmeasured disturbances, and changes in the economic factors and production specifications may cause the optimal solution to deviate from the nominal operating conditions (at which the model parameters have been estimated) thus increasing the modeling error. Sensitivity analysis aims to determine the change in the optimal solution given an estimated error in the model parameters (Gal, 1979, Fiacco, 1983). In this work, only deterministic model parameter variations are considered.

The objective is to develop a systematic methodology for sensitivity analysis in process optimization. The main interest lies in the investigation of the changes in the optimal variable values and the optimal objective function value under multiple simultaneous parameter perturbations over an expected range of uncertainty. This will provide useful information about the relationship between the optimal solution and combinations of parameter perturbations. Nonlinear effects may appear in the optimal solution under multiple parameter variations that cannot be predicted by a local sensitivity analysis, that evaluates the behaviour of the optimal solution around a reference point. Sensitivity analysis will expose the importance of the model parameters to the optimal solution which can be utilized in the parameter estimation stage by updating the estimates of those parameters whose impact on the optimal solution is the most significant. Furthermore, the acquired sensitivity information can be used to determine the largest magnitude for single or multiple parameter variations for which the process becomes infeasible. In process optimization, with many process units, sensitivity analysis can be utilized to investigate the interaction between the different units under the influence of parameter estimate variations.

The method for sensitivity analysis is based on the pathfollowing of the KKT set using continuation methods for parameter variation along specified directions. Finite

parameter perturbations may cause the optimal solution characteristics (current active constraints set, type of extremum) to change, in contrary to local sensitivity results (Fiacco, 1983). Pathfollowing of the optimal solution attempts to identify the range of variation for the parameter estimates for which the characteristics of the optimal solution remain the same. For example active set changes will provide useful information about the importance of process constraints, such as product specifications and capacity constraints, in the presence of model uncertainty.

### 1.3 Thesis Outline

A schematic of the thesis outline is summarized in Figure 1.2. The first section involves the modeling of distillation units for steady-state optimization using orthogonal collocation, discussed in Chapters 2 and 3, and the second section deals with the study of the sensitivity analysis in process optimization in Chapters 4 and 5.

Chapter 2 describes the formulation of the OCFE models for distillation units and the improvements that have been introduced for existing collocation models. The performance of the OCFE models in steady-state optimization is then assessed by a number of multicomponent distillation column examples.

Chapter 3 follows with the development of a new procedure for the adaptive placement of the element breakpoints in the OCFE model so that a more accurate economic optimal solution is obtained. The approximation error in the optimal solution of the proposed adaptive procedure for OCFE distillation models is compared to the accuracy achieved by an existing adaptive procedure that is commonly used in continuous systems. A number of examples examine the efficiency of the proposed approach.

A sensitivity analysis methodology is presented in Chapter 4. Based on established theoretical results, an algorithm that traces the optimal solution path for different parameter values is described. The algorithm is modified to handle multiple

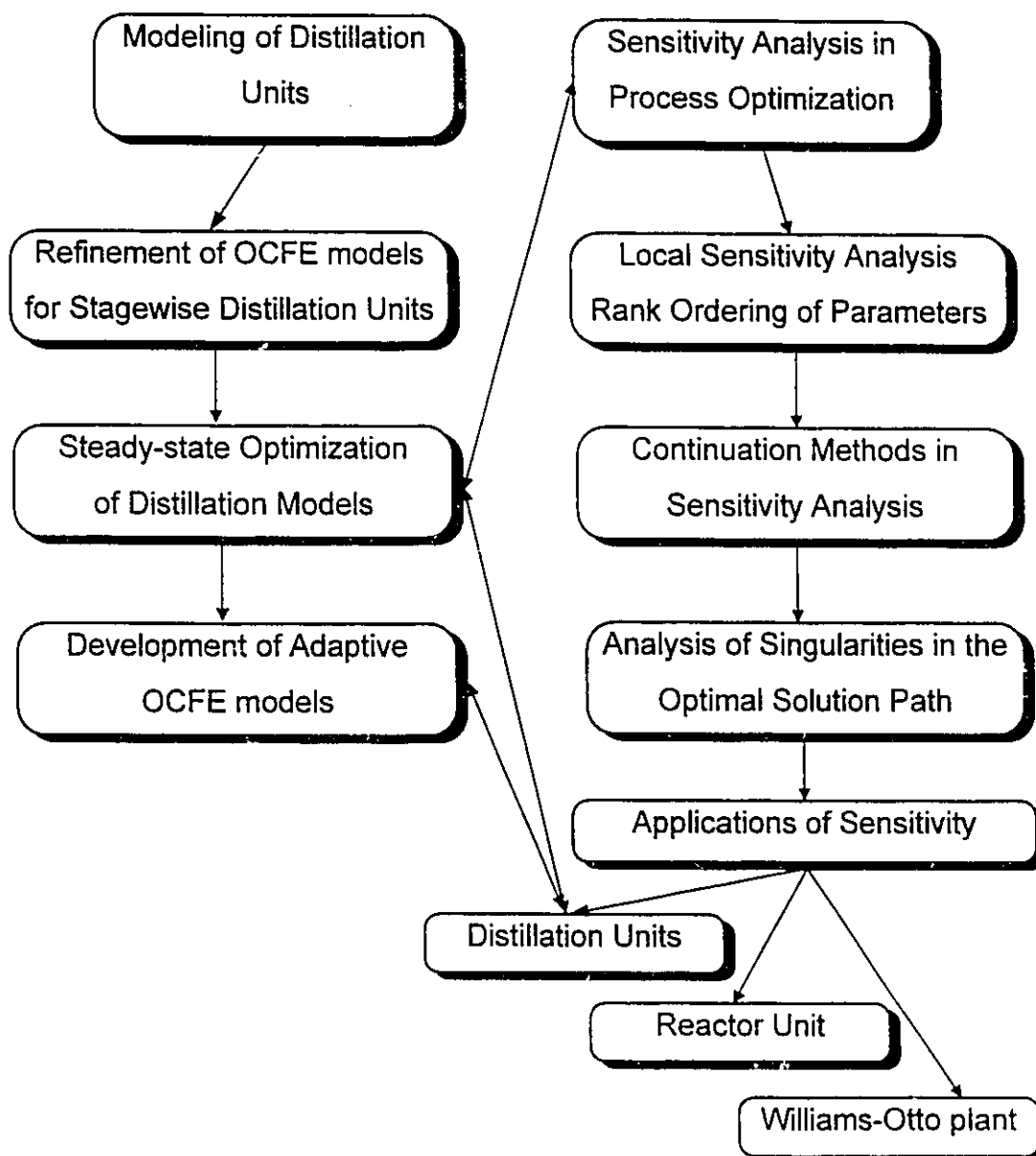


Figure 1.2 Thesis outline.

simultaneous parameter variations. Special attention is given in situations where singularities in the optimal solution path occur.

A large variety of sensitivity analysis applications are studied in Chapter 5. The Williams-Otto plant is used to examine the behaviour of the optimal solution for multiple parameter variations. Active set variations are studied for a multicomponent distillation unit and the interaction of different process units under parameter uncertainty is investigated in a distillation column train example. The sensitivity of OCFE distillation models (developed in Chapter 2) is calculated using the proposed methodology. Another application that involves the OCFE distillation models is the study of the sensitivity of the economic optimal solution to variations in the element partition, which links directly to the subject of Chapter 3. The parametric sensitivity of a reactor model described by a set of differential and algebraic equations completes the set of applications studied.

Chapter 6 summarizes the conclusions and the contributions achieved by this work.

## **2. Orthogonal Collocation on Finite Elements Models for Distillation Units**

### **2.1 Equilibrium Stage Distillation Models - An Overview**

A large variety of modeling options have been developed for stagewise separation columns. Accuracy and simplicity of structure are two very important features for distillation models. The discussion considers equilibrium stage distillation models which can be classified into four categories depending on their structure: full-order, compartmental, collocation and short-cut models. The most popular full-order model is the tray-by-tray model, that generally results in an acceptable level of accuracy for both steady-state and dynamic simulations. However, the large dimensionality of the resulting set of nonlinear equations makes the solution of the tray-by-tray models tedious and time consuming.

There have been a large number of models developed using simplifying assumptions in order to reduce the size of the model. Some of the most widely applied methods for distillation modelling that are based on empirical short-cut techniques are: the Fenske-Underwood-Eduljee equations (Eduljee, 1975), Smoker's equation, the Smith-Brinkley method (Smith and Brinkley, 1960) and the methods proposed by Glinos and Malone (1984) for multicomponent mixtures. The degree of simplification of short-cut models does not allow them to recognize the same optimal solution as the rigorous tray-by-tray model. The major reason is that even though short-cut models may result in reasonable predictions of the steady-state behaviour of the process, valuable gradient information has been lost as a result of the simplified assumptions that are made.

Another category of model size reduction is based on compartmental methods that were first introduced by España and Landau (1978). The dynamic behaviour of a number of stages was assumed to be well represented by a single equilibrium stage. They

proposed a separation of the distillation column into three compartments; the condenser, the rectifying section and the stripping section with the reboiler. Each group of stages was described as a homogeneous mixture with constant liquid and vapour enthalpies within each compartment and liquid holdup equal to the sum of the liquid holdup of the stages in the given compartment. The formulation of the model does not include energy balances and the values of the equilibrium constants were estimated using input-output data from the column. A similar approach was followed by Georgakis and Stoever (1982a, b) for the solution of the dynamic behaviour of linearized separation models. A large number of compartments (lumps of stages) of unequal number of stages was used to represent a staged absorber. They transformed the resulting tridiagonal matrix that corresponds to each lump of stages into an equivalent diagonal matrix, so that calculations are facilitated.

A further refinement of the compartmental method is due to Benallou et al. (1986). In their work the full nonlinear characteristics of the distillation process introduced by the energy balances were incorporated. The material balances around each compartment were expressed as a function of the *sensitive tray* and the distillate or bottoms concentration depending whether the compartment was located in the rectifying or stripping section of the column. The *sensitive tray* corresponds to an actual tray that best represents the dynamics of the given group of trays. However, the location of the *sensitive tray* for each compartment and the sufficient number of the compartments required to actually simulate the behaviour of the column are selected arbitrarily. Furthermore, the material balances around the compartments require the evaluation of the equilibrium K-values at all the locations of the actual trays which leads to a substantial increase in computations. Bequette and Edgar (1988) used a singular value decomposition technique for the selection, from a group of trays, of the most sensitive tray to the input variables. Horton et al. (1991) suggested some guidelines regarding the choice of the *sensitive tray*, which plays an important role in the time required for the

simulation, and the division of the column into compartments for binary distillation processes.

Orthogonal collocation techniques belong to the group of methods of weighted residuals (Villadsen and Michelsen, 1978; Finlayson, 1980) that solve boundary value problems of the form:

$$y^{(m)} = \Psi(y^{(m-1)}, y^{(m-2)}, \dots, y^{(1)}, y, x) \quad x \in [a, b] \quad (2.1)$$

$$\text{with } y^{(j)}(a) = y_{a,j} \quad \text{and} \quad y^{(j)}(b) = y_{b,j} \quad j = 0, \dots, m \quad (2.1a)$$

where  $x$  is the independent variable,  $y$  is the dependent variable,  $y^{(m)}$  denotes the  $m$ -th order derivative of  $y$  and  $y_{a,j}$ ,  $y_{b,j}$  are the fixed boundary values for the derivatives of  $y$ . The main aspect of the methods of weighted residuals (MWR) is the approximation of the solution of (2.1) by a polynomial series such as:

$$\tilde{y} = \sum_{i=0}^N a_i x^i \quad (2.2)$$

where (2.2) satisfies the boundary conditions (2.1a) associated with problem (2.1). Substitution of the polynomial approximation,  $\tilde{y}$ , into (2.1) results in a set of residual equations.

$$\tilde{y}^{(m)} - \Psi(\tilde{y}^{(m-1)}, \tilde{y}^{(m-2)}, \dots, \tilde{y}^{(1)}, \tilde{y}, x) = R(x, \tilde{y}; N) \quad (2.3)$$

Since  $\tilde{y}$  is only an approximation of the exact solution, the residuals are not usually zero and must be minimized in some optimal sense over the entire domain. This is achieved by requiring the weighted residuals to be zero.

$$\int_a^b \hat{W}_k R(x, \tilde{y}; N) dx = 0 \quad k = 1, \dots, N \quad (2.4)$$

Depending on the choice of the weighting function  $\hat{W}_k$ , different MWR arise. In the collocation method  $\hat{W}_k = \delta(x - x_k)$ , where  $\delta$  is the Dirac delta function, and then

$R(x_k, \tilde{y}; N) = 0$ , which means that the residuals are satisfied exactly at certain points, called *collocation points*. If we divide the interval  $[a, b]$  into subdomains and choose  $\hat{W}_k = 1$  within a given subdomain,  $x_{k-1} < x < x_k$ , and zero elsewhere then we have the subdomain method. Other methods include the method of the moments and the Galerkin method, where the residual function is forced to be orthogonal to a family of weighting functions which implies that the residuals approach zero as the number of approximation terms  $N$  tends to infinity. In the least squares method  $\hat{W}_k = \partial R / \partial a_k$  and the residuals satisfy

$$\int_a^b R^2(x, \tilde{y}; N) dx \quad (2.5)$$

which results in the minimization of the residuals in a least squares sense.

In orthogonal collocation methods, the points at which the residual equations are exactly satisfied are chosen to be the roots of orthogonal polynomials which result in the least approximation error. The solution in every point in the domain is usually expressed as a function of the values of the state variables at the collocation points and can take the form:

$$\tilde{y}(x) = \sum_{j=0}^N \psi_j(x) \tilde{y}(x_j) \quad (2.6)$$

where  $\psi(x)$  are known basis functions and  $\tilde{y}(x_j)$  are the values of the state variables at the collocation points,  $x_j$ . First and higher-order derivatives of the solution can then be easily derived by direct differentiation of (2.6) as follows:

$$\frac{d\tilde{y}(x)}{dx} = \sum_{j=0}^N \frac{d\psi_j(x)}{dx} \tilde{y}(x_j) \quad , \quad \frac{d^2\tilde{y}(x)}{dx^2} = \sum_{j=0}^N \frac{d^2\psi_j(x)}{dx^2} \tilde{y}(x_j) \quad (2.7)$$

Relations (2.7) imply that the derivatives of the states at every point depend on the values of the state variables at the collocation points.

Orthogonal collocation techniques have been used extensively for the solution and optimization of process systems described by mixed differential/algebraic equations (Villadsen and Michelsen, 1978; Finlayson, 1980; Renfro, 1986; Cuthrell and Biegler, 1987). The residual equations are nonlinear algebraic equations that can be solved with a standard equation-based process simulator or optimizer.

Dynamic models of stagewise separation processes using tray-by-tray models involve the solution of a set of differential equations with time as the independent variable. The equations describe the behaviour of the state variables (component composition, temperature) at the equilibrium stages. In steady-state the model becomes a set of difference equations relating conditions among consecutive stages.

Orthogonal collocation techniques consider the distance from the top of the column as an additional independent variable in the system and assume that the spatial dimension is a continuous domain. Composition and temperature are then considered to be continuous functions of position in the column. This approach consists the major difference from the tray-by-tray model, where composition and temperature are discontinuous and evaluated only at the locations of the equilibrium stages. Orthogonal collocation can be used for the spatial dimension variation to obtain the solution. Eventually one may use fewer collocation points than the number of actual trays in the column, thus obtaining a reduced number of equations in the process model.

The first attempt to implement orthogonal collocation as a model reduction method was discussed by Wong and Luus (1980). They converted the linearized model equations into a continuous analog described by a set of partial differential equations (PDE) in time and one spatial dimension which was solved by collocation at the roots of Legendre polynomials. However, Cho and Joseph (1983a) showed that the approximation scheme that was used for the derivation of the PDE system in the work by Wong and Luus (1980) did not satisfy material conservation in the column.

Cho and Joseph (1983a, b) proposed two different procedures for the model reduction of dynamic distillation models using collocation techniques. The first method is similar to that described by Wong and Luus (1980) but satisfies the material balances around any inscribed envelope in the column. The second method is a direct implementation of the orthogonal collocation in the equation set. They used the roots of Jacobi polynomials as collocation points. Jacobi polynomials treat the spatial domain as a continuum. However, as mentioned by Stewart et al. (1985) Jacobi polynomials do not recover the full-order model whenever the number of collocation points is equal to the number of actual trays that they represent. This disadvantage of the Jacobi polynomials prompted Stewart and coworkers to use the roots of the Hahn discrete polynomials as collocation points. The roots of such polynomials coincide with the equilibrium stages in the limiting case of equal number of collocation points and stages in the tray-by-tray model.

All these collocation models treat the number of stages as a continuous variable with the composition and temperature varying continuously throughout the column. The tray-by-tray equations material and energy balances and equilibrium relations are assumed to be satisfied exactly at the collocation points. The residual equations are then solved to obtain the values of the state variables at the collocation points. Although the collocation point locations do not necessarily have any physical meaning in the model, since they need not correspond to the location of any stage, the nature of the full-order, tray-by-tray, model is preserved.

Stewart et al. (1985) and Srivastava and Joseph (1985) studied the effects of different polynomials and the parameters in the weighting function in the orthogonality relation of the polynomials, on the accuracy of the solution. These parameters govern the distribution of the collocation points in the domain. Hahn polynomials with uniformly distributed collocation points proved to be superior to Jacobi polynomials in terms of the magnitude of approximation error achieved.

Discontinuities in the composition and temperature profiles due to feed streams and sidestreams were treated by applying different interpolating polynomials above and below the point of discontinuity (Stewart et al., 1985; Srivastava and Joseph, 1987a. Pinto and Biscaia, 1988). This formulation is similar to orthogonal collocation on finite elements (OCFE) with the breakpoints of the finite elements at the points of discontinuities. However, these approaches do not accurately estimate the distribution of the feed stream in the two phases. A new approach to handle the feed tray discontinuity will be presented in Section 2.3.1. Swartz and Stewart (1987) used finite elements in the simulation of multiphase distillation, where the element breakpoints were located at the moving miscibility front of the two liquid phases.

Recently, Huss and Westerberg (1994) suggested a variable transformation for both the stage number and the component mole fractions. Their motivation was to straighten the composition profiles, in order to represent more accurately flat regions in the column profiles. However, low-order polynomial interpolation can also provide a good approximation of flat composition profiles as will be shown in the following sections.

Swartz and Stewart (1986) used orthogonal collocation methods for the optimal design of stagewise distillation columns by transforming the discrete problem into a continuous one that can be solved by standard nonlinear programming (NLP) methods.

## **2.2 Full-order Model**

### **2.2.1 Tray-by-tray Model Formulation**

The full-order model used for the steady-state simulation and optimization of a stagewise distillation column is a tray-by-tray model applying mass and energy balances and equilibrium relations at each tray in the column.

Similar to Stewart et al. (1985), the major assumptions made are:

- a. Complete mixing of each phase at each stage.
- b. Constant holdups of liquid and no vapour phase holdup on each stage.
- c. No liquid entrainment from stage to stage.
- d. Adiabatic stages; no heat losses from the column.
- e. Thermal equilibrium between the leaving liquid and vapour stream from each stage.

On every tray,  $i$ , the MESH equations (Material balances, Equilibrium relations, Summation relations and Heat enthalpy or energy balances) are applied as follows:

$$l_{m,i-1} + v_{m,i+1} - l_{m,i} - v_{m,i} + f_{m,i} = 0 \quad m = 1, \dots, NC \quad (2.8)$$

$$L_{i-1}H_{i-1}^L + V_{i+1}H_{i+1}^V - L_iH_i^L - V_iH_i^V + F_iH_i^F = 0 \quad (2.9)$$

where

$$L_i = \sum_{m=1}^{NC} l_{m,i} \quad (2.10)$$

$$V_i = \sum_{m=1}^{NC} v_{m,i} \quad (2.11)$$

$$v_{m,i} = K_{m,i}(T_i, P_i, l_{m,i}, v_{m,i}) \frac{l_{m,i}}{L_i} V_i \quad m = 1, \dots, NC \quad (2.12)$$

$$H_i^L = \sum_{m=1}^{NC} \frac{l_{m,i}}{L_i} H_{m,i}^L(T_i) \quad (2.13)$$

$$H_i^V = \sum_{m=1}^{NC} \frac{v_{m,i}}{V_i} H_{m,i}^V(v_{m,i}, T_i, P_i) \quad (2.14)$$

Index  $i$  denotes the tray number and  $m$  denotes the component.  $l_{m,i}$ ,  $v_{m,i}$  and  $L_i$ ,  $V_i$  are the component and total liquid and vapour molar flow rates, respectively.  $T_i$  and  $P_i$  are the temperature and pressure at each equilibrium stage.  $H_i^L$  and  $H_i^V$  are the liquid and vapour total molar enthalpies at every stage and  $H_{m,i}^L$  and  $H_{m,i}^V$  are the liquid and vapour

component molar enthalpies. A schematic of a conventional tray distillation column is shown in Figure 2.1.

A Murphree stage efficiency may be used for each stage

$$\left( \frac{v_{mj+1}}{V_{i+1}} - \frac{v_{mj}}{V_i} \right) = E_{MV,mj} \left( \frac{v_{mj+1}}{V_{i+1}} - \frac{v_{mj}^*}{V_i} \right) \quad m = 1, \dots, NC \quad (2.15)$$

where  $v_{mj}^*$ , is the vapour flow rate of the  $m$ -th component if phase equilibrium was established.

The total number of equations in the model is further reduced by eliminating the component vapour molar flows using the equilibrium relations (2.12) as suggested by Holland (1981). The total number of variables involved in a tray-by-tray model for a fixed feed stream composition and temperature and fixed pressure in the column is equal to  $NT(NC+3)$ , where  $NT$  and  $NC$  are the numbers of trays and components in the column respectively. The formulation in liquid flow rates evaluates the equilibrium relations for each component in every tray, only once for every Newton-Raphson iteration. The advantage of this elimination is that the total number of nonlinear constraints and variables is reduced and hence the efficiency and the speed of the NLP solver may be improved, even though the Jacobian matrix becomes denser. On the other hand the block-tridiagonal form of the Jacobian is preserved. For a typical case involving a four component distillation column the solution time was reduced by a factor of 2, using MINOS 5.3 as the equation solver, as a direct result of this formulation.

Equilibrium coefficients, liquid and vapour stream enthalpies are evaluated on each tray using simplified regressed equations based on fitting rigorous thermodynamic models. Thermodynamic data were determined for single liquid phase solutions at the operating conditions of the columns used in the examples and regressed equations were fit to these data (Bailey, 1991). K-values are determined at each stage using regressed equations of the form:

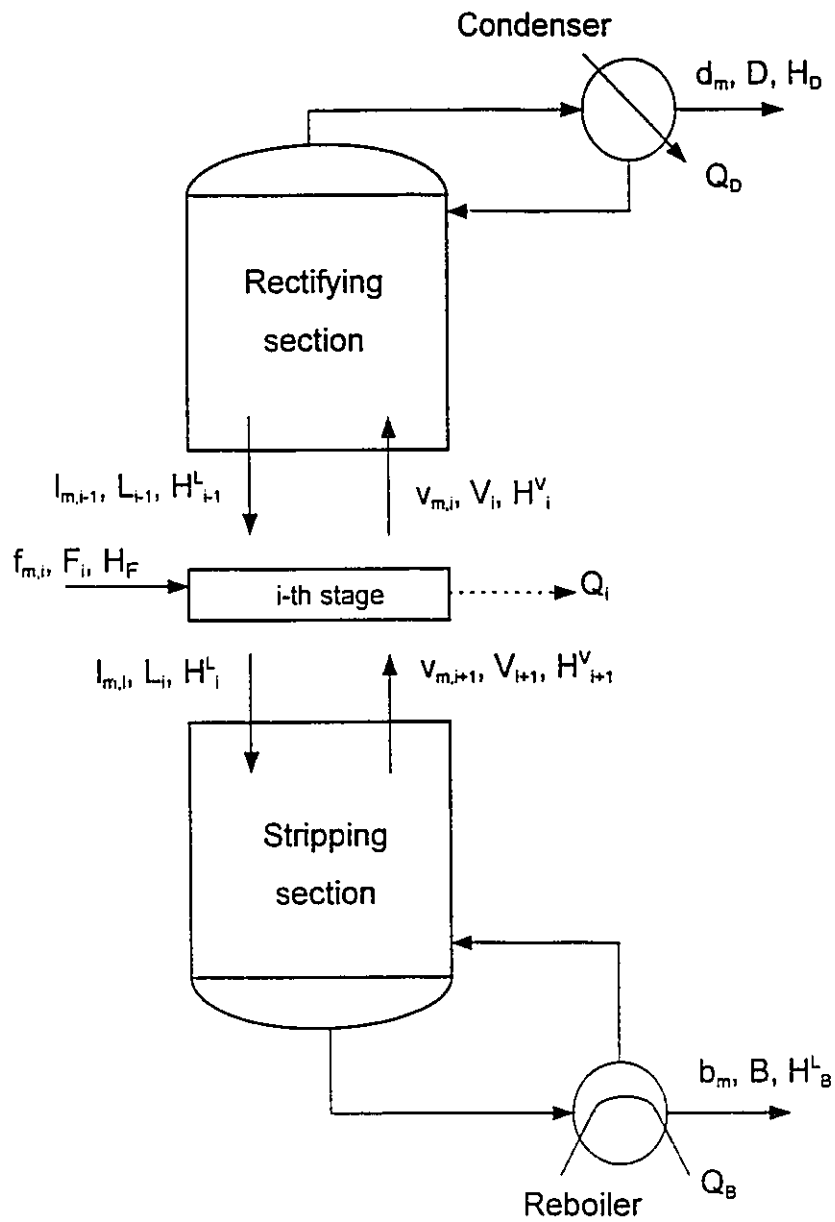


Figure 2.1 Schematic of a conventional tray distillation column.

$$K_{m,i} = \exp(a_{m,1} + a_{m,2}T_i + a_{m,3}T_i^2 + a_{m,4}P_i) \quad m = 1, \dots, NC \quad (2.16)$$

The component molar liquid enthalpy is given by the following regressed equation:

$$H_{m,i}^L = b_{m,1} + b_{m,2}T'_{corr,m,i} + b_{m,3}T'^2_{corr,m,i} + b_{m,4}T'^3_{corr,m,i} \quad m = 1, \dots, NC \quad (2.17)$$

where  $T'_{corr,m,i}$  is a corrected temperature defined as:

$$T'_{corr,m,i} = T_i T_{c,m} \left( \sum_{k=1}^{NC} x_{k,i} V_{c,k} \right) / \left( \sum_{k=1}^{NC} x_{k,i} V_{c,k} T_{c,k} \right) \quad m = 1, \dots, NC \quad (2.18)$$

where  $V_{c,m}$  and  $T_{c,m}$  are the critical volume and temperature of the  $m$ -th component respectively and  $x_{m,i}$  are the liquid molar fractions of each component. Finally liquid molar enthalpy is given by (2.13).

The molar vapour enthalpy for each component is given by the expression:

$$H_{m,i}^V = c_{m,1} + c_{m,2}p_{r,m,i}^2 + c_{m,3}p_{r,m,i} + c_{m,4}T_{r,m,i}p_{r,m,i} + c_{m,5}T_{r,m,i} + c_{m,6}T_{r,m,i}^2 \quad m = 1, \dots, NC \quad (2.19)$$

where

$$p_{r,m,i} = P_{r,m,i} \exp(1 - T_{r,m,i}) \quad m = 1, \dots, NC \quad (2.20)$$

$T_{r,m,i}$  and  $P_{r,m,i}$  are the reduced temperature and pressure of the  $m$ -th component at the  $i$ -th tray. The total molar vapour enthalpy is then calculated by (2.14).

### 2.2.2 Solution Methods of the MESH Equations

The solution methods for the MESH equations can be classified into two main categories: simultaneous convergence methods and equation decoupling methods. The methods of the first category attempt to obtain the solution by working in the full set of equations simultaneously. The latter methods are based on a partition of the equation set that are being solved in a layered approach. An extensive review of most of these

strategies that have developed for the solution of the MESH equations can be found in Wang and Wang (1981).

The most commonly used method for the simultaneous solution of the MESH equations is Newton-Raphson method. The convergence rate of Newton-Raphson method accelerates as it approaches the solution, but the method may fail if the initial guesses for the variables are away from the solution. Naphtali and Sandholm (1971) applied the method and showed that the Jacobian matrix is a block-tridiagonal matrix which can be easily solved by a Gaussian elimination scheme. Buzzi-Ferraris (1981) showed however that the block tridiagonal structure is destroyed when nonstandard specifications are incorporated or interlinking between columns exists. For such cases efficient solution algorithms were proposed by Buzzi-Ferraris (1981). Since the computational effort to evaluate the Jacobian matrix may become extremely large, a quasi-Newton approximation to the Jacobian may be used (Rheinboldt, 1984).

In order to alleviate some of the problems of Newton-Raphson method many different strategies were developed, including a damped Newton method (Naphtali and Sandholm, 1971) and continuation methods that can guarantee convergence from a wider range of initial guesses (Vickery and Taylor, 1986, and Vickery et al., 1988).

The category of equation decoupling solution algorithms include the  $\theta$ -method of convergence by Holland (1980) and the "inside-out" algorithms. The main philosophy behind the inside-out algorithms is that a simpler problem, based on a subset of the total equations, is solved in an inner iteration loop keeping some of the variables fixed. Upon convergence in the inner loop the fixed variables are updated in an outer loop. Different pairings of equations with variables are possible which result in efficient algorithms (Boston and Sullivan, 1974, Russell, 1983, and Wu and Bishnoi, 1988).

## 2.3 Orthogonal Collocation on Finite Elements Models

### 2.3.1 Orthogonal Collocation on Column Sections

The development of the reduced order models is based on the same assumptions made for the tray-by-tray model. Distillation columns are separated into sections, each defined as the group of trays between two sidestreams leaving or entering the column. A column with a single feed stream, two product streams and no sidestreams is separated into two sections, the rectifying and the stripping sections. The number of stages in each section is considered to be a continuous variable. The condenser, feed tray and reboiler are treated as discrete equilibrium stages. The formulation of the model can be applied in any column, regardless of the number of sidestreams, by locating the breakpoints of the elements at the trays where the sidestreams enter or leave the column.

Liquid and vapour component molar flows, as well as liquid and vapour phase enthalpies, are expressed as polynomial functions of position in the given column section. These functions are to be adjusted so that the equations which describe the material, energy and equilibrium relationships in the column are satisfied exactly at the collocation points. In every section, the number of  $n$  interior collocation points is specified, with the restriction that  $n$  must be no greater than the number of stages,  $NT$ , contained in that section. Also, the boundary points of each section  $s_0=0$  and  $s_{n+1}=NT+1$  are used as interpolation points for liquid and vapour states respectively. Beginning with the general formulation of the model, the approximation functions that are used in the collocation scheme are:

$$\tilde{l}_m(s) = \sum_{j=0}^n W_{lj} \tilde{l}_m(s_j) \quad 0 \leq s \leq NT, \quad m = 1, \dots, NC \quad (2.21)$$

$$\tilde{v}_m(s) = \sum_{j=1}^{n+1} W_{vj} \tilde{v}_m(s_j) \quad 1 \leq s \leq NT + 1, \quad m = 1, \dots, NC \quad (2.22)$$

$$\tilde{L}(s)\tilde{H}^L(s) = \sum_{j=0}^n W_{lj} \tilde{L}(s_j)\tilde{H}^L(s_j) \quad 0 \leq s \leq NT \quad (2.23)$$

$$\tilde{V}(s)\tilde{H}^V(s) = \sum_{j=1}^{n+1} W_{vj} \tilde{V}(s_j)\tilde{H}^V(s_j) \quad 1 \leq s \leq NT+1 \quad (2.24)$$

where

$$\tilde{L}(s) = \sum_{m=1}^{NC} \tilde{l}_m(s) \quad (2.25)$$

$$\tilde{V}(s) = \sum_{m=1}^{NC} \tilde{v}_m(s) \quad (2.26)$$

The functions,  $W_{lj}$  and  $W_{vj}$ , are Lagrange interpolation polynomials of order  $n+1$ , given by the expressions:

$$W_{lj}(s) = \prod_{\substack{k=0 \\ k \neq j}}^n \frac{s - s_k}{s_j - s_k} \quad j = 0, \dots, n \quad (2.27)$$

$$W_{vj}(s) = \prod_{\substack{k=1 \\ k \neq j}}^{n+1} \frac{s - s_k}{s_j - s_k} \quad j = 1, \dots, n+1 \quad (2.28)$$

The Lagrange polynomials  $W_{lj}$  and  $W_{vj}$  are equal to zero at collocation points  $s_k$ , that  $k \neq j$  and equal to unity when  $k = j$ . The numbering in the approximation polynomials for the liquid and vapour states (2.27 and 2.28) is not the same because interpolation points are shifted by one to take into account the condenser and the reboiler.

A set of residual equations results from substituting the approximation relations for the variables (2.21-2.24) into the material and energy balance equations (2.8, 2.9) at the collocation points. The residuals of these equations are required to be zero at the collocation points,  $s_j$ .

*Material balance residual equations*

$$\tilde{L}_m(s_j - 1) + \tilde{v}_m(s_j + 1) - \tilde{L}_m(s_j) - \tilde{v}_m(s_j) = 0 \quad m = 1, \dots, NC \quad j = 1, \dots, n \quad (2.29)$$

*Equilibrium equations*

$$\frac{\tilde{v}_m(s_j)}{\tilde{V}(s_j)} - K_m(\tilde{T}(s_j), \tilde{P}(s_j), \tilde{L}_m(s_j), \tilde{v}_m(s_j)) \frac{\tilde{L}_m(s_j)}{\tilde{L}(s_j)} = 0 \quad m = 1, \dots, NC \quad j = 1, \dots, n \quad (2.30)$$

*Energy balance residual equations*

$$\tilde{L}(s_j - 1)\tilde{H}^L(s_j - 1) + \tilde{V}(s_j + 1)\tilde{H}^V(s_j + 1) - \tilde{L}(s_j)\tilde{H}^L(s_j) - \tilde{V}(s_j)\tilde{H}^V(s_j) = 0 \quad j = 1, \dots, n \quad (2.31)$$

Similar to the procedure used in the full-order model, the molar vapour component flows are eliminated from (2.29) and (2.31) by using the equilibrium equations (2.30). The vapour component molar flow rates are not included in the set of nonlinear variables. The formulation requires the evaluation of the equilibrium parameters only once per collocation point and iteration.

Those points within the column in which discontinuities in the liquid or vapour composition occur (such as the condenser, feed plate and the reboiler) are treated as discrete equilibrium stages by applying separate mass and energy balances. This approach is similar to that proposed by Stewart et al. (1985) with the exception that in the present work the feed plate is treated as a separate equilibrium stage. Stewart et al. (1985) proposed that the liquid and vapour part of the feed stream must be added to the liquid and vapour streams connecting the two column sections which is correct only in the case of adiabatic columns of constant molar overflow. In general, the temperature and composition at the feed plate change in order to satisfy the product quality specifications. In addition, feed stream conditions strongly affect the temperature and the distribution of the feed stream into the liquid and vapour phases. Srivastava and Joseph (1987) and Pinto and Biscaia (1988) suggested that the feed plate should be a collocation

point for the approximation schemes in both column sections. However, such a formulation does not isolate the discontinuity in the composition and temperature profiles since the feed plate acts as an interpolation and collocation point for the continuous Lagrange polynomials. This formulation will diminish the accuracy of the approximation using Lagrange interpolation. Pinto and Biscaia (1988) explored the performance of several collocation schemes in predicting the full-order behaviour and used a special type of discrete polynomial in order to place a collocation point at the feed plate that does not follow the properties of the Hahn polynomials at the limit of equal number of collocation points and trays. Kim et al. (1989) suggested a sequential modular approach on the column sections to deal with the feed tray discontinuity; however, this method requires an additional iterative procedure to obtain the solution.

Mass balance, equilibrium and energy balance relations are solved at the feed plate given the feed flow rate and feed enthalpy. The model equations for the condenser, the feed plate and the reboiler are given below:

*condenser*

$$\sum_{j=1}^{n_R+1} W_{vj}^R(1) \tilde{v}_m^R(s_{Rj}) - \tilde{l}_m^R(s_0) - d_m = 0 \quad m = 1, \dots, NC \quad (2.32)$$

$$\sum_{j=1}^{n_R+1} W_{vj}^R(1) \tilde{V}_R(s_{Rj}) \tilde{H}_R^V(s_{Rj}) - \tilde{L}_R(s_0) \tilde{H}_R^L(s_0) - DH_D + Q_D = 0 \quad (2.33)$$

$$\frac{d_m}{D} - K_m^D(\tilde{T}_R(s_0), \tilde{P}_R(s_0)) \frac{\tilde{l}_m^R(s_0)}{\tilde{L}_R(s_0)} = 0 \quad m = 1, \dots, NC \quad (2.34)$$

*feed tray*

$$\sum_{j=1}^{n_V+1} W_{vj}^S(1) \tilde{v}_m^S(s_{Sj}) + \sum_{j=0}^{n_R} W_{lj}^R(NT_R) \tilde{l}_m^R(s_{Rj}) - \tilde{v}_m^R(s_{n_R+1}) - \tilde{l}_m^S(s_0) + f_m = 0 \quad m = 1, \dots, NC \quad (2.35)$$

$$\sum_{j=1}^{n_r+1} W_{vj}^S(1) \tilde{V}_S(s_{Sj}) \tilde{H}_S^V(s_{Sj}) + \sum_{j=0}^{n_r} W_{lj}^R(NT_R) \tilde{L}_R(s_{Rj}) \tilde{H}_R^L(s_{Rj}) - \tilde{V}_R(s_{n_r+1}) \tilde{H}_R^V(s_{n_r+1}) - \tilde{L}_S(s_0) \tilde{H}_S^L(s_0) + FH^F = 0 \quad (2.36)$$

$$\frac{\tilde{v}_m^R(s_{n_r+1})}{\tilde{V}_R(s_{n_r+1})} - K_m^F(\tilde{T}_S(s_0), \tilde{P}_S(s_0)) \frac{\tilde{l}_m^S(s_0)}{\tilde{L}_S(s_0)} = 0 \quad m = 1, \dots, NC \quad (2.37)$$

*reboiler*

$$\sum_{j=0}^{n_s} W_{lj}^S(NT_S) \tilde{l}_m^S(s_{Sj}) - \tilde{v}_m^S(s_{n_s+1}) - b_m = 0 \quad m = 1, \dots, NC \quad (2.38)$$

$$\sum_{j=0}^{n_s} W_{lj}^S(NT_S) \tilde{L}_S(s_{Sj}) \tilde{H}_S^L(s_{Sj}) - \tilde{V}(s_{n_s+1}) \tilde{H}_S^V(s_{n_s+1}) - B H_B^L + Q_B = 0 \quad (2.39)$$

$$\frac{\tilde{v}_m^S(s_{n_s+1})}{\tilde{V}_S(s_{n_s+1})} - K_m^B(\tilde{T}_S(s_{n_s+1}), \tilde{P}_S(s_{n_s+1})) \frac{b_m}{B} = 0 \quad m = 1, \dots, NC \quad (2.40)$$

Index R is used for the rectifying section and index S is used for the stripping section of the column. Figure 2.2 shows the formulation of the feed stage. The composition and the enthalpy of the vapour stream entering the condenser, the liquid stream entering the reboiler, and the liquid and vapour streams entering the feed plate are determined by extrapolation using the Lagrange polynomial of the section in which each stream is located. For the liquid state, component molar flow rates and total enthalpy are evaluated by extrapolation at points  $s=NT_R$  and  $s=NT_S$  for the rectifying and stripping sections respectively, which correspond to the endpoints of each column section for the liquid states, and for the vapour state at point  $s=1$  for both column sections.

Equilibrium coefficients and component enthalpies are calculated using the regressed equations (2.16), (2.17) and (2.19).

Stewart et al. (1985) investigated the approximation error using different families of orthogonal polynomials for the selection of collocation points and showed that the

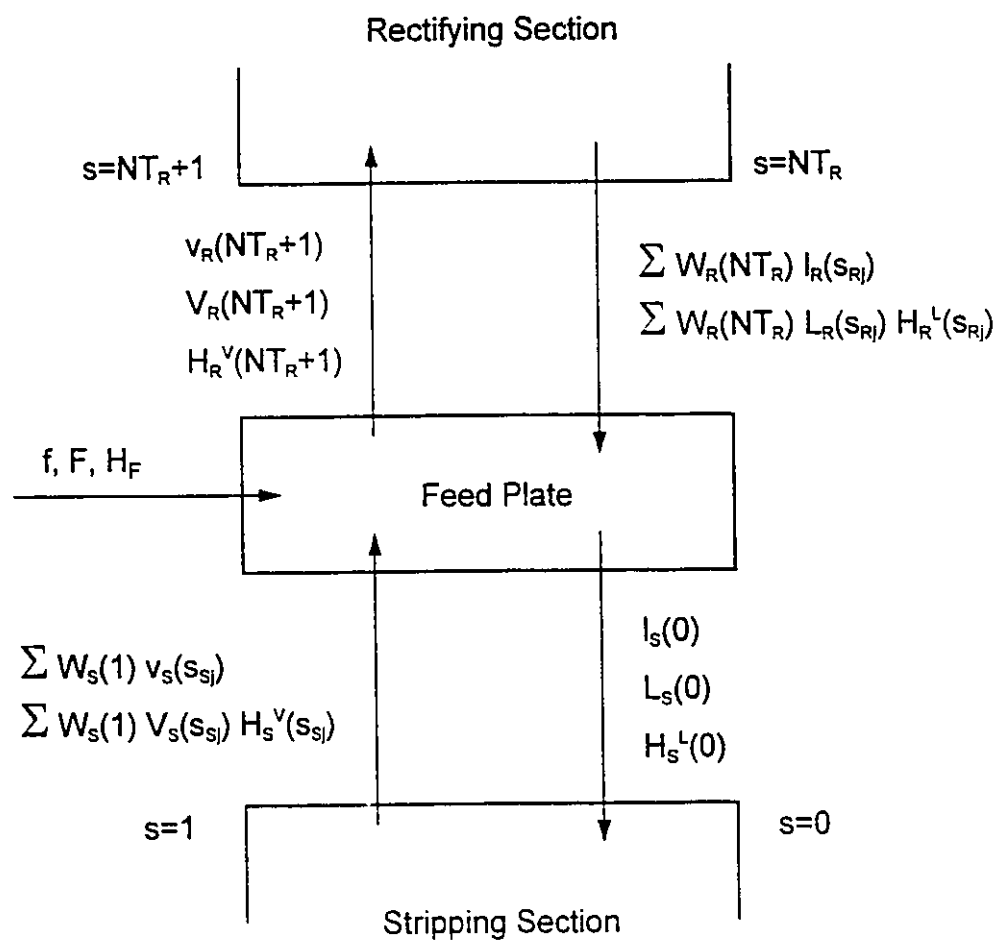


Figure 2.2 Feed tray formulation in the OCFE model.

roots of the Hahn orthogonal polynomials are the best selection. Hahn polynomials  $Q_n(x; \alpha, \beta, M)$  obey the weighted orthogonality condition:

$$\sum_{x=0}^M w(x; \alpha, \beta, M) Q_m(x; \alpha, \beta, M) Q_n(x; \alpha, \beta, M) = 0 \quad (m \neq n) \quad (2.41)$$

where

$$w(x; \alpha, \beta, M) = \frac{(\alpha + 1)_x (\beta + 1)_{M-x}}{x! (M-x)!} \quad (2.42)$$

Stewart et al. (1985) reported that when both parameters  $\alpha$  and  $\beta$  have the value zero, which results in a uniform weighting to the residuals, then the approximation error becomes the least among other selections for the values of the parameters. The collocation points in such a case are distributed uniformly in the given column section and are the roots of a Hahn orthogonal polynomial (2.41) with  $x=s-1$  and  $M=NT-1$ .

Another useful property of the Hahn polynomials is that whenever the number of interior collocation points is equal to the number of stages in this section then the roots of the polynomials coincide with the discrete stages and thus the full model is recovered. The collocation model retains the stagewise structure of the full-order (tray-by-tray) model and approximates it with fewer equations. At the limit where the number of trays and collocation points approaches infinity the roots of the Hahn and Jacobi polynomials become identical and the complete continuous domain is recovered. For more details about the properties of Hahn polynomials such as analytical expressions for the roots of up to fourth order polynomials, the reader is referred to Stewart et al. (1985) and Askey (1975).

### 2.3.2 Orthogonal Collocation on Finite Elements of Column Sections

The collocation method on the column sections described in the previous section uses  $(n+1)$ -th order approximation polynomials for each column section where  $n$  is the

total number of collocation points in each column section. When the composition profiles in the column are steep or change rapidly, then a large number of collocation points would be required to track the steep fronts in the solution and obtain an accurate approximation. Thus each section is divided into smaller parts, named finite elements.

A more accurate representation can be achieved if the division of each column section into smaller subdomains is made such that the density of collocation points is greater in those regions where significant changes in the composition or temperature occur. Fewer collocation points can be used where the profiles in the column follow a smooth behaviour. A  $(k_i+1)$ -th order polynomial is defined on every element, where  $k_i$  is the number of collocation points in the element and a set of piecewise continuous polynomials (2.27, 2.28) is used for the approximation. This results in the use of more low-order Lagrange interpolation polynomials compared with collocation schemes of the same total number of collocation points and only one element per column section. Each finite element is bounded by two endpoints (breakpoints). At the breakpoints of each element, continuity of the polynomials is required, so that the piecewise approximation function is continuous throughout the entire column section. The formulation of this technique for a conventional distillation column with two finite elements on each section is shown in Figure 2.3.

Similar to the method described in the preceding section,  $k_i$  interior collocation points, which are the roots of Hahn orthogonal polynomials, are selected for every finite element. Also  $s_{i,0}=0$  and  $s_{i,k_i-1} = NT_i + 1$ , where  $NT_i$  is the number of stages in the  $i$ -th element, are interpolation points for liquid and vapour phase approximation polynomials respectively.

The boundary conditions between finite elements obey zero-order continuity and are given by:

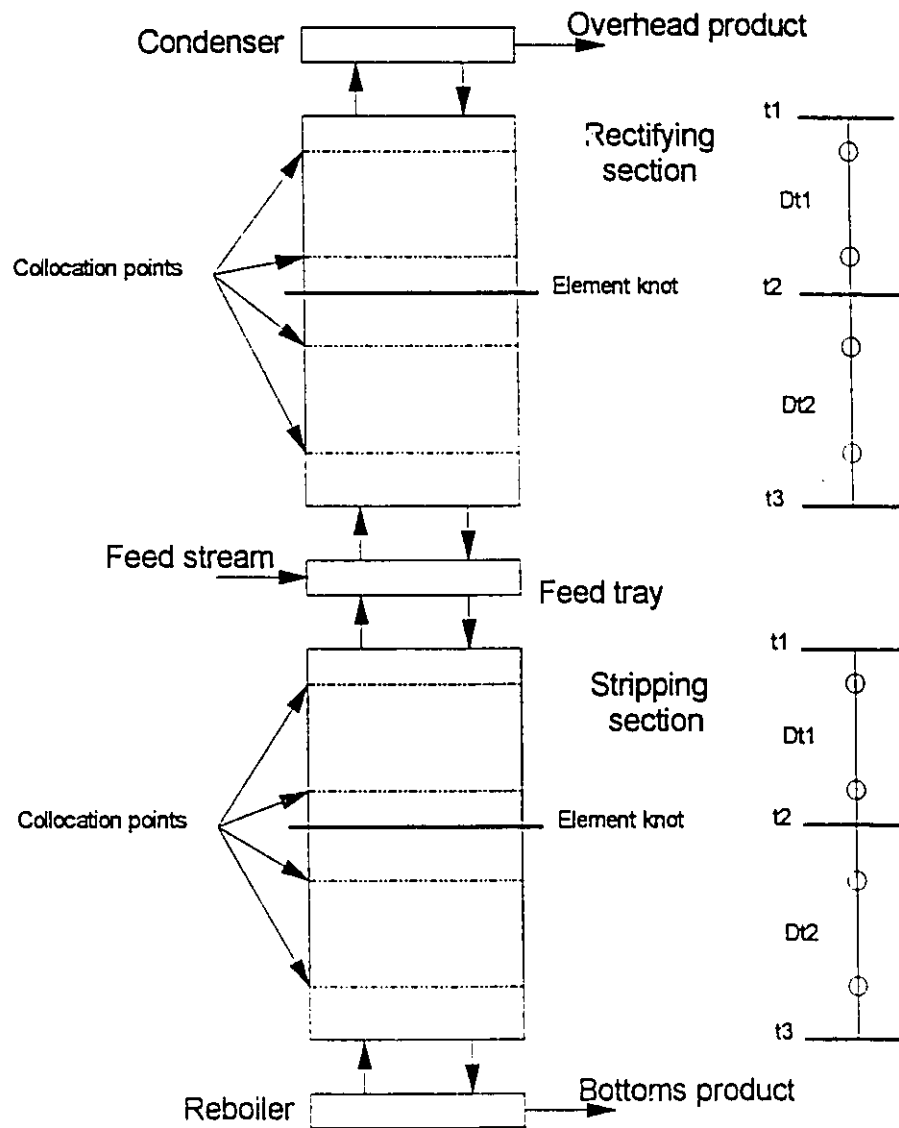


Figure 2.3 OCFE model formulation for a conventional distillation column.

*liquid phase*

$$\sum_{j=0}^{k_i} W_{i,j} (NT_i) \tilde{l}_{m,j} (s_{i,j}) = \tilde{l}_{m,i+1} (s_{i+1,0}) \quad m = 1, \dots, NC \quad (2.43)$$

*vapour phase*

$$\tilde{v}_{m,i} (s_{i,k_i+1}) = \sum_{j=1}^{k_{i+1}+1} W_{v,j+1,j} (1) \tilde{v}_{m,i+1} (s_{i+1,j}) \quad m = 1, \dots, NC \quad (2.44)$$

where index  $i$  denotes the element. Similar relations are used for the total liquid and vapour stream enthalpy. Detailed representation of the boundary conditions of the elements is shown in Figure 2.4. Liquid molar flow rates and enthalpy of the stream leaving the  $i$ -th element are evaluated by extrapolation at point  $NT_i$  using the Lagrange polynomial for  $i$ -th element. An analogous procedure is used for the vapour molar flow rates and enthalpy of the stream entering the  $(i+1)$ -th element. They are calculated by extrapolation at point  $s_{i+1}=1$  using the Lagrange polynomial for the  $(i+1)$ -th element.

The size of each finite element can be determined such that the total approximation error in every column section is minimized. Such a procedure will be presented in Chapter 3. Hahn polynomials can be applied not only for integer values but also for real values of  $NT_i$ ; the length of every finite element can be any real number. The only requirement is that the sum of all the finite element lengths in each column section is equal to the integer number of equilibrium stages in that section. In addition the order of the interpolation polynomial used to approximate the behaviour of the variables in a given element can not exceed the number of equilibrium stages included in the element.

An alternative method for approximating composition and temperature profiles in the column is to use cubic splines instead of Lagrange polynomials. Cubic splines may allow the second derivative of the piecewise cubic interpolation functions to be continuous at the knots connecting the elements of each section which implies continuity of curvature (de Boor, 1985). However, since derivative information is not available

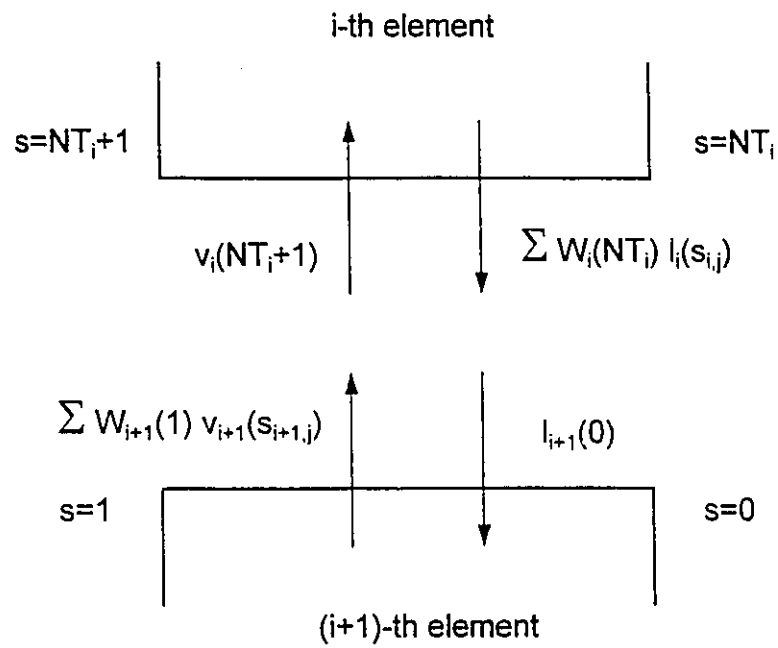


Figure 2.4 Boundary conditions between finite elements.

regarding the approximated functions of component composition and temperature, because of the discrete nature of the full-order model, the properties of splines are not helpful. Although the models using cubic spline interpolation polynomials approach the optimum solution, there is no definite advantage both in computational time and accuracy of the spline collocation model. The set of equations becomes more complicated because the derivatives of the approximated function need to be estimated, thus making the optimization problem more difficult to solve. Cubic spline methods were not explored any further in this work. Higher-order continuity may though be beneficial in the simulation of packed distillation columns where the spatial domain is by its nature continuous. Such a situation was examined by Wardle and Hapoglu (1994) who incorporated the use of Hermite interpolating polynomials within each element.

## **2.4 Steady-State Optimization of Distillation Columns**

The performance of the OCFE models in steady-state optimization is tested with four distillation columns. Two different NLP solvers have been used to determine the optimal solution for the distillation columns: MINOS 5.3, an augmented projected Lagrangian algorithm (Murtagh and Saunders, 1990), and a reduced sequential quadratic programming (r-SQP) algorithm developed for large-scale problems (Schmid and Biegler, 1994).

### **2.4.1 Case I: Propylene-propane (C<sub>3</sub>) splitter**

This example involves the optimization of a propylene-propane splitter. The main characteristics of this type of distillation column are: high reflux ratios (which increases the operating costs) and a large number of equilibrium stages (because of the low relative volatility of the two components). The conditions of the feed stream as well as other characteristics and specifications of the column are shown in Table 2.1. The regressed equations (2.16, 2.17 and 2.19) are used for the evaluation of the thermodynamic properties of the liquid and vapour phases except that absolute temperatures were used for

Table 2.1 Column specifications.

	Case I C <sub>3</sub> splitter	Case II DIB	Case III C <sub>3</sub> -C <sub>4</sub> splitter	Case IV EB/S
<b>Feed</b>				
Total flowrate (Mmol/d)	1.0734	6.4240	7.4544	0.19397
Temperature (°C)	46.11	94.80	69.88	110.0
Pressure (kPa)	1860.60	1730.40	1741.00	43.40
<b>Composition (%mol)</b>				
ethane	-	-	0.09	-
propylene	89.73	-	-	-
propane	10.27	3.83	22.11	-
i-butane	-	63.76	52.47	-
n-butane	-	28.22	23.09	-
i-pentane	-	4.19	2.07	-
pentane	-	-	0.17	-
ethyl-benzene (EB)	-	-	-	53.52
styrene	-	-	-	46.48
Condenser type	equilibrium	equilibrium	equilibrium	equilibrium
Reboiler type	equilibrium	equilibrium	equilibrium	equilibrium
<b>Ideal stages</b>				
rectifying section	115	14	9	25
stripping section	60	19	11	45
<b>Product specifications</b>				
Overhead product (%mol)	propane ≤ 0.25	n-butane ≤ 3.0	i-butane ≤ 0.6	styrene ≤ 3.06
Bottoms product (%mol)	propylene ≤ 0.50	i-butane ≤ 5.0	propane ≤ 4.0	EB ≤ 0.30

the calculation of the liquid enthalpy. The values of the parameters that are used in the regressed equations are given in Appendix A. The assumption of ideal solutions was made for the evaluation of the thermodynamic properties and the present method requires modification as suggested by Swartz and Stewart (1987) when applied to multiphase distillation. Pressure is fixed for every tray at the values given by a simulation case. The pressure at each collocation point is calculated by a linear interpolation of the pressure values at the two neighbouring trays. If the pressure is not specified at every tray, then given the total pressure drop within the column and the pressure at the condenser, the pressure of each tray is calculated by linear interpolation between the values of pressure at the top and the bottom of the column. The initial point for the optimization is the solution of a simulation case using HYSIM 1.51 (Hyprotech, 1991) and interpolating linearly between the equilibrium stages to obtain the values of the variables at the collocation points. The total number of nonlinear constraints for an OCFE model with  $n$  collocation points, after elimination of the vapour component molar flow rates using the equilibrium relations, is calculated as follows:

Mass balances:  $[n + 3] NC$

Energy balances:  $[n + 3]$

Summation equations:  $[n + 3] 2$

Molar fractions at the overhead and bottoms products:  $2 NC$

Reflux ratio relation

In the mass and energy balances, the equations for the three discrete equilibrium stages in the model (condenser, feed plate and reboiler) are included. There are two degrees of freedom for the column because pressure and feed conditions are specified.

Two different cases are examined. The first case involves the minimization of a linear objective function that penalizes the utility costs (steam used in the reboiler and coolant used in the condenser) required for the separation which takes the form:

$$Cost_1 = C_B Q_B - C_D Q_D \quad (2.45)$$

The second case-study has a nonlinear objective function which includes the cost of the utilities and the differential value of the components in the two product streams,

$$Cost_2 = C_B Q_B + C_D Q_D + C_{hk} x_{D,hk} D + C_{jk} x_{B,jk} B \quad (2.46)$$

The values of the cost parameters are given in Appendix B.

Optimization results for the C<sub>3</sub>-splitter are shown in Tables 2.2 and 2.3. Both tray-by-tray and OCFE models converge to the same optimal solution and the same set of constraints is active at the optimum for both case-studies. In the case of the linear objective the optimal solution is constrained (Table 2.2), which implies that there are no degrees of freedom associated with the optimal solution. The Lagrange multipliers (marginal values) of the active product specification constraints are nearly identical for tray-by-tray and OCFE models. The Lagrange multiplier of an active constraint indicates the magnitude of change in the objective function per unit increase or decrease in the right-hand-side term of the constraint and show the sensitivity of the optimal solution to the relaxation or tightening of the given constraint. This is only valid for infinitesimal changes in the right-hand-side term of the constraints. As a reminder, Lagrange multipliers should not be confused with Lagrange interpolation polynomials being used in the development of the OCFE models. Optimization results show that a short-cut model based on the Fenske-Underwood-Eduljee equations failed to predict the same optimal solution as the tray-by-tray model (Table 2.2 and 2.3).

In the case with the nonlinear objective function the optimal solution is unconstrained and the optimal solutions obtained by both the OCFE and the full-order model are in good agreement.

The OCFE model consists of three elements in each section and three collocation points are used in every element for fourth-order Lagrange interpolation polynomials. The model size is reduced by a factor of 8 compared to the corresponding tray-by-tray

Table 2.2 Propylene-propane splitter optimization results with linear objective.

	Tray-by-tray	OCFE	<i>modified</i> Stewart et al. approach	Short-cut
Reflux ratio	19.708	19.701	19.835	17.785
Condenser heat duty (GJ/d)	-239.056	-238.972	-240.595	-210.955
Reboiler heat duty (GJ/d)	237.743	237.659	239.282	222.815
Overhead product:				
mol% propylene	99.75	99.75	99.75	99.75
Lagrange multiplier for propane = 0.25 %mol (\$/mol frac.)	-61.004	-60.949	-62.235	-41.788
Flow (Mmol/d)	0.965	0.965	0.965	0.965
Bottoms product:				
mol% propane	99.50	99.50	99.50	99.50
Lagrange multiplier for propylene = 0.50 %mol (\$/mol frac.)	-10,358	-10,317	-10,543	-12,209
Flow (Mmol/d)	0.108	0.108	0.108	0.108
VAX 3500 CPU time (s)				
r-SQP	49.5	13.7	-	-
MINOS 5.3	326.0	18.0	17.8	1.3
number of equations	880	110	110	7
number of variables	882	112	112	9
Objective function value (\$/d)	666.205	665.971	670.515	623.883
MINOS 5.3 Options				
Lagrangian	No	No	No	No
Penalty parameter	0.0	0.0	0.0	0.0
Minor Iterations	100	100	100	Default

OCFE model: 3 elements/section (equispaced), 3 collocation points/element.

Short-cut model: Fenske-Underwood-Eduljee equations.

Table 2.3 Propylene-propane splitter optimization results with nonlinear objective.

Solver r-SQP	Tray-by-tray	OCFE	Short-cut
Reflux ratio	20.310	20.309	17.804
Condenser heat duty (GJ/d)	-246.229	-246.215	-
Reboiler heat duty (GJ/d)	244.909	244.896	-
Overhead product:			
mol% propylene	99.793	99.793	99.875
mol% propane	0.207	0.207	0.125
Flow (Mmol/d)	0.965	0.965	0.963
Bottoms product:			
mol% propylene	0.597	0.596	0.101
mol% propane	99.403	99.404	99.909
Flow (Mmol/d)	0.109	0.109	0.109
RS/6000 355 CPU time (s)	17.9	5.4	0.2
number of equations	880	110	7
number of variables	882	112	9
Objective function value (\$/d)	898.139	897.910	809.128

OCFE model: 3 elements/section (equispaced), 3 collocation points/element.

Short-cut model: Fenske-Underwood-Eduljee equations.

model, and as a consequence, the computational time to obtain the solution is reduced significantly. The CPU time to obtain the solution on a VAX 3500, using MINOS 5.3 as the NLP solver, is decreased by a factor of 11 for the OCFE model for the linear objective case. The OCFE model is about 3.5 times faster than tray-by-tray when the r-SQP code is used for the optimization for both cases. The reflux ratio and the bottoms product flow rate are selected as the independent variables in the r-SQP for the decomposition of the Hessian matrix. The large model size reduction in the OCFE formulation is mainly due to the large flat regions in the component profiles of the column as shown in Figures 2.5 and 2.6. These flat regions allow the use of only a few collocation points for an accurate representation of the tray-by-tray solution.

The temperature and liquid composition profiles at the optimum for both models are shown in Figures 2.5 and 2.6 respectively. Clearly, OCFE models perform well in predicting the optimal profile of the  $C_3$ -splitter.

#### **2.4.2 Case II: Deisobutanizer (DIB)**

This case involves the optimization of a four component deisobutanizer (DIB). The column specifications are shown in Table 2.1. The setpoints for the control scheme are the purity levels in the two product streams. The two objective functions (2.45) and (2.46) are considered in the DIB optimization.

Tables 2.4 and 2.5 show the optimization results for the DIB using the two different objective functions. The OCFE model for the DIB consists of three elements for every column section and two and three collocation points per element for the rectifying and stripping sections respectively. Finite elements of different sizes are used because an equispaced OCFE model with the same total number of collocation points fails to converge to the optimal solution. Both models converge to the same solution but OCFE requires about half of the tray-by-tray CPU time using MINOS 5.3 as the optimization algorithm. OCFE models converge with difficulty when the r-SQP algorithm is used.

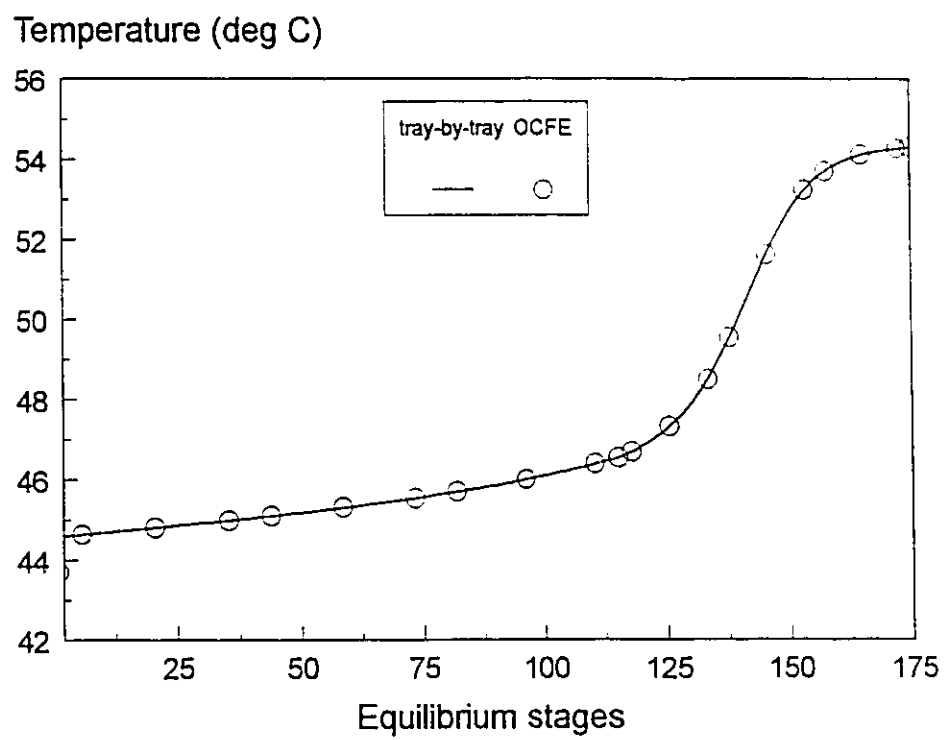


Figure 2.5 Comparison of the temperature profiles at the optimum in the tray-by-tray and OCFE models for the C<sub>3</sub>-splitter.

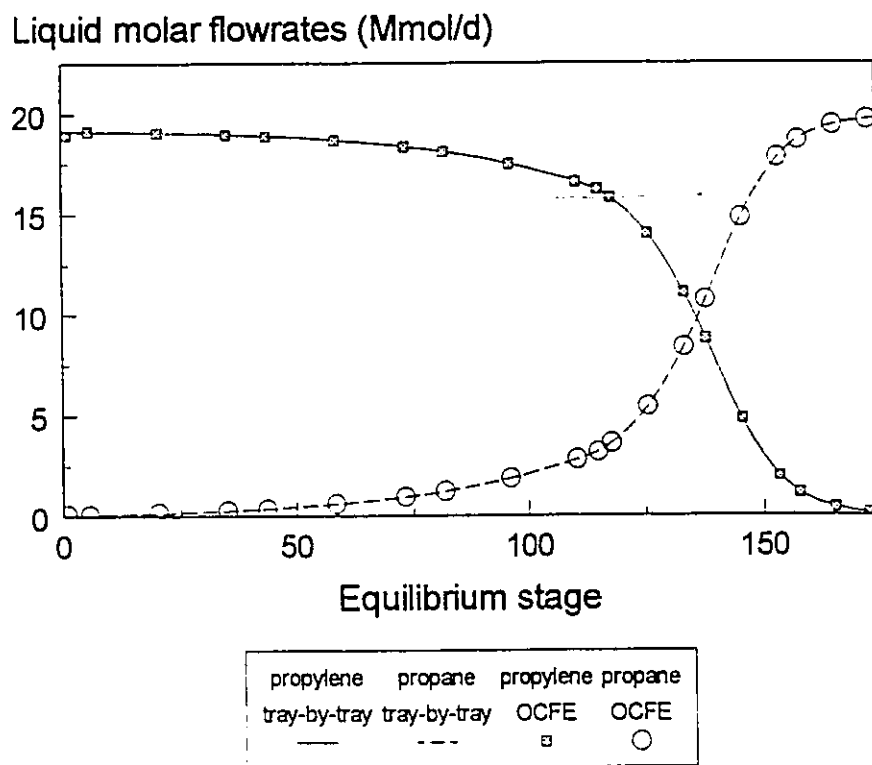


Figure 2.6 Comparison of the liquid composition profiles at the optimum in the tray-by-tray and OCFE models for the C<sub>3</sub>-splitter.

Table 2.4 Deisobutanizer (DIB) optimization results with linear objective.

	Tray-by-tray	Tray-by-tray	OCFE A	OCFE B	Short-cut
Solver	r-SQP	MINOS 5.3	r-SQP	MINOS 5.3	MINOS 5.3
Reflux ratio	7.043	7.043	7.043	7.043	7.358
Condenser heat duty (GJ/d)	-565.206	-565.206	-565.205	-565.205	-671.317
Reboiler heat duty (GJ/d)	584.191	584.191	584.191	584.190	694.694
Overhead product:					
mol% propane	5.63	5.63	5.63	5.63	5.63
mol% i-butane	91.37	91.37	91.37	91.37	91.37
Lagrange multiplier for n-butane = 3.0 %mol (\$/mol frac.)	-25,737	-25,741	-25,737	-25,737	-21,218
Flow (Mmol/d)	4.370	4.370	4.370	4.370	4.370
Bottoms product:					
mol% n-butane	81.89	81.89	81.89	81.89	81.89
mol% i-pentane	13.11	13.11	13.11	13.11	13.11
Lagrange multiplier for i-butane = 5.0 %mol (\$/mol frac.)	-7,195	-7,196	-7,195	-7,194	-11,621
Flow (Mmol/d)	2.054	2.054	2.054	2.054	2.054
VAX 3500 CPU time (s)	29.3	55.5	40.1	29.0	3.5
number of equations	240	240	177	135	14
number of variables	242	242	179	137	16
Objective function value (\$/d)	1628.14	1628.14	1628.14	1628.12	1903.66
MINOS 5.3 Options					
Lagrangian	-	No	-	No	No
Penalty parameter	-	0.0	-	0.0	Default
Minor Iterations	-	100	-	100	100

OCFE A model: 3 elements/section (equispaced), 3 collocation points/element in rectifying section, 4 collocation points/element in stripping section.

OCFE B model: 3 elements/section, 2 collocation points/element in rectifying section, 3 collocation points/element in stripping section. element lengths: rectifying section: 3.805, 3.740, 4.455, stripping section: 5.784, 4.927, 7.289.

Short-cut model: Fenske-Underwood-Eduljee equations.

Table 2.5 Deisobutanizer (DIB) optimization results with nonlinear objective.

Solver MINOS 5.3	Tray-by-tray	OCFE
Reflux ratio	10.078	10.077
Condenser heat duty (GJ/d)	-810.458	-810.409
Reboiler heat duty (GJ/d)	831.339	831.292
Overhead product:		
mol% propane	5.617	5.617
mol% i-butane	92.241	92.240
mol% n-butane	2.142	2.143
Flow (Mmol/d)	4.380	4.380
Bottoms product:		
mol% i-butane	2.720	2.718
mol% n-butane	84.110	84.111
mol% i-pentane	13.170	13.170
Flow (Mmol/d)	2.044	2.044
RS/6000 355 CPU time (s)	18.7	9.0
number of equations	240	135
number of variables	242	137
Objective function value (\$/d)	4560.32	4560.33
MINOS 5.3 Options		
Lagrangian	Yes	Yes
Penalty parameter	10.0	120.0
Minor iterations	100	100

OCFE model: 3 elements/section, 2 collocation points/element in rectifying section, 3 collocation points/element in stripping section. element lengths: rectifying section: 3.900, 3.900, 4.200, stripping section: 5.230, 4.903, 7.867.

The minimal OCFE model size for which a feasible solution is obtained using r-SQP is greater than the one achieved with MINOS 5.3. The r-SQP algorithm has proved to be more sensitive to the initial point than MINOS 5.3. Tables 2.4 and 2.5 report also the options parameters that are used for MINOS 5.3. In the first case, with the linear objective, both tray-by-tray and OCFE models converge faster when the augmented Lagrangian function is not used as the objective function in the linearized subproblems, but in the nonlinear objective case the use of the Lagrangian is crucial. A penalty parameter equal to 100 is used with the OCFE model since the initial infeasibilities are higher than in the tray-by-tray model.

The i-butane and n-butane liquid molar flow rates at the optimal solution for both models are shown in Figure 2.7 and verify the agreement of the optimal solution obtained by the two different process models. The liquid composition profiles for the non-key components propane and i-pentane are shown in Figure 2.8. The profiles show that OCFE models predict the composition of nonkey components accurately. Figure 2.9 shows the temperature profile at the optimum as calculated by the two modeling options.

The proposed OCFE models are compared to the existing collocation models proposed by Stewart et al. (1985). The collocation model proposed by Stewart et al. (1985) uses only one interpolation polynomial for each column section. However, for these simulations, Stewart et al. model is implemented with an equal number of finite elements as the proposed OCFE model and will be called the *modified* Stewart et al. model. The only difference between the original and *modified* models is in the treatment of the feed plate discontinuity. For the C<sub>3</sub>-splitter, the optimal solution obtained with the *modified* Stewart et al. model is not very different from the tray-by-tray solution but worse than the solution of the proposed OCFE approach (Table 2.2). However, for the case of the more complex DIB column, no feasible optimal solution is obtained with Stewart et al. formulation due to large errors introduced in the feed plate equations.

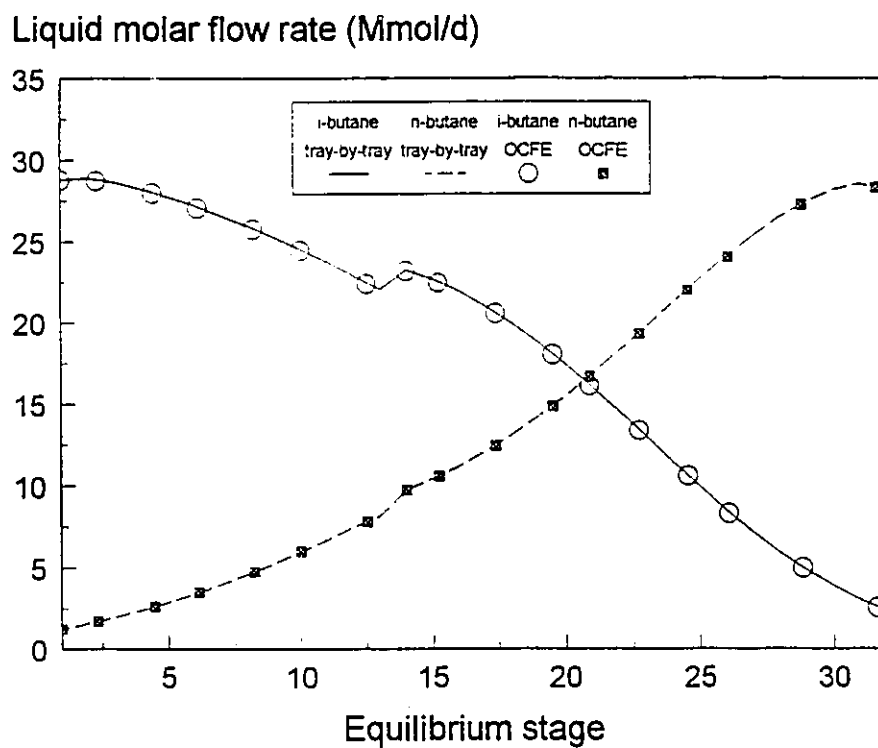


Figure 2.7 Comparison of the liquid composition profiles for the key components (at the optimum) in the tray-by-tray and OCFE models for the DIB.

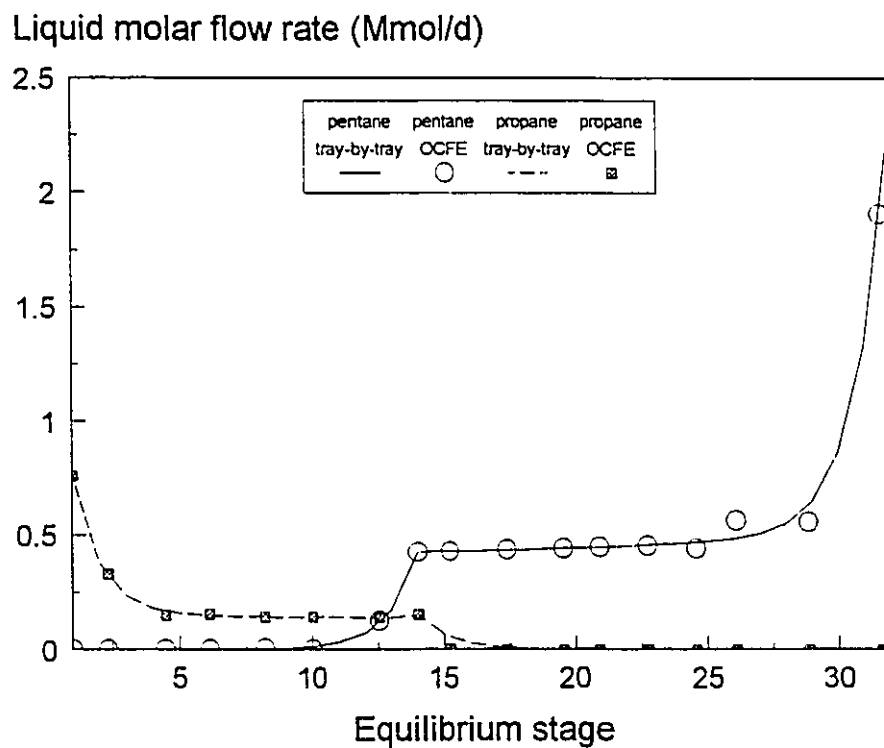


Figure 2.8 Comparison of the liquid composition profiles for the nonkey components (at the optimum) in the tray-by-tray and OCFE models for the DIB.

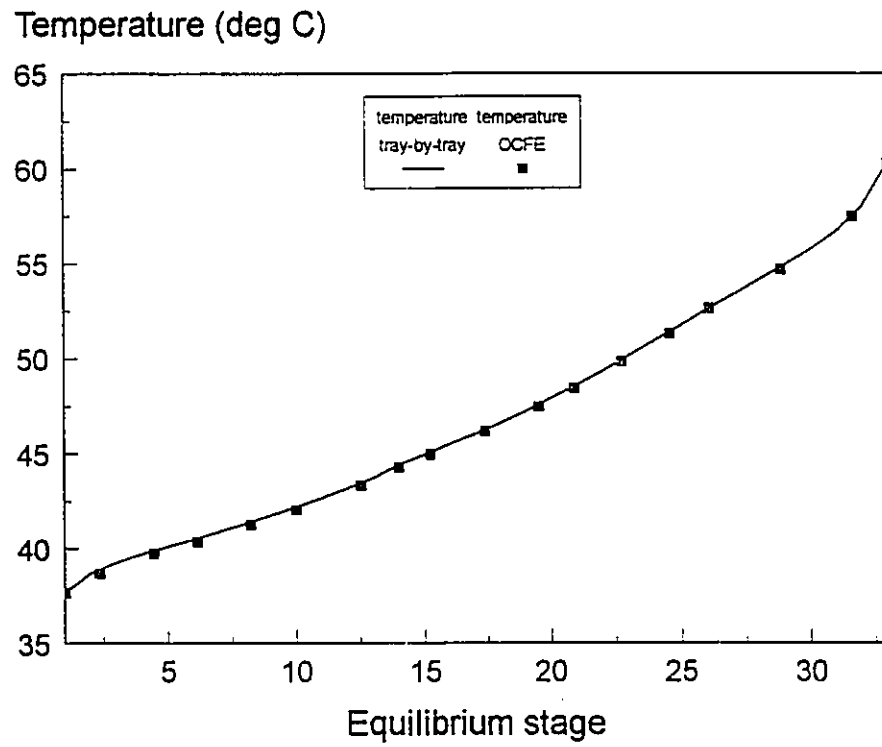


Figure 2.9 Comparison of the temperature profiles at the optimum in the tray-by-tray and OCFE models for the DIB.

The OCFE model is tested for its accuracy when the set of independent variables change. The independent variables are fixed at their optimal solution value of the original optimization problem and the simulation solution is obtained using MINOS 5.3. Two cases are examined. In the first case, the reflux ratio and the reboiler duty are the independent variables. In the second case, the overhead distillate flow rate and the reboiler duty are the degrees of freedom. In both cases the solutions are identical to the original case and in very good agreement with the tray-by-tray solution. The initial starting point is the same for all the cases.

#### **2.4.3 Case III. C<sub>3</sub>-C<sub>4</sub> splitter**

The C<sub>3</sub>-C<sub>4</sub> splitter is a more complex distillation column with six components. The linear cost objective (2.45) is used in the optimization. The OCFE model that results in a feasible optimal solution consists of two elements per column section. Each element in the rectifying section has three collocation points while the two elements in the stripping section have three and two collocation points respectively. The model size reduction is smaller in this case and as a consequence only a 20% decrease in the total solution time is achieved using the OCFE model (Table 2.6). The main reason for this behaviour is attributed to the increased complexity of the C<sub>3</sub>-C<sub>4</sub> splitter compared to the previous two examples. The C<sub>3</sub>-C<sub>4</sub> splitter is modeled with only 20 equilibrium stages. The ratio of the total number of collocation points used in the OCFE model (11) to the number of equilibrium stages in the tray-by-tray model (17, excluding the condenser, reboiler and the feed tray) is greater than in the previous two cases as a result of the increased complexity of the column.

#### **2.4.4 Case IV. Ethylbenzene-styrene (EB/S) Column**

In this example a binary ethylbenzene-styrene column (King, 1980) is optimized using the nonlinear objective (2.46) with cost parameters given in Appendix B. The liquid component enthalpy calculation using Equation (2.17) is based on the tray

Table 2.6 C<sub>3</sub>-C<sub>4</sub> splitter optimization results with linear objective.

	Tray-by-tray	OCFE
Reflux ratio	10.146	10.145
Condenser heat duty (GJ/d)	-184.716	-184.690
Reboiler heat duty (GJ/d)	224.184	224.184
Overhead product:		
mol% ethane	0.47	0.47
mol% propane	98.91	98.91
mol% n-butane	0.02	0.02
Lagrange multiplier for i-butane = 0.6 %mol (\$/mol frac.)	-29.460	-29.451
Flow (Mmol/d)	1.422	1.422
Bottoms product:		
mol% i-butane	64.70	64.70
mol% n-butane	28.53	28.53
mol% i-pentane	2.56	2.56
mol% pentane	0.21	0.21
Lagrange multiplier for propane = 4.0 %mol (\$/mol frac.)	-3.760	-3.670
VAX 3500 CPU time (s)		
r-SQP	28.5	-
MINOS 5.3	37.7	31.4
number of equations	193	139
number of variables	191	141
Objective function value (\$/d)	611.99	611.92
MINOS 5.3 Options		
Lagrangian	No	No
Penalty parameter	0.0	0.0
Minor Iterations	100	100

OCFE model: 2 elements/section, 3 collocation points/element in rectifying section, 3-2 collocation points in elements in stripping section. element lengths: rectifying section: 3.500, 3.500, stripping section: 5.400, 4.600.

temperature. The OCFE model consists of three elements per column section with three collocation points per element. Table 2.7 compares the optimal solution obtained by tray-by-tray and OCFE models. The agreement of the two solutions is very good even though the OCFE model uses about a third of the number of the equations in the tray-by-tray model. The OCFE model is about 12 times faster than the tray-by-tray model for this column using MINOS 5.3 as the solver. A dense Jacobian formulation is used for the tray-by-tray which increases the solution time.

#### 2.4.5 Initial Point Dependence

The dependence of the initial set of variable values for both the full-order and the OCFE models on the performance and computational effort required to converge to the optimal solution is investigated. The initial points tested are constructed by specifying poor estimates for the component molar flow rates and temperature at the two endpoints of the column and then calculating the values for the variables in the interior of the column by linear interpolation. These poor estimates of the variables increase the magnitude of the initial infeasibilities of the nonlinear constraints. For the OCFE models the values of the variables at the collocation points are evaluated by linear interpolation of the tray-by-tray initial variable values for the same starting point at adjacent trays.

The initial profiles for the *i*-butane molar flow rates are shown in Figure 2.10. In Table 2.8, the optimization results using MINOS 5.3 for different initial points for the DIB are shown. OCFE models are more robust than tray-by-tray models to poor initial variable values. As the initial point moves further from a feasible initial point, the ratio of the CPU time required for the tray-by-tray solution to that for the OCFE model increases. For some initial sets of variable values the tray-by-tray model fails to converge to the optimal solution.

For the  $C_3$ -splitter, the tray-by-tray model fails to converge whenever the initial temperature profile is assumed to be linear. The reason for this behaviour is that the tray-

Table 2.7 EB/S column optimization results with nonlinear objective.

Solver MINOS 5.3	Tray-by-tray	OCFE
Reflux ratio	10.166	10.166
Condenser heat duty (GJ/d)	-38.993	-38.993
Reboiler heat duty (GJ/d)	44.762	44.762
Overhead product:		
mol% ethyl-benzene	97.887	97.887
mol% styrene	2.113	2.113
Flow (Kmol/d)	105.093	105.092
Bottoms product:		
mol% ethyl-benzene	1.058	1.058
mol% styrene	98.942	98.942
Flow (Kmol/d)	88.877	88.878
RS/6000 355 CPU time (s)	121.4	9.4
number of equations	355	110
number of variables	357	112
Objective function value (1,000 \$/d)	161.03	161.03
MINOS 5.3 Options		
Lagrangian	Yes	Yes
Penalty parameter	Default	Default
Minor Iterations	100	100

OCFE model: 3 elements/section, 3 collocation points/element, equispaced.

i-butane liquid molar flowrates (Mmol/d)

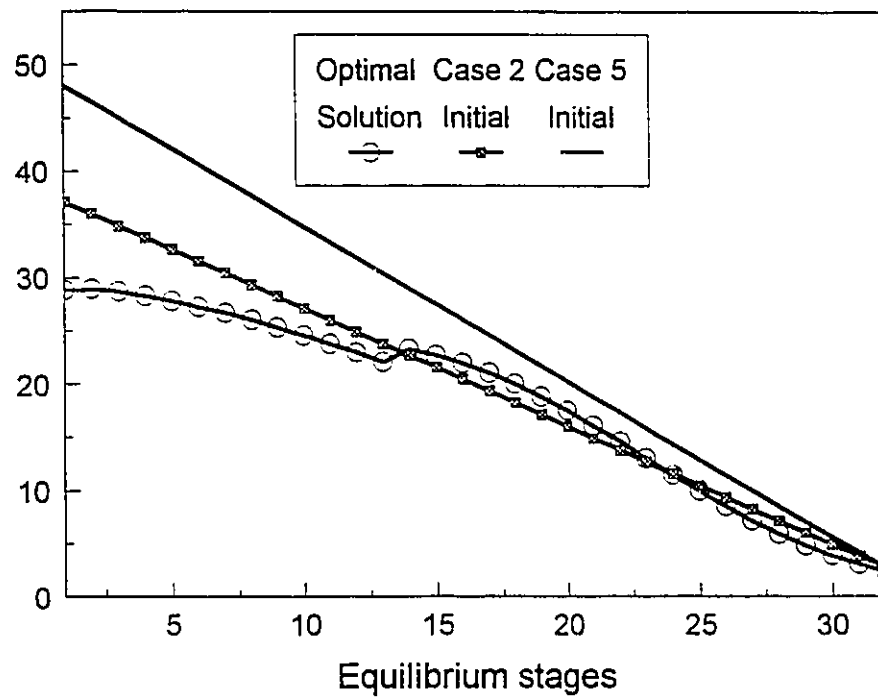


Figure 2.10 Comparison between the initial and optimal  $iC_4$  liquid composition profiles for the DIB.

Table 2.8 Optimization results for the DIB for different initial variable value sets.

Solver: MINOS 5.3	VAX 3500	Tray-by-tray	OCFE
Case 1			
i-butane: 37.1 - 2.7 Mmol/d	CPU time (s)	55.8	33.5
n-butane: 0.9 - 38.0 Mmol/d	CPU ratio	1.67	1.00
temperature: 35 - 60 °C	Major itns	8	7
Simulation solution (HYSIM)	Minor itns	110	103
Case 2			
i-butane: 37.1 - 2.7 Mmol/d	CPU time (s)	55.3	29.0
n-butane: 0.9 - 34.1 Mmol/d	CPU ratio	1.90	1.00
temperature: 35 - 60 °C	Major itns	8	6
Linear interpolation	Minor itns	116	84
Case 3			
i-butane: 40.0 - 2.7 Mmol/d	CPU time (s)	104.1	42.5
n-butane: 0.9 - 38.0 Mmol/d	CPU ratio	2.45	1.00
temperature: 30 - 65 °C	Major itns	10	8
Linear interpolation	Minor itns	59	200
Case 4			
i-butane: 45.0 - 2.7 Mmol/d	CPU time (s)	232.6	60.0
n-butane: 1.0 - 42.0 Mmol/d	CPU ratio	3.88	1.00
temperature: 30 - 65 °C	Major itns	11	10
Linear interpolation	Minor itns	601	323
Case 5			
i-butane: 48.0 - 2.7 Mmol/d	CPU time (s)	No convergence	74.6
n-butane: 1.0 - 45.0 Mmol/d	Major itns	-	10
temperature: 30- 65 °C	Minor itns	-	483
Linear interpolation			

by-tray model formulation may induce singularities in the problem due to the large flat regions in the temperature profile in the rectifying section (Figure 2.5). In addition, the discrepancy between the final solution profile and the initial linear profile is significant. The magnitude of infeasibilities in the material and energy balances using the initial variable values becomes significantly large. The OCFE model converged to the optimal solution when a linear temperature profile is provided as an initial estimate of the temperature variation in the column.

The improved ability of the OCFE models to converge to the optimal solution with a poor initial guess for the variables may be a very useful advantage, when OCFE models are used under a real-time (on-line) optimization framework. Disturbances in the real plant may result in the optimal operating conditions moving far away from the initial point estimate and then the robustness in convergence of the process model becomes very important.

#### **2.4.6 Approximation Error Analysis**

An important issue, for the use of OCFE models for distillation optimization, is the selection of the proper combination of number of elements for every column section and number of collocation points within each element. The approximation error defined as the difference of the OCFE solution from the tray-by-tray solution decreases asymptotically, as the total number of collocation points in the column increases. Such behaviour is expected since the use of the Hahn polynomials guarantee that the full-order model is recovered when the number of collocation points equals the number of equilibrium stages in a given column section. OCFE and global collocation models that use a single element per column section will eventually become identical at the full-order limit.

The approximation error analysis has two major requirements:

- a. Given an expected level of model accuracy, determine a sufficient combination of number of elements per element and number of collocation points per element.
- b. Given the configuration of the OCFE model, determine the optimal partition of the domain so that the approximation error is minimized.

It would be desirable to provide a method that can fulfill both requirements. However, the main goal is to achieve the minimum possible size of the OCFE model for which the tray-by-tray solution is obtained.

The approximation error of a given OCFE scheme depends mainly on the shape of the composition and temperature profiles in the given column section. The approximation error can be minimized by varying the length of the finite elements so that an optimal distribution of the collocation points (with respect to approximation error) in the column is achieved, for a constant total number of collocation points. Adaptive finite element formulation will be investigated in Chapter 3. The order of the approximation polynomial within a given element length that can represent the tray-by-tray model cannot be determined *a priori*. As a result optimization results using polynomials of different order are analyzed to determine a proper collocation scheme.

The optimal combination of number of elements and number of collocation points per element is difficult to determine *a priori*. Carta et al. (1995) developed charts by extensive simulations in order to determine the model reduction using OCFE for a given approximation error. The varying parameters are the relative volatility for a binary mixture and the purity levels of the product streams. However, the results are valid for a limited number of simplified distillation columns that cannot be generalized easily. A factor that is critical to the minimum size of the OCFE model is the complexity of the mixture (comparison of the results between the  $C_3$  and the  $C_3$ - $C_4$  splitters) and the thermodynamic model (e.g. rigorous evaluation versus constant relative volatility assumption) that is used.

The approximation error for the temperature and composition is calculated for the C<sub>3</sub>-splitter to investigate the dependence of the accuracy of the OCFE model on different collocation schemes. The approximation error is defined as the sum of squares of the differences of the variables (temperature or composition) obtained by the tray-by-tray model from the values of the same variables evaluated at the location of the equilibrium stages using the OCFE solution and the Lagrange interpolation polynomials. The error in composition and temperature for a single tray  $t$ , is given by the following relations:

$$e_{Temp,t} = T_t - \sum_{j=0}^{k_i} W_{i,j}(s_t) \tilde{T}_i(s_{ij}) \quad (2.47)$$

$$e_{flow,m,t} = l_{m,t} - \sum_{j=0}^{k_i} W_{i,j}(s_t) \tilde{l}_{m,i}(s_{ij}) \quad m = 1, \dots, NC \quad (2.48)$$

where  $s_t$  is the location of the actual  $t$ -th tray inside the  $i$ -th element and  $\tilde{T}_i(s_{ij})$ ,  $\tilde{l}_{m,i}(s_{ij})$  are the temperatures and the component liquid molar flow rates at the collocation points of the  $i$ -th element respectively.

Table 2.9 shows the error behaviour for different collocation schemes. For the cases of 2 and 3 elements per column section, with 2 collocation points per element, convergence to the optimal solution is not possible, which implies that 3rd order Lagrange polynomials are not very effective in predicting the tray-by-tray solution. In addition, one can assess the performance of different collocation schemes, with equal total number of collocation points, in identifying the optimal full-order solution. For instance, the approximation error is smaller when 3 elements per section with 4 collocation points per element are used compared with a scheme that uses 4 elements per section with 3 collocation points per element.

Table 2.9 Approximation error in different OCFE schemes for the C<sub>3</sub>-splitter

	2 elements per section	3 elements per section	4 elements per section
2 collocation points per element	<b>No convergence</b>	<b>No convergence</b>	1.483 1.696 2.934
3 collocation points per element	1.794 2.160 3.043	0.491 0.163 2.394	0.374 0.044 1.879
4 collocation points per element	0.460 0.117 2.306	0.340 0.025 1.715	0.252 0.007 1.262

Table entries are sum of squares of errors for propylene and propane liquid molar flow rates and temperature.

## 2.5 Chapter Summary

Orthogonal collocation on finite elements techniques are used for the model size reduction of distillation units. Each column section is divided into subdomains in which orthogonal collocation is applied. The number of equilibrium stages as well as the component molar flow rates and the total enthalpies are treated as continuous variables of position in the column. The collocation points are chosen to be the roots of the Hahn orthogonal polynomials. The condenser, the reboiler and the plates, where a sidestream leaves or enters the column, are treated as discrete equilibrium stages. This new formulation allows the accurate representation of the column behaviour under the presence of discontinuities in column variable profiles due to feed and side product streams.

OCFE models are used for steady-state optimization of distillation units and the optimal solutions are compared to those obtained by the tray-by-tray model. Both models converge to the same optimal solution but OCFE models require less computational effort. OCFE formulations are advantageous for columns that have a large number of equilibrium stages with relatively smooth profiles, since the reduction in model size and solution time is substantial. As the complexity of the distillation column increases, due to the addition of more components or the use of more rigorous thermodynamic models, the minimum number of collocation points for a feasible optimal solution increases.

OCFE models show improved robustness in converging to the optimal solution when a poor initial point is provided, mainly because of their compact size. For a constant number of collocation points there is a combination of number of elements per column section and number of collocation points per element for which a measure of the approximation error is minimized. At present, the minimum number of elements and collocation points, which provide the least approximation error, cannot be determined without a previous solution of the column available.

## 3. Adaptive Collocation on Finite Elements Models for Distillation Units

### 3.1 Introduction

In Chapter 2 an OCFE model is developed for the steady-state optimization of distillation units. There is a minimum number of elements per column section and collocation points per element for which a feasible optimal solution exist for a given column. However, this lower bound of the approximation model depends on the operating conditions in the column. The error associated with a given OCFE formulation depends strongly upon the distribution of the collocation points in the column sections. The distribution of the collocation points, for a given total number of points, can be controlled by varying the sizes of the finite elements. Element breakpoint locations may be used as additional adjustable parameters for the structure of the OCFE model in order to achieve an optimal element partition of the column sections in terms of the approximation error.

The adaptation of the element breakpoint locations may allow small OCFE models, in total number of collocation points, to achieve a more accurate approximation compared to the corresponding OCFE model with fixed breakpoint locations. Generally, the approximation error for a given collocation scheme of a distillation process depends on the shape and the characteristics of the approximated composition and temperature profiles. However, the features of the state profiles at the optimal solution are unknown *a priori* and therefore it can be difficult to select the element sizes. An estimate of the approximation error, that will be updated as the optimal solution is approached, may provide a measure of the local “goodness” of the approximation.

The choice of equally spaced finite elements does not necessarily result in an optimal partition. For a steep variation in the column profiles, a large number of collocation points is required for an accurate representation of the actual solution. On the other hand, a few collocation points would be sufficient to match the solution when changes with small slope occur in the column profiles. A criterion for the adaptive element breakpoint placement may be the distribution of the approximation error equally throughout the column. An element partition methodology based on error equidistribution, with a given number of elements per column section and a given number of collocation points per element, will attempt to place small elements in those regions where steep changes in the state variables occur and larger elements in those regions where relatively small changes occur. Since the behaviour of the profiles in the column play such a decisive role in the element partition procedure, it is desirable that the procedure is carried out using the profiles at the economic optimal solution. The procedure for the adjustment of the element lengths is embedded into the nonlinear program that aims to determine the optimal operating conditions for the separation process. Therefore, the element partition is based on the shapes of the profiles as they evolve towards the economic optimal solution.

Simultaneous solution of the error equidistribution and economic optimum problem has been successfully applied to the optimization of systems described by a set of differential and algebraic equations, for example by Cuthrell and Biegler (1985). The method was extended by including a procedure that determines a sufficient number of finite elements for a flowsheet reactor model using OCFE by Vasantharajan and Biegler (1990).

Two different methods are used to determine the optimal element length distribution in OCFE models for distillation processes with a given total number of collocation points. Both methods are based on the equidistribution of the approximation error, but they use different techniques for the calculation of an estimate of the approximation error. The first method uses the residuals of the material and energy

balances around pre-defined envelopes in the column while the second method uses the derivatives of the polynomial approximation solution.

### 3.2 Adaptive OCFE Model for Distillation Units

Error analysis of piecewise polynomial approximations to an isolated solution of an  $m$ -th order nonlinear ordinary differential equation, with the polynomials determined by collocation at Gaussian points, was made by de Boor and Swartz (1973). De Boor (1974) proposed a method to determine the optimal location of the element breakpoints when approximating a function, given implicitly as the solution of an ordinary differential equation, by piecewise polynomials. The method is based on the asymptotic equidistribution of the approximation error associated with each element and determines the optimal distribution of element breakpoints rather than the optimal location of each breakpoint independently. This approach was later implemented in the code COLSYS developed for the solution of boundary value problems using collocation and piecewise polynomials or B-splines (Ascher et al., 1979). The method requires the evaluation of the approximation error associated with each element. However, the actual solution is usually not known and thus an estimate of the error must be calculated. Christiansen and Russell (1978) provided an overview of the most popular methods for estimating the approximation error resulting from piecewise polynomials using collocation. The estimates can be calculated by either the derivatives of the approximate solution or by using the residuals of the differential equations at non-collocation points.

White (1979, 1982) introduced a transformation, based on the equidistribution of the arc length of the state variable profile, of the original problem such that the new problem can be accurately represented by a small number of equally spaced breakpoints.

However, the previous methods deal with problems in a continuous domain. In the case of approximating the solution of a stagewise separation process, the reduced order model is applied in a spatially discrete domain. The compositions and temperatures in the tray-by-tray model are defined only at certain points where phase equilibrium is

usually assumed. Therefore the comparison between the tray-by-tray and the OCFE models can be made reasonably only at the equilibrium stages.

The element boundaries may be adjusted according to the shape of the composition profiles in the column. Srivastava and Joseph (1987) used different collocation schemes to approximate the behaviour of key and nonkey components. Usually, the composition profiles of nonkey components exhibit flat regions for large sections in the column, where the composition of the nonkey components is very small, and steep changes towards the two column endpoints. For nonkey components, more collocation points are used in those regions where their composition changes rapidly, while fewer points are used in the regions where the mole fraction is very small and no significant changes occur. A global collocation scheme for key components is used and overall material and energy balances are applied at a given total number of collocation points in this scheme. Interpolation at the collocation points of the global scheme, using the nonkey collocation scheme, is required in order to transfer the information for the nonkey components to the points where the overall balances are applied. This strategy requires *a priori* knowledge of the profiles in order to determine the regions where steep fronts exist.

Drozdowicz and Martinez (1988) implemented similar global and local collocation schemes and used the absorption factor, defined as  $L/KV$ , to determine the location of the steep changes for the state variables in the column. A value of the absorption factor much different from unity, indicates the presence of steep regions in the composition profile and then a local collocation scheme with more collocation points is introduced in this region. This procedure is embedded in a flowsheet solution framework and the location of the steep regions can be determined during the course of the solution.

Swartz (1987) used the residuals of the material and energy balances at non-collocation points as an error estimate and located the breakpoints by minimizing the weighted sum of the residuals. Stewart et al. (1985) gave physical meaning to the

element breakpoints by locating them at the points where discontinuities in the flow rates are introduced due to sidestreams entering or leaving the column. In multiphase distillation with two liquid phases, the moving miscibility boundary separates the column section in which one liquid phase exists from the section in which two liquid phases are present. The boundary provides a natural way to locate the element breakpoint (Swartz and Stewart, 1987).

Huss and Westerberg (1994) proposed a transformation of the component mole fractions so that the new variable has a straight profile in the column. This transformation aims to approximate more accurately those regions in the column where some of the components have mole fractions close to one or zero. It was argued that in such a situation, a polynomial approximation within each element may cause the composition profile to oscillate thus creating problems by reaching the low bound for the composition (zero mole fraction) inside the column. The proposed variable transformation of the mole fraction that was proposed has the form:

$$2x_{L,m} - 1 = \tanh(\hat{x}_{L,m}) \quad m = 1, \dots, NC \quad (3.1)$$

where  $x_{L,i}$  is the liquid phase mole fraction for the  $m$ -th component. The transformed variable  $\hat{x}_{L,m}$ , goes to negative or plus infinity when  $x_{L,i}$  approaches one or zero, respectively. An equispaced element partition was then imposed on the straight profile of the transformed variables.

### 3.2.1 Residual-based Breakpoint Placement

The residuals of the system equations at non-collocation points can provide an estimate of the approximation error (Ferguson and Finlayson, 1972; Carey and Finlayson, 1975). Swartz (1987) suggested a residual-based hybrid method for adaptive placement of the element knots for a collocation model in a distillation column. This method uses polynomial interpolation to approximate the residuals inside the element. The interpolation points are roots of a Hahn orthogonal polynomial of order  $k_i+1$ , where  $k_i$  is

the number of collocation points in the given element. Each residual is evaluated at these  $k_i+1$  points, and each interpolated residual is then made to vanish at the zeros of a  $k_i$ -th order Hahn polynomial. A weighted sum of the square of the residuals at the roots of the  $(k_i+1)$ -th order Hahn polynomial provides a measure of the residuals for every element. These measures from different elements are forced to be equal and are embedded into the formulation of the OCFE model.

Russell and Christiansen (1978) used the residual at the midpoint of the element to define a bound for the local approximation error given by:

$$\|e\|_i = C' R(x_{i+1/2}) \Delta t_i^m + O(\Delta t_i^{k_i+1}) \quad (3.2)$$

where  $C'$  is a computable constant,  $R(x_{i+1/2})$  is the residual of the system equations evaluated at the midpoint of the  $i$ -th element,  $m$  is the order of the differential equation, and  $\Delta t_i$  is the length of the  $i$ -th element. An error equidistribution criterion may be then constructed using (3.2) by requiring that:

$$\Delta t_i^m |R(x_{i+1/2})| = \text{const.} \quad i = 1, \dots, NE \quad (3.3)$$

However, Koster et al. (1993) found that when (3.3) is used as the equidistribution relation the adaptive element placement problem does not provide an accurate representation of the actual solution. Therefore they proposed a modification of (3.3) expressed by

$$\Delta t_i^{m+k_i} |R(x_{i+1/2})| = \text{const.} \quad i = 1, \dots, NE \quad (3.4)$$

where  $k_i$  is the order of the approximation polynomial used at the  $i$ -th element. Error equidistribution based on the criterion (3.4) proved to result in element partitions that provided an accurate solution.

Vasantharajan and Biegler (1990) used an error criterion based on the condition that the residuals at some selected non-collocation points should be less than a specified

tolerance. However, the selection of the non-collocation points is arbitrary and evaluation of the residuals at one point does not necessarily reflect the behaviour of the residuals throughout the entire domain.

A method that is closely related to the nature of the distillation process is proposed. The methodology uses the residuals of the material and energy balances evaluated around envelopes encribed within the column. More specifically, the envelopes for the rectifying section contain the condenser and the trays included between the top of the column and the end of each element in the rectifying section. For the stripping section, the residuals are evaluated around envelopes that contain the reboiler and the trays included from the bottom of the column till the top of each element. A schematic of the envelope configuration is shown in Figure 3.1. The method utilizes the fact that the material and energy balances must be satisfied around any encribed envelope in the column.

The residual equations for the component material balances, with the finite elements numbered from top to bottom for every column section, take the form:

*Rectifying section:*

$$\begin{aligned} R_{MAT,m,i} &= d_m + \tilde{l}_{m,i+1}(s_0) - \tilde{v}_{m,i}(s_{k_i+1}) & i = 1, \dots, NE_R - 1 \text{ and } m = 1, \dots, NC \\ R_{MAT,m,i} &= d_m + \sum_{j=0}^{k_i} W_{l,j,i}(NT_i) \tilde{l}_{m,i}(s_{i,j}) - \tilde{v}_{m,i}(s_{k_i+1}) & i = NE_R \end{aligned} \quad (3.5)$$

*Stripping section:*

$$\begin{aligned} R_{MAT,m,i} &= b_m + \tilde{l}_{m,i}(s_0) - \tilde{v}_{m,i-1}(s_{k_i+1}) & i = 2, \dots, NE_S \text{ and } m = 1, \dots, NC \\ R_{MAT,m,i} &= b_m + \tilde{l}_{m,i}(s_0) - \sum_{j=1}^{k_i+1} W_{v,j,i}(1) \tilde{v}_{m,i}(s_{i,j}) & i = 1 \end{aligned} \quad (3.6)$$

Similarly the residual equations for the energy balances become:

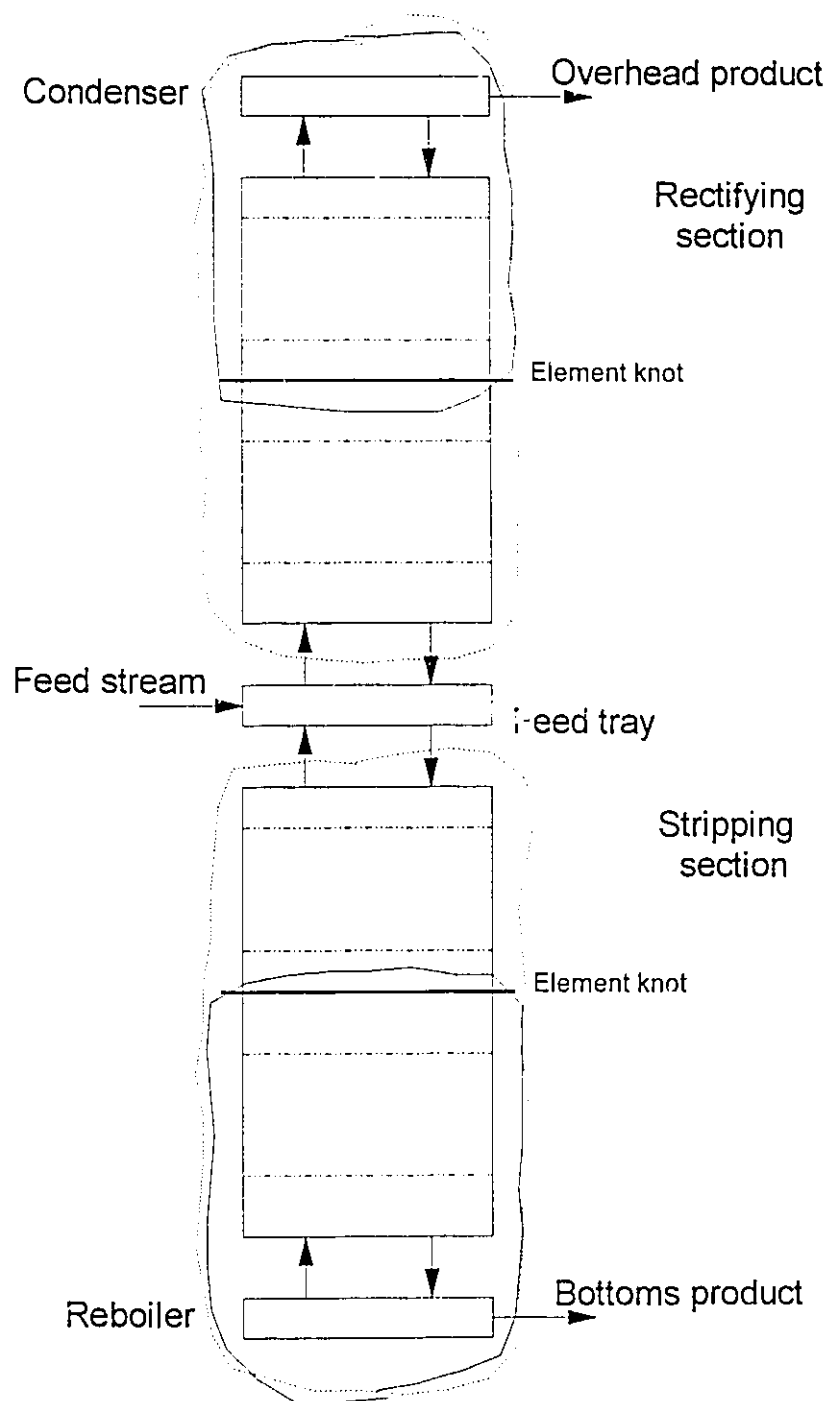


Figure 3.1 Material and energy balance envelopes for a typical adaptive OCFE distillation model.

*Rectifying section:*

$$\begin{aligned} R_{ENG,i} &= D H_D + Q_D + \tilde{L}_{i+1}(s_0) \tilde{H}_{i-1}^L(s_0) - \tilde{V}_i(s_{k+1}) \tilde{H}_i^V(s_{k+1}) & i = 1, \dots, NE_R - 1 \\ R_{ENG,i} &= D H_D + Q_D + \tilde{L}_i(NT_i) \tilde{H}_i^L(NT_i) - \tilde{V}_i(s_{k+1}) \tilde{H}_i^V(s_{k+1}) & i = NE_R \end{aligned} \quad (3.7)$$

*Stripping section:*

$$\begin{aligned} R_{ENG,i} &= B H_B^L + Q_B + \tilde{L}_i(s_0) \tilde{H}_i^L(s_0) - \tilde{V}_{i-1}(s_{k+1}) \tilde{H}_{i-1}^V(s_{k+1}) & i = 2, \dots, NE_S \\ R_{ENG,i} &= B H_B^L + Q_B + \tilde{L}_i(s_0) \tilde{H}_i^L(s_0) - \tilde{V}_i(1) \tilde{H}_i^V(1) & i = 1 \end{aligned} \quad (3.8)$$

Index  $i$  denotes the element. The residual relations around the envelopes make use of the zero-order continuity boundary condition between the elements (Equations 2.43 and 2.44); the liquid stream leaving the  $i$ -th element is equal to the liquid entering the  $(i+1)$ -th element.

The magnitude of the total residual for a given element is calculated using the 2-norm of the residuals of the component material balances and the total energy balance.

$$R_{TOT,i} = \left\{ R_{ENG,i}^2 + \sum_{m=1}^{NC} R_{MAT,m,i}^2 \right\}^{1/2} \quad i = 1, \dots, NE \quad (3.9)$$

The total residual of each envelope is forced to be equal to the total residual of the subsequent envelopes. The equidistribution constraints are embedded in the economic optimization problem which takes the following form:

$$\begin{aligned} & \text{Min} \quad \{\text{Costs}\} & (P3.1) \\ & \text{s. t. Material \& Energy Balances (2.29 - 2.31)} \\ & R_{TOT,i} - R_{TOT,i+1} = 0 \quad i = 1, \dots, NE - 1 \end{aligned}$$

Problem (P3.1) determines both the optimal operating conditions of the distillation column and an element partition such that the envelope balance residuals equidistribution constraints are satisfied within the feasibility tolerance specified for the nonlinear constraints.

The residual-based adaptive breakpoint placement for OCFE models for distillation columns is based on the closure of the material and energy balances around envelopes of adjustable size. The envelope size depends on the lengths of the elements included within a given envelope. The use of the max-norm of the material and energy balance residuals as a measure of the total envelope residual in (3.9) would increase the difficulty of the problem because of the non-differentiabilities introduced by such a norm.

In cases of multiphase distillation, where more than one liquid phase is present within the column, or for heterogeneous azeotropic distillation, an element breakpoint should be placed at the point where the phase discontinuity occurs. In a formulation suggested by Swartz and Stewart (1987), the phase stability criteria were solved with the balance equations simultaneously in order to determine the miscibility boundary of the two liquid phase mixture. The proposed OCFE model with the adaptive element breakpoint placement can be used in the region of the two liquid phases provided that an element breakpoint separates the single phase from the two phase regions.

### 3.2.2 Error Equidistribution using Spline Approximation to the Derivatives

Following de Boor's methodology (1974) the breakpoints are located such that a local error term associated with each element is made constant. The function  $y$ , which satisfies an  $m$ -th order differential equation, is approximated by piecewise polynomials of order  $k+1$  (degree  $< k+1$ ) with breakpoint sequence:

$$a = t_1 < t_2 < \dots < t_{NE+1} = b$$

where  $NE$  is the number of elements. The breakpoints correspond to the boundaries of the finite elements.

If  $y$  is sufficiently smooth then the local approximation error satisfies the following inequality (de Boor, 1974):

$$\|y - \tilde{y}\|_{[t_i, t_{i+1}]} \leq C \Delta t_i^{k+1} \|y^{(k+1)}\|_i + O(\Delta t_i^{k+2}) \quad (3.10)$$

where:

$\|y - \tilde{y}\|_{[t_i, t_{i+1}]}$  is the max-norm of the local approximation error term between the function  $y$  and the piecewise polynomial approximation function  $\tilde{y}$ . In the case of a distillation column, the function  $y$  represents the composition and temperature profiles determined by the tray-by-tray model and  $\tilde{y}$  represents the solution obtained by the OCFE model. The function  $y$  is defined only at the equilibrium stages.  $\Delta t_i$  is the length of the  $i$ -th interval.  $\|y^{(k+1)}\|_i$  is the max-norm of the  $(k+1)$ th derivative of the function  $y$  in the interval  $[t_i, t_{i+1}]$ .  $C$  is a constant that depends only upon  $k$  and  $m$  for a given collocation scheme. The global error term is  $\mathcal{O}(\Delta t^{k+2})$  and for sufficiently small elements it can be neglected (de Boor, 1974).

The accuracy of the approximation can be improved by reducing the size of those intervals where the  $(k+1)$ -th derivative of  $y$  is large, for a given number of collocation points within each element, or by adding more collocation points. In the development of the adaptive OCFE models, the number of collocation points per element is kept constant. The approximation error minimization can be formulated as a nonlinear programming problem.

$$\begin{aligned} \text{Min}_{t_i} \quad \text{Max}_j \quad \Delta t_j \left\| y^{(k+1)} \right\|_j^{1/(k+1)} \quad & i = 2, \dots, NE \quad \text{and} \quad j = 1, \dots, NE \quad (\text{P3.2}) \\ \text{s.t.} \quad \Delta t_i \geq k \quad & i = 1, \dots, NE \\ \text{with} \quad t_1 = 0, \quad t_{NE+1} = NT \end{aligned}$$

where  $NT$  is the number of trays in every column section and  $k$  is the number of collocation points in each element, which is assumed to be equal for all elements without any loss of generality. The problem (P3.2) can be solved to obtain the optimal breakpoint placement that minimizes the local approximation error, while satisfying the constraint that an element can have no more interior collocation points than the number of equilibrium stages in that element.

The optimization problem (P3.2) is difficult to solve since it contains non-differentiable functions and the function  $y$  which is only known approximately. The goal is not to locate each breakpoint to attain a global optimum, but rather to obtain a local optimal distribution of element lengths for which the approximation error associated with each element is constant. The optimality conditions for problem (P3.2), when  $y$  is continuous and there are no active constraints, satisfy the relation (de Boor, 1974):

$$\Delta t_i \|y^{(k+1)}\|_i^{1/(k+1)} = \text{const.} \quad i = 1, \dots, NE \quad (3.11)$$

De Boor (1974) showed that the distribution of breakpoints that satisfy (3.11) is asymptotically equivalent to that determined by  $t_2, \dots, t_{NE}$  such that (Pereyra and Sewell, 1975):

$$\int_{t_i}^{t_{i+1}} |y^{(k+1)}(s)|^{1/(k+1)} ds = \frac{1}{NE} \int_a^b |y^{(k+1)}(s)|^{1/(k+1)} ds \quad i = 1, \dots, NE \quad (3.12)$$

The collocation solution is used to approximate  $y^{(k+1)}$  in the domain. However, the  $(k+1)$ -th derivative of the collocation solution is equal to zero because the piecewise polynomials are of degree less than  $(k+1)$ . Hence the piecewise constant  $k$ -th derivative of the collocation solution is used and then  $y^{(k+1)}$  is estimated based on a first order difference approximation over the elements which is given as follows (de Boor, 1974):

$$\xi^{(k+1)}(s) = \begin{cases} \frac{2|\Delta\Theta_{3/2}|}{t_3 - t_1}, & \text{on } (t_1, t_2) \\ \frac{|\Delta\Theta_{i-1/2}|}{t_{i+1} - t_{i-1}} + \frac{|\Delta\Theta_{i+1/2}|}{t_{i+2} - t_i}, & \text{on } (t_i, t_{i+1}) \quad i = 2, \dots, NE - 1 \\ \frac{2|\Delta\Theta_{NE-1/2}|}{t_{NE+1} - t_{NE-1}}, & \text{on } (t_{NE}, t_{NE+1}) \end{cases} \quad (3.13)$$

where  $\Theta_{i+1/2} = \tilde{y}^{(k)}(s)$  on  $(t_i, t_{i+1})$ , and  $\Delta\Theta_{i-1/2} = \Theta_{i+1/2} - \Theta_{i-1/2}$ . A schematic of the approximation of the  $(k+1)$ -th derivative of the true solution is given in Figure 3.2.

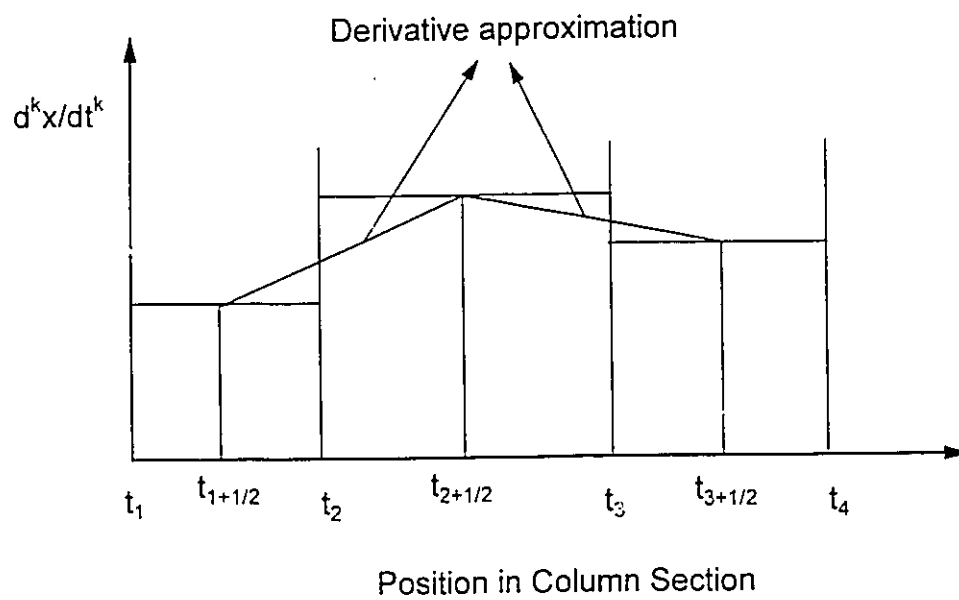


Figure 3.2 Approximation of the  $(k+1)$ -th derivative of the state variable profile (de Boor, 1974).

In particular, for the case of a staged distillation column, the approximated state variables are the liquid and vapour component molar flow rates and the total stream enthalpies. The derivatives of the functions that represent the behaviour of these variables in the interior of the column are given by the  $k$ -th derivatives of the Lagrange interpolation polynomials within each element.

$$\tilde{l}^{(k)}(s) = k! \sum_{i=0}^k \left\{ \tilde{l}(s_i) \prod_{\substack{j=0 \\ j \neq i}}^k \frac{1}{(s_i - s_j)} \right\} \quad (3.14)$$

$$\tilde{v}^{(k)}(s) = k! \sum_{i=1}^{k+1} \left\{ \tilde{v}(s_i) \prod_{\substack{j=1 \\ j \neq i}}^{k+1} \frac{1}{(s_i - s_j)} \right\} \quad (3.15)$$

$s_j$  denotes the location of the  $j$ -th collocation point. Similar relations evaluate the liquid and vapour total enthalpies.

In the case of a distillation column, there are multiple state variable profiles to be approximated. The objective is to equidistribute the approximation error associated with all the variables of interest. The 2-norm of the derivatives is used to determine the total approximation error (Cuthrell and Biegler, 1987). The max-norm is desirable, but non differentiable (Equation 3.11); however, the 2-norm is considered to be a good compromise. The error equidistribution relation thus becomes:

$$\Delta t_i \left\{ \sum_{j=1}^q \left( \xi_{j,i}^{2/(k+1)} \right) \right\}^{1/2} = \text{const.} \quad i = 1, \dots, NE \quad (3.16)$$

where  $q$  denotes the total number of state variables that are approximated.

It is assumed that  $|\xi^{(k+1)}|$  behaves like  $|y^{(k+1)}|$ . The local error term is equidistributed among the finite elements in each column section. A continuous and monotonically increasing function  $G(s)$ , that calculates the additive local error term as a function of the position in the column is constructed.

$$G(s) = \int_a^s (\xi(s))^{1/(k+1)} ds \quad (3.17)$$

The new location of the breakpoints is determined by the following expression:

$$t_{new} = t_1 + G(s)^{-1} (i-1) \frac{G(\beta)}{NE} \quad i = 1, \dots, NE + 1 \quad (3.18)$$

The algorithm that calculates the optimal placement of the breakpoints is utilized in an outer-loop of the optimization problem, that determines the economic optimum of the given distillation column and consists of the following steps:

1. Obtain a solution for the economic optimization problem with equispaced elements.
2. Estimate the error within each element using the obtained solution (Equation 3.13).
3. Adjust the element lengths so that the error is equidistributed (Equations 3.16 and 3.18).
4. If the element lengths do not change more than a defined tolerance, stop. Otherwise continue.
5. Solve the economic optimization problem for the new partition.
6. Go to step (2).

The procedure may encounter some difficulties in determining the optimal breakpoint sequence when some of the intermediate problems (step 5) become infeasible. In such a situation, the error estimates are calculated using state variables that do not satisfy the constraints of the model (2.29-2.31) and are subject to discrepancies. The element lengths are not expected to have a large effect on the economic optimal solution based on the results of the residual equidistribution approach. There is typically a range of variation for the element breakpoints for which an optimal solution can be found. The OCFE model fails to converge if the element breakpoints fall outside a range of breakpoint placements.

An approach that simultaneously determines the economic optimum and the optimal element partition using (3.11) (Vasantharajan and Biegler, 1990) failed to converge in our implementation of the OCFE models for distillation columns. Such an approach involved the solution of a sequence of subproblems in order to deal with the absolute values in (3.13). However, some of these subproblems did not result in a feasible solution which caused the failure of the whole procedure.

### **3.3 Steady-State Optimization with Approximation Error Criteria**

Both methods for the adaptive element breakpoint placement are applied to the steady state optimization of distillation columns. MINOS 5.3 is used for the optimization. In a real-time optimization framework, it is not necessary to adjust the size of the elements of the OCFE model each time a new optimal solution is to be determined. The adaptive placement of the breakpoints can be performed every time there is evidence that (due to a measured or unmeasured disturbance) the profiles in the distillation column have changed such that the plant optimum has shifted significantly. A new element partition may be required to improve the accuracy of the OCFE model. The values of the material and energy balance residuals may be used to determine whether an update of the element length distribution is required.

#### **3.3.1 Deisobutanizer (DIB) example**

The DIB separates a mixture of 4 components and is modeled with 33 equilibrium stages, including a partial condenser and reboiler, with 100% tray efficiency (Bailey, 1991). The feed stream properties and the product specifications are shown in Table 2.1. The OCFE model consists of 3 elements per column section, with 2 collocation points per element in the rectifying section and 3 collocation points per element in the stripping section. This implies that third and fourth order Lagrange interpolation polynomials are used for the rectifying and stripping section respectively. Regressed equations are used for the calculation of the equilibrium constants and the liquid and vapour enthalpy. The

objective function of the economic optimization problem is the minimization of the utility costs (2.45) that are required for the satisfaction of the product specifications.

The OCFE model with this structure does not converge to a feasible optimal solution when equispaced breakpoints are used. An OCFE model with equispaced breakpoints required the addition of more collocation points in order to obtain convergence thus increasing the number of equations in the model.

Simultaneous solution of the economic optimization and the optimal breakpoint selection problem, using the residual-based approach, resulted in a feasible solution close to the optimal solution obtained by the tray-by-tray model (Table 3.1). The augmented optimization problem (P3.1) includes an envelope residual equidistribution constraint for every breakpoint that is allowed to move. Thus the number of degrees of freedom in the augmented problem (P3.1) are the same as in the original cost minimization problem. The solution time increases when the material balance residuals are neglected and only the residuals of the energy balances are equidistributed among the elements. There is no significant difference between the optimal values of the independent variables in the column obtained by either formulation of the residual measure, even though the resulted element partition is different. The optimal composition and temperature profiles for this column are shown in Figures 2.7-2.9.

There are multiple combinations of element lengths that satisfy the equidistribution constraints of (P3.1). The problem may become ill-conditioned if too many breakpoints are allowed to vary and the optimization algorithm fails to converge. The characteristic of such cases, using MINOS 5.3, is that the infeasibilities of the model constraints fall below the specified tolerance (most typically  $10^{-6}$ - $10^{-8}$ ) but the changes in the Lagrange multipliers between consecutive major iterations remain significantly large. This is an indication that the residual equidistribution has no unique element partition that results in an economic optimal solution. In order to avoid such a situation, some of the element lengths are kept fixed or their changes are restricted by imposing upper and

Table 3.1 Optimization results with adaptive breakpoint placement for the DIB (linear objective).

		Mesh A	Mesh B	Mesh C	Mesh D
	Tray-by-tray	Equispaced	Mass & Energy Residuals Equidistribution	Energy Residuals Equidis- tribution	Derivative Equidis- tribution
Reflux ratio	7.057	7.057	7.057	7.057	7.040
Condenser heat duty (MJ/d)	-566.948	-566.850	-566.852	-566.849	-565.488
Reboiler heat duty (MJ/d)	585.936	585.839	585.837	585.834	584.751
Marginal value					
Overhead prod. (\$/mol fr)	-25.899	NA	-25.899	-25.899	NA
Bottom prod. (\$/mol fr.)	-7.239	NA	-7.238	-7.239	NA
Objective (\$/d)	1633.03	1632.75	1632.75	1632.74	1629.60
	<b>Feasible</b>	<b>Infeasible</b>	<b>Feasible</b>	<b>Feasible</b>	<b>Infeasible</b>
VAX 3500 CPU (sec) Solver MINOS 5.3					
Optimization only	69.3	57.0	33.2	41.0	58.0
Optimization with Elem. Adaptivity	NA	NA	103.2	134.1	NA
Rectifying section element lengths					
1st	-	4.000	3.838	3.205	2.714
2nd	-	4.000	3.679	4.317	3.282
3rd	-	4.000	4.483	4.478	6.004
Stripping section element lengths					
1st	-	6.000	5.807	5.840	7.526
2nd	-	6.000	4.819	6.345	5.516
3rd	-	6.000	7.374	5.815	4.958

lower bounds on the element size. The final element length distribution depends on the initial values of the variable set. However, the economic objective value and the optimal set of variable values were insensitive, in this particular example, to different breakpoint distributions. In Table 3.1, the optimization results for different element partitions are shown and are compared to the tray-by-tray optimal solution. The solutions obtained from the OCFE models are in good agreement with the tray-by-tray model, but the CPU solution time varied for different element partitions from the same starting point.

Breakpoint placement using the derivative equidistribution results in an element partition for which convergence to a feasible optimal point is not possible. After typically 5 iterations the equidistribution constraints are satisfied. The resulting breakpoint placement is different from the one obtained using the residual-based approach (Table 3.1). In the stripping section the element breakpoints move in opposite directions depending on the method for adapting the element lengths. For instance, the residual based method reduces the top element length in that section from its equispaced value (6.0) to 5.807, while the derivative equidistribution method increases the length to 7.526 in response to larger errors in the bottom of the column. The error measure is scale dependent and careful scaling of all variables is necessary. No substantial difference is observed in the element partition when the error associated with fewer state variables is used in Equation 3.16.

The failure of the derivative equidistribution approach may be attributed to the fact that this method is developed to estimate the approximation error for a continuous function. However, the approximated solution in distillation models is defined in a spatially discrete domain with the derivatives of the approximation polynomials having no physical meaning. According to the requirements of the OCFE models the distance between two collocation points cannot be greater than the distance between two stages (equal to unity) in the fictitious stage number domain.

Table 3.2 compares the error sum of squares of the component molar flow rates and temperature for different breakpoint sequences. Using the OCFE solution, the values of the state variables are calculated at the locations of the equilibrium stages by Lagrange interpolation. The calculated values are then compared with those from the tray-by-tray model. The error sum of squares is comparable for all of the different breakpoint partitions. Another error measure is the sum of the absolute values of the material and energy balance residuals when applied to the locations of the equilibrium stages using the OCFE solution and Lagrange interpolation. Residual-based methods result in element partitions that have the smallest sum of balance residuals.

Figures 3.3 and 3.4 show the maximum absolute error in composition and temperature for each element for different breakpoint sequences. The meshes obtained by the residual-based approach have the smallest errors in most of the elements. The partition obtained by the derivative equidistribution strategy has the largest errors mainly because they correspond to an infeasible solution. The largest errors appear at the elements closer to the two end-points of the column.

As a second case, the nonlinear objective function (2.46) is used. As shown in Chapter 2 the optimal solution of the tray-by-tray model has two degrees of freedom. An OCFE model with equispaced elements converges to a totally different optimal solution having only one degree of freedom (Table 3.3). The reason is that a nonkey flow rate (propane flow rate in the second element of the stripping section) is set to zero with a large Lagrange multiplier associated with the active variable bound resulting in an unrealistic composition profile. This is an indication that the given element is too large to provide an accurate representation and its size should be reduced. The residual-based approach determined an element partition that results in an optimal solution that is very close to the tray-by-tray solution. The derivative equidistribution method fails once more in this example and results in an infeasible solution.

Table 3.2 Error sum of squares of composition and temperature and sum of absolute values of balance residuals for different element partitions (meshes) for the DIB.

	Mesh A	Mesh B	Mesh C	Mesh D
	Equispaced	Mass & Energy Residual Equidistribution	Energy Residuals Equidistribution	Derivative Equidistribution
Error sum of squares				
propane (Mmol/d)	$7.274 \cdot 10^{-2}$	$6.576 \cdot 10^{-2}$	$3.943 \cdot 10^{-2}$	$3.211 \cdot 10^{-2}$
i-butane (Mmol/d)	$8.328 \cdot 10^{-2}$	$7.960 \cdot 10^{-2}$	$4.759 \cdot 10^{-2}$	0.447
n-butane (Mmol/d)	$7.484 \cdot 10^{-2}$	0.127	$7.116 \cdot 10^{-2}$	0.376
pentane (Mmol/d)	$8.066 \cdot 10^{-2}$	0.143	$7.544 \cdot 10^{-2}$	$5.767 \cdot 10^{-2}$
Temperature (°C)	0.151	0.172	$9.836 \cdot 10^{-2}$	$7.762 \cdot 10^{-2}$
Sum of absolute values				
material balance residuals	$2.337 \cdot 10^{-3}$	$1.335 \cdot 10^{-6}$	$4.592 \cdot 10^{-6}$	0.206
energy balance residuals	$3.955 \cdot 10^{-5}$	$6.404 \cdot 10^{-6}$	$2.778 \cdot 10^{-5}$	1.591
	<b>Infeasible</b>	<b>Feasible</b>	<b>Feasible</b>	<b>Infeasible</b>

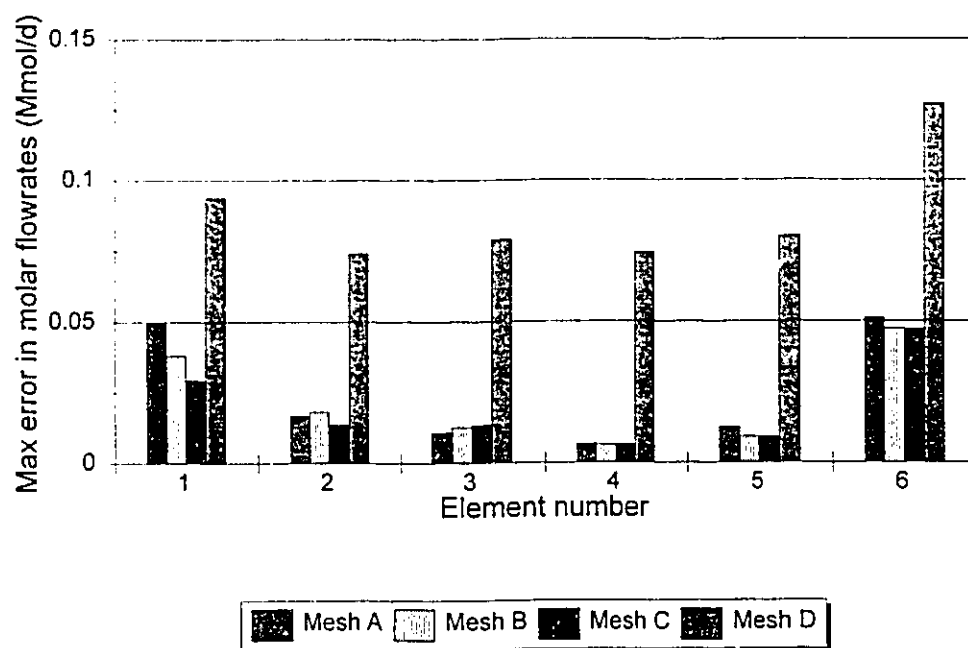


Figure 3.3 Maximum absolute error in liquid composition in every element for different element partitions in the DIB. See Tables 3.1 and 3.2.

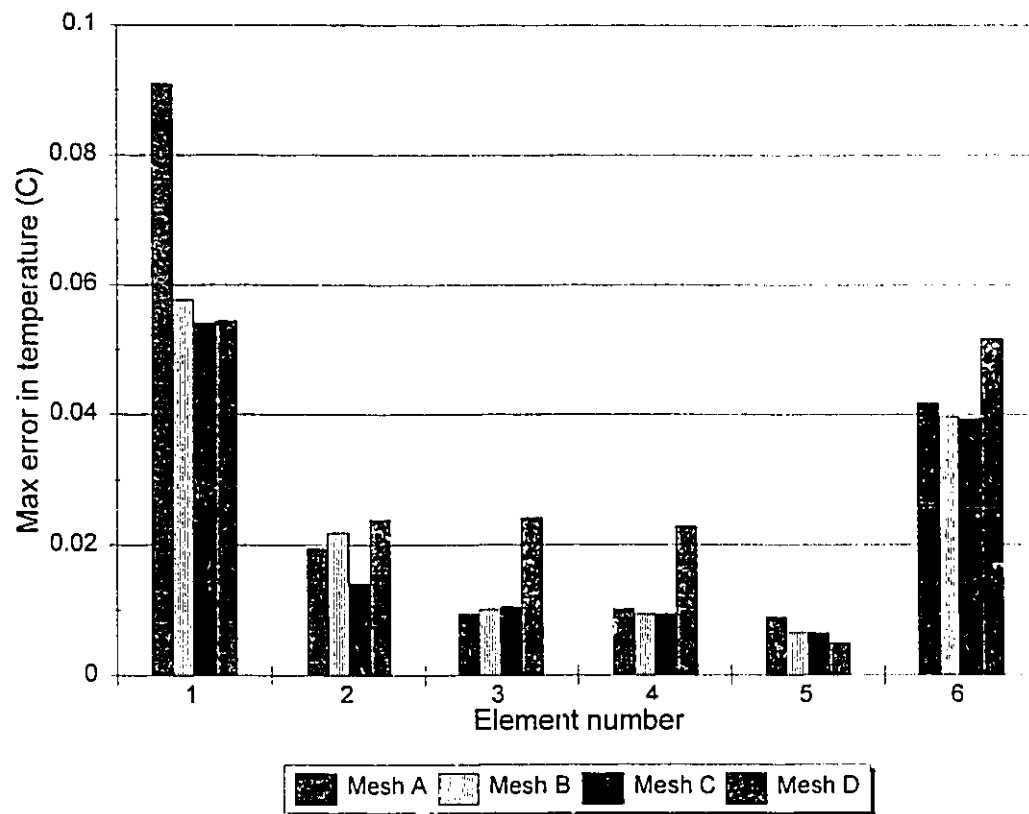


Figure 3.4 Maximum absolute error in temperature in every element for different element partitions in the DIB. See Tables 3.1 and 3.2.

Table 3.3 Optimization results with adaptive breakpoint placement for the DIB  
(nonlinear objective).

		Mesh A	Mesh B	Mesh C
	Tray-by-tray	Equispaced	Mass & Energy Residuals Equidistribution	Derivative Equidistribution
Reflux ratio	10.078	6.273	10.077	5.000
Condenser heat duty (MJ/d)	-810.458	-566.850	-810.387	-411.284
Reboiler heat duty (MJ/d)	831.339	585.839	831.270	469.591
n-butane in overhead (%mol)	2.142	3.033	2.143	9.417
i-butane in bottoms (%mol)	2.720	10.314	2.719	1.492
Objective (\$/d)	4560.32	6716.18	4560.35	8399.49
	<b>Feasible</b>	<b>Feasible</b>	<b>Feasible</b>	<b>Infeasible</b>
RS/6000 355 CPU (sec) Solver MINOS 5.3				
Optimization only	18.7	7.4	9.5	NA
Optimization with Elem. Adaptivity	NA	NA	28.5	NA
Rectifying section element lengths				
1st	-	4.000	3.900	2.787
2nd	-	4.000	3.900	3.354
3rd	-	4.000	4.200	6.853
Stripping section element lengths				
1st	-	6.000	5.611	7.838
2nd	-	6.000	4.969	5.395
3rd	-	6.000	7.420	4.767

This example shows the significance of the selection of a suitable element partition of the domain for the OCFE models. A poor selection of the element breakpoints, as in the equispaced case, may result in a different optimal solution which will cause undesirable consequences in a real-time optimization situation.

### 3.3.2 C<sub>3</sub>-splitter example

Another column example consists of a binary propylene-propane splitter (Hyprotech, 1991). Due to the low relative volatility of the system the separation requires a large number of equilibrium stages. As a result, only small changes occur in the composition and temperature profiles in the rectifying section and most of the variation in the variables is in the stripping section (Figures 2.5 and 2.6). The column specifications are shown in Table 2.1. The OCFE model that is used for this column has 3 elements per column section with 3 collocation points per element.

Both methods for the adaptive breakpoint placement are implemented and the optimization results are shown in Table 3.4. The residual-based approach results in multiple element partitions, depending on the initial variable values, mainly because of the large flat region in the column profiles. Upper and lower bounds are imposed on the element sizes in order to improve the convergence rate to the optimal solution. The breakpoint sequences obtained by the residual based approach converge to an optimal solution that is slightly different from the one given by the full-order model. The derivative equidistribution method converges to an element partition in 5 iterations and the optimal solution is in good agreement with the one obtained by the tray-by-tray model. However, all OCFE models have the same set of active constraints in the final solution. The small discrepancies in the solution obtained by the residual-based approach may be attributed to the greater sensitivity of the optimal solution to the element length partition. The optimizer attempts to adjust the element partition so that the objective

Table 3.4 Optimization results with adaptive breakpoint placement for the C<sub>3</sub>-splitter.

		Mesh A	Mesh B	Mesh C	Mesh D
	Tray-by-tray	Equispaced	Mass & Energy Residuals Equi- distribution	Energy Residuals Equidis- tribution	Derivative Equidis- tribution
Reflux ratio	20.140	20.129	20.082	20.031	20.131
Condenser heat duty (MJ/d)	-243.861	-243.726	-243.147	-242.535	-243.734
Reboiler heat duty (MJ/d)	242.548	242.413	241.834	241.222	242.431
Marginal values					
Overhead prod. (\$/mol fr)	-63.973	-63.894	-63.592	-63.281	-63.904
Bottom prod. (\$/mol fr.)	-10,420	-10,357	-9,915	-9,158	-10,365
Objective (\$/d)	679.66	679.28	677.66	675.95	679.33
VAX 3500 CPU (sec) Solver MINOS 5.3					
Optimization only	326.0	18.0	22.3	22.3	22.6
Optimization with Elem. Adaptivity	NA	NA	72.2	98.2	NA
Rectifying section element lengths					
1st	-	37.667	38.000	38.000	40.734
2nd	-	37.667	40.000	40.000	37.304
3rd	-	37.666	35.000	35.000	34.962
Stripping section element lengths					
1st	-	19.667	20.000	20.779	19.923
2nd	-	19.667	15.000	11.000	19.661
3rd	-	19.666	24.000	27.221	19.416

function reaches a minimum, since a wide range of different element partitions satisfy the equidistribution constraints.

Table 3.4 provides the element partition resulting from different error equidistribution methods. The derivative equidistribution method locates the breakpoints in an almost equispaced fashion in the stripping section, while the residual-error method reduces the size of the middle element.

The error sum of squares, the sum of the material and the energy balance residuals (Table 3.5) and the maximum absolute error in composition and temperature for every element (Figures 3.5 and 3.6) show that the equispaced and the derivative equidistribution OCFE models result in the smallest discrepancies from the tray-by-tray solution. However, the residual equidistribution method has the smallest sum of balance residuals. As expected, the largest error in terms of maximum absolute error in composition and temperature is concentrated in the stripping section of the column.

### 3.3.3 EB/S column example

The last example involves the optimization of a ethylbenzene-styrene column (Table 2.1). The column is modeled with 3 elements for every section with 3 collocation points in every element. The derivative equidistribution method requires 4 elements with 3 collocation points per element in the stripping section.

Optimization results for the styrene column shown in Table 3.6 suggest that OCFE models approach the same optimal solution as the tray-by-tray model with significantly less computational effort. Different error criteria lead to different element partitions but the optimal solution is not very sensitive to the element breakpoint sequence. The composition and temperature profiles at the optimal solution are shown in Figure 3.7.

The envelope residual-based approach encounters some convergence difficulties because there is a wide range of breakpoint sequences for which the residual

Table 3.5 Error sum of squares of composition and temperature and sum of absolute values of balance residuals for different element partitions for the C<sub>3</sub>-splitter.

	Mesh A	Mesh B	Mesh C	Mesh D
	Equispaced	Mass & Energy Residuals Equidistribution	Energy Residuals Equidistribution	Derivative Equidistribution
Error sum of squares				
propylene (Mmol/d)	0.182	0.743	1.375	0.170
propane (Mmol/d)	0.213	0.945	1.751	0.195
Temperature (°C)	$8.277 \cdot 10^{-3}$	0.315	0.581	0.154
Sum of absolute values				
material balance residuals	$1.006 \cdot 10^{-8}$	$6.315 \cdot 10^{-11}$	$5.464 \cdot 10^{-8}$	$1.987 \cdot 10^{-8}$
energy balance residuals	$3.036 \cdot 10^{-8}$	$1.489 \cdot 10^{-10}$	$1.642 \cdot 10^{-7}$	$6.090 \cdot 10^{-8}$

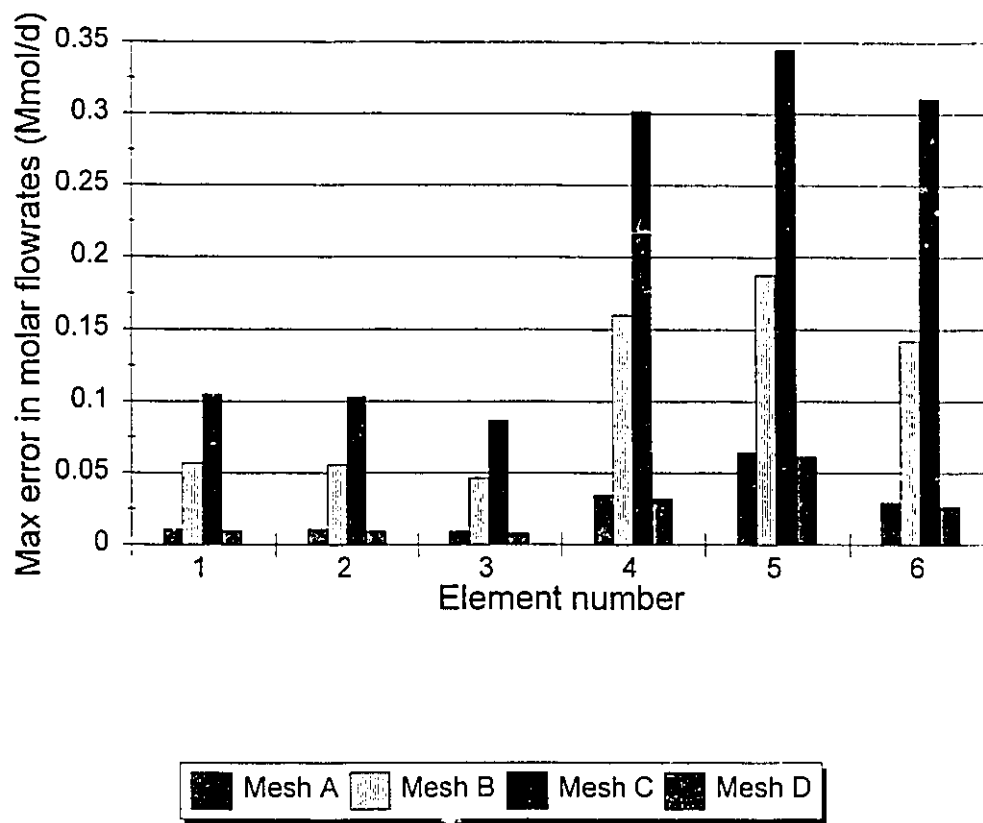


Figure 3.5 Maximum absolute error in liquid composition in every element for different element partitions in the  $C_3$ -splitter. See Tables 3.4 and 3.5.

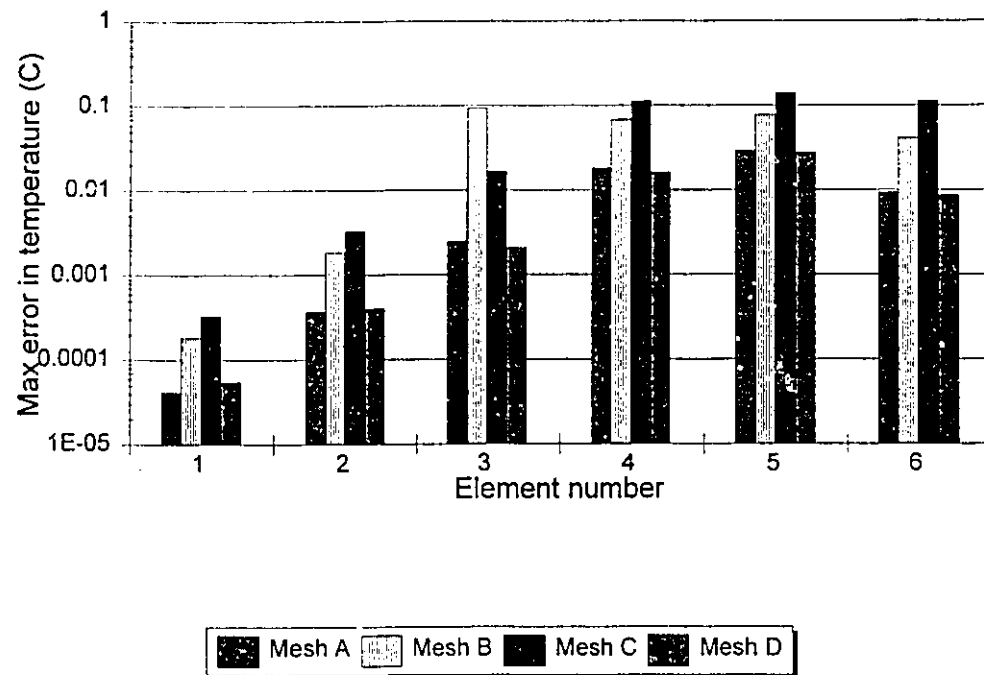


Figure 3.6 Maximum absolute error in temperature in every element for different element partitions in the  $C_3$ -splitter. See Tables 3.4 and 3.5.

Table 3.6 Optimization results with adaptive breakpoint placement for the EB/S column.

		Mesh A	Mesh B	Mesh C	Mesh D
	Tray-by-tray	Equispaced	Mass & Energy Residuals Equidistribution	Energy Residuals Equidis- tribution	Derivative Equidis- tribution
Reflux ratio	9.654	9.654	9.657	9.657	9.654
Condenser heat duty (GJ/d)	-37.635	-37.653	-37.644	-37.643	-37.659
Reboiler heat duty (GJ/d)	43.446	43.441	43.455	43.455	43.448
Marginal value					
Overhead prod. (\$/mol fr)	-961.2	-960.6	-961.7	-961.7	-961.2
Bottom prod. (\$/mol fr.)	-2,965.2	-2,956.3	-2,972.0	-2,970.8	-2,967.9
Objective (\$/d)	119.32	119.32	119.35	119.35	119.34
VAX 3500 CPU (sec)					
Optimization only	186.2	20.3	23.8	23.2	25.3
Optimization with Elem. Adaptivity	NA	NA	111.5	100.4	NA
Rectifying section element lengths					
1st	-	7.667	8.000	8.222	6.279
2nd	-	7.667	9.000	6.251	7.140
3rd	-	7.666	6.000	8.526	9.581
Stripping section element lengths					
1st	-	14.667	18.000	17.723	14.953
2nd	-	14.667	13.000	13.277	9.204
3rd	-	14.667	13.000	13.000	8.854
4th	-	-	-	-	10.989

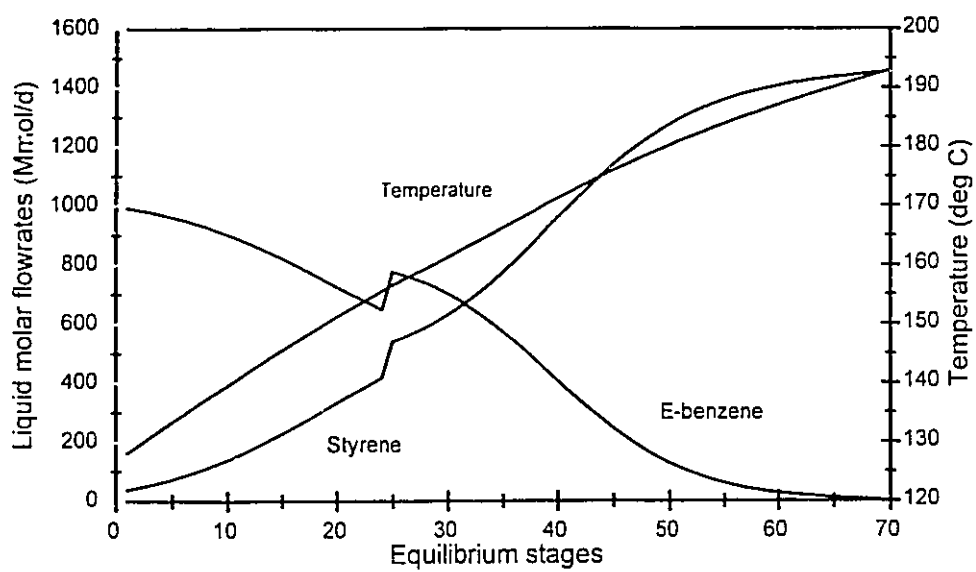


Figure 3.7 Optimal composition and temperature profiles for the EB/S column.

equidistribution constraints are satisfied. In order to improve the efficiency of the optimizer, upper and lower bounds are imposed for the element breakpoints. The derivative equidistribution method requires the addition of another element in the stripping section in order to converge in 11 iterations.

### 3.4 Chapter Summary

OCFE models with adaptive placement of the breakpoints between the finite elements are developed for multicomponent distillation units. The location of the breakpoints is calculated by forcing the approximation error to be equidistributed throughout the column. An estimate of the approximation error is evaluated using the residuals of the material and energy balances around envelopes in the column. The residual-based approach is very efficient in determining an element partition that provides an OCFE model of increased accuracy in steady-state optimization. Consequently, the optimal solution is close to the tray-by-tray optimum but is obtained with less computational effort for the economic optimization. Adaptive breakpoint placement allows OCFE models with smaller total number of collocation points than the corresponding equispaced OCFE model, to converge to the tray-by-tray optimum. Hence a greater model size reduction is achieved. Multiple element length distributions may satisfy the residual equidistribution constraints of problem (P3.1) but they do not affect the optimal solution significantly in the studied cases. However, an arbitrary selection of element breakpoints may lead to an erroneous optimal solution.

The derivative equidistribution method, that uses the derivative of the approximation function as an estimate for the error, is satisfactory for the  $C_3$ -splitter and EB/S column examples but fails in the DIB example.

## 4. Sensitivity Analysis in Chemical Process Optimization

### 4.1 Introduction

A systematic methodology for sensitivity analysis of the optimal solution with respect to deterministic type of changes in the model parameters is presented in this Chapter. The proposed sensitivity analysis method aims to estimate the change in the optimal solution (optimal objective function value and optimal variable values) given an estimated error, but not a statistical distribution for the error, in the model parameters. A very sensitive solution, where large changes in the optimal solution result from small changes in the parameter estimates, will not generally be desirable. This implies that in a real-time optimization framework the setpoints to the controllers calculated by the optimizer may have a large range of possible values even for small model mismatch (Koninckx, 1988). Model parameters that have a relatively large influence on the optimal solution would require a more accurate estimate. Sensitivity information has been utilized in order to develop process models and designs that are robust to model error (Uber and Brill, 1990) and to determine a criterion for the adequacy of a process model for use in real-time optimization (Forbes and Marlin, 1994).

Sensitivity analysis methods can be separated into two main categories: a) local sensitivity methods that calculate the local gradients of the solution with respect to infinitesimal parameter variations and b) global sensitivity methods that determine the behaviour of the solution under simultaneous parameter perturbations of arbitrary magnitude.

Tilden et al. (1981) and Rabitz et al. (1983) survey numerous sensitivity analysis methods that have been developed for the study of the effects of model parameter variations to the solution trajectory of a system of differential equations. The sensitivity analysis of chemical process flowsheets was studied by Volin and Ostrovskiy (1981a, b)

where they presented an adjoint method for a sequential modular process simulation environment. Leis et al. (1987) utilized the structure of the system and the sparsity pattern of the Jacobian matrix in order to improve the efficiency of the sensitivity calculations. Sensitivity analysis methods of nonlinear programs can be grouped as local sensitivity methods (Fiacco, 1983) and nonlinear parametric programming methods (Guddat et al., 1990). The details of both groups of methods will be examined extensively in the following sections.

## 4.2 Local Sensitivity Analysis in Nonlinear Programming

### 4.2.1 Theoretical Background

The main theoretical results for the stability and the local sensitivity of nonlinear programs (NLP) are described in Fiacco (1976, 1983). The results describe the behaviour of the optimal solution subject to parametric variations around a nominal point. The standard form of the nonlinear parametric program is:

$$\begin{aligned} & \text{Min}_x f(x, \varepsilon) \\ \text{s.t. } & h_i(x, \varepsilon) = 0 \quad i \in I \quad I = \{1, \dots, m_1\} \\ & g_j(x, \varepsilon) \leq 0 \quad j \in J \quad J = \{1, \dots, m_2\} \end{aligned} \quad (\text{P4.1})$$

where  $x$  is the  $n$ -dimensional vector of the process (state) variables,  $\varepsilon$  is the  $p$ -dimensional vector of the model parameters,  $h_i(x, \varepsilon)$ ,  $i \in I$ ,  $g_j(x, \varepsilon)$ ,  $j \in J$  are the equality and inequality constraints in the process model respectively and  $f(x, \varepsilon)$  is the objective function for the NLP. The process constraints as well as the objective function depend on the set of model parameters. The Lagrangian of (P4.1) is defined as:

$$L(x, \varepsilon, \lambda, \mu) = f(x, \varepsilon) + \sum_{i \in I} \lambda_i h_i(x, \varepsilon) + \sum_{j \in J} \mu_j g_j(x, \varepsilon) \quad (4.1)$$

where  $\lambda_i, i \in I, \mu_j, j \in J$  are the Lagrange multipliers that correspond to the equality and inequality constraints, respectively.

The necessary and sufficient conditions for point  $x^*$  to be an isolated local minimizer for (P4.1), at a fixed point of the parameter vector  $\varepsilon^*$ , are (Fletcher, 1987):

*First-order Karush-Kuhn-Tucker conditions:*

$$\nabla_x L(x^*, \lambda^*, \mu^*, \varepsilon^*) = \nabla_x f(x^*, \varepsilon^*) + \sum_{i \in I} \lambda_i^* \nabla_x h_i(x^*, \varepsilon^*) + \sum_{j \in J_0} \mu_j^* \nabla_x g_j(x^*, \varepsilon^*) = 0 \quad (\text{a})$$

$$\mu_j^* g_j(x^*, \varepsilon^*) = 0 \quad j \in J \quad (\text{b})$$

$$\mu_j^* > 0 \quad j \in J_0 \quad (\text{c})$$

$$h_i(x^*, \varepsilon^*) = 0 \quad i \in I \quad (\text{d})$$

$$g_j(x^*, \varepsilon^*) \leq 0 \quad j \in J \quad (\text{e})$$

(4.2)

*Second-order conditions:*

$$z^T \nabla_x^2 L(x^*, \lambda^*, \mu^*, \varepsilon^*) z > 0 \quad \text{for all nonzero } z \in \mathbb{R}^n \text{ such that}$$

$$\text{a. } \nabla_x h_i(x^*, \varepsilon^*) z = 0 \quad \text{for all } i \in I \quad (\text{4.3})$$

$$\text{b. } \nabla_x g_j(x^*, \varepsilon^*) z \geq 0 \quad \text{for all } j \in J_0$$

$$\text{c. } \nabla_x g_j(x^*, \varepsilon^*) z = 0 \quad \text{for all } j \in J_+$$

$J_0$  is the index set of the active inequalities at point  $x^*$  defined as  $J_0 = \{j \in J / g_j(x^*, \varepsilon^*) = 0\}$  and  $J_+$  is the index set of the active inequalities that have positive Lagrange multipliers,  $J_+ = \{j \in J / \mu_j^* > 0\}$ . The gradients of the active constraints  $\{\nabla_x h_i, \nabla_x g_{j_0}\}$  at point  $x^*$  are assumed to form a set of linearly independent vectors, known as the *linear independence constraint qualification* (LICQ) which guarantees the uniqueness of the Lagrange multipliers at point  $x^*$ .

The main sensitivity result given by Fiacco is summarized in the following theorem:

---

Theorem (4.1) (Fiacco, 1983)

Given that the functions in (P4.1) are twice continuously differentiable in  $x$  and once continuous differentiable in  $\varepsilon$ , in a neighbourhood of  $(x^*, \varepsilon^*)$ , the second-order sufficiency conditions hold at point  $(x^*, \varepsilon^*)$  with  $\lambda^*, \mu^*$  being the corresponding Lagrange multipliers, LICQ holds at  $(x^*, \varepsilon^*)$  and that  $\mu_j^* > 0$  for all  $i \in J_0$ , then

1.  $x^*$  is a local isolated minimization point of (P4.1) for  $\varepsilon^*$  and the Lagrange multipliers  $\lambda^*, \mu^*$  are unique.
2. for  $\varepsilon$  in a neighbourhood of  $\varepsilon^*$ , there exist a unique once continuously differentiable function  $\varphi(\varepsilon) = [x(\varepsilon), \lambda(\varepsilon), \mu(\varepsilon)]$  that satisfy the second-order conditions for a local minimizer with  $\varphi(\varepsilon^*) = (x^*, \lambda^*, \mu^*)$  and hence  $x(\varepsilon)$  is a locally unique minimization point of (P4.1) for  $\varepsilon$ , with Lagrange multipliers  $\lambda(\varepsilon)$  and  $\mu(\varepsilon)$ .
3. the set of active constraints for  $\varepsilon$  near  $\varepsilon^*$  remains unchanged, the strict complementarity condition (4.2c) and the LICQ hold at  $x(\varepsilon^*)$ .

---

The local sensitivity theorem is a direct result of the implicit function theorem and guarantees the existence of points that satisfy the optimality conditions for infinitesimal parameter variations around the nominal point.

Differentiation of the first-order optimality conditions (4.1a, b, d) with respect to the parameter vector  $\varepsilon$  yields an explicit expression for the variation of the process variables and the Lagrange multipliers as a function of the model parameters  $\varepsilon$ . In order to reduce the dimensionality of the system only the active constraints at point  $(x^*, \varepsilon^*)$  are considered. The inactive inequalities can then be eliminated since the corresponding

Lagrange multipliers are equal to zero. The result is summarized by the following linear system

$$\begin{bmatrix} \nabla_x^2 L & \nabla_x h^T & \nabla_x g_{J_0}^T \\ \nabla_x h & 0 & 0 \\ \nabla_x g_{J_0} & 0 & 0 \end{bmatrix} \begin{bmatrix} \nabla_\varepsilon x^* \\ \nabla_\varepsilon \lambda^* \\ \nabla_\varepsilon \mu^* \end{bmatrix} = - \begin{bmatrix} \nabla_{x\varepsilon}^2 L \\ \nabla_\varepsilon h \\ \nabla_\varepsilon g_{J_0} \end{bmatrix} \quad (4.4)$$

where  $\nabla_\varepsilon x^*$ ,  $\nabla_\varepsilon \lambda^*$  and  $\nabla_\varepsilon \mu^*$  are the local gradients, or local sensitivities, of the process variables and the Lagrange multipliers with respect to  $\varepsilon$ , at point  $(x^*, \varepsilon^*)$ . The gradients of the Lagrangian and the active constraints of system (4.4) are evaluated at point  $(x^*, \varepsilon^*)$ .

The calculation of the sensitivity of the objective function value to the model parameters is based on the observation that at an optimal solution the value of the Lagrangian (4.1) equals the objective function value. Hence the local gradient of the objective function,  $\nabla_\varepsilon f^*$ , at point  $(x^*, \varepsilon^*)$ , equals the gradient of the Lagrangian with respect to the parameters at that point. Differentiation of the Lagrangian with respect to the parameter vector, using the chain rule, will result in an expression for the gradient of the objective function for problem (P4.1) (Fiacco, 1983):

$$\nabla_\varepsilon f^* = \nabla_\varepsilon f + \lambda^T \nabla_\varepsilon h + \mu^T \nabla_\varepsilon g \quad (4.5)$$

where  $\nabla_\varepsilon f$ ,  $\nabla_\varepsilon h$  and  $\nabla_\varepsilon g$  are the partial derivatives of the objective function and the constraints with respect to  $\varepsilon$ . In the case where the parametric NLP has the form

$$\begin{aligned} & \text{Min}_x f(x) \\ \text{s.t. } & h_i(x) = \varepsilon_i \quad i \in I \quad I = \{1, \dots, m_1\} \\ & g_j(x) \leq \varepsilon_{m_1+j} \quad j \in J \quad J = \{1, \dots, m_2\} \end{aligned} \quad (P4.2)$$

where the parameters appear only in the right-hand-side terms of the constraints, then the sensitivity of the objective function is equal to the Lagrange multipliers of the corresponding active constraints.

A large amount of research has been carried out on local sensitivity analysis of NLPs that does not have any direct link to engineering applications. However, the work by Shapiro (1985) examined the second-order local gradients of the optimal variable values and the optimal objective function value and the asymptotic behaviour of the optimal solution of problem (P4.1) given the asymptotic probability distribution of the model parameters.

#### 4.2.2 Computational Considerations

The solution of the linear system (4.4) involves the evaluation of the Hessian of the Lagrangian which is a matrix of dimension  $n \times n$ . Hessian evaluation is a computationally intensive procedure since it requires the evaluation of the gradients of the nonlinear constraints  $n$  times. Fiacco and Armacost (1979) and Fiacco (1983) proposed different methodologies for the solution of the linear system (4.4). They attempted to utilize the information available after the termination of the optimization algorithm in order to accelerate the sensitivity computations. Ganesh and Biegler (1987) presented a procedure based on a block elimination and a finite difference scheme that accelerate the computational time for the solution of system (4.4).

In most chemical engineering applications, the Hessian matrix is sparse since only a few variables are involved in every constraint. Powell and Toint (1979) and Coleman and More (1984) developed efficient procedures for the evaluation of the symmetric Hessian matrix, given the sparsity structure of the matrix, with the least number of evaluations of the Jacobian.

A technique that is commonly used for large-scale systems (Gill et al., 1981) is to examine the reduced space of the optimization problem. The technique is based on the

partition of the process variables into dependent and independent variables. Even though the total number of variables may be large, the number of independent variables, or the degrees of freedom, is relatively small in most applications. This observation is utilized both in the solution of large-scale optimization problems and in the solution of system (4.4) for the estimation of the sensitivities.

Following Wolbert et al. (1994), a matrix  $\mathbf{Z}$  of dimension  $n \times (n-m)$  is constructed, where  $m$  is the total number of active constraints at the given optimal point. The columns of  $\mathbf{Z}$  form a basis for the null space of the gradients of active constraints,  $\nabla_x \mathbf{H} = \begin{bmatrix} \nabla_x h \\ \nabla_x g_{j_0} \end{bmatrix}$ , i.e.  $\nabla_x \mathbf{H} \mathbf{Z} = 0$ . Matrix  $\mathbf{Y}$  is a  $n \times m$  matrix, whose columns span the range space of  $\nabla_x \mathbf{H}^T$ , which implies that  $\mathbf{Y}^T \mathbf{Z} = 0$ . Matrices  $\mathbf{Z}$  and  $\mathbf{Y}$  can be obtained by performing a QR decomposition of  $\nabla_x \mathbf{H}^T$ .

$$\nabla_x \mathbf{H}^T = [\mathbf{Y} \quad \mathbf{Z}] \begin{bmatrix} \mathbf{R} \\ 0 \end{bmatrix} \quad (4.6)$$

where  $\mathbf{R}$  is an upper triangular matrix of dimension  $m \times m$ .

Decomposing the sensitivities of the variables into their null and range space components, system (4.4) takes the following form:

$$\begin{bmatrix} \mathbf{Z}^T \nabla_x^2 L \mathbf{Z} & \mathbf{Z}^T \nabla_x^2 L \mathbf{Y} & 0 \\ \mathbf{Y}^T \nabla_x^2 L \mathbf{Z} & \mathbf{Y}^T \nabla_x^2 L \mathbf{Y} & \mathbf{Y}^T \nabla_x \mathbf{H}^T \\ 0 & \nabla_x \mathbf{H} \mathbf{Y} & 0 \end{bmatrix} \begin{bmatrix} \nabla_\epsilon x_z^* \\ \nabla_\epsilon x_y^* \\ \nabla_\epsilon \Lambda^* \end{bmatrix} = - \begin{bmatrix} \mathbf{Z}^T \nabla_{x\epsilon}^2 L \\ \mathbf{Y}^T \nabla_{x\epsilon}^2 L \\ \nabla_\epsilon \mathbf{H} \end{bmatrix} \quad (4.7)$$

where  $\nabla_\epsilon x_z^*$  and  $\nabla_\epsilon x_y^*$  are the sensitivities in the null and range space, respectively and

$\nabla_\epsilon \Lambda^* = \begin{bmatrix} \nabla_\epsilon \lambda^* \\ \nabla_\epsilon \mu^* \end{bmatrix}$ . The sensitivity of the process variables is then given as the sum of the

parametric variation in the two subspaces as:

$$\nabla_{\epsilon} x^* = \mathbf{Z} \nabla_{\epsilon} x_z^* + \mathbf{Y} \nabla_{\epsilon} x_y^* \quad (4.8)$$

The individual terms in (4.8) are given by the following relations:

$$\nabla_{\epsilon} x_y^* = -(\nabla_x \mathbf{H} \mathbf{Y})^{-1} \nabla_{\epsilon} \mathbf{H} \quad (4.9a)$$

$$\nabla_{\epsilon} x_z^* = -(\mathbf{Z}^T \nabla_x^2 L \mathbf{Z})^{-1} (\mathbf{Z}^T \nabla_{x\epsilon}^2 L + \mathbf{Z}^T \nabla_x^2 L \mathbf{Y} \nabla_{\epsilon} x_y^*) \quad (4.9b)$$

The first-order derivatives of the process constraints and the objective function are calculated analytically. Large-scale optimization algorithms calculate an approximation to the reduced-Hessian of the system,  $\mathbf{Z}^T \nabla_x^2 L \mathbf{Z}$ , which is updated at every iteration using a quasi-Newton approximation (Fletcher, 1987), and is available after an optimal solution is reached. Ganesh and Biegler (1987) showed that even though the approximation of the Hessian may be adequate for the purpose of optimization, its use may lead to erroneous sensitivity results, because the range space components of the approximate Hessian are not correct, even upon convergence. The second order information is determined by numerical perturbation of the gradient of the Lagrangian along the orthonormal directions of the columns of  $\mathbf{Z}$  (Gill et al. pg. 160, 1981). Such a procedure results in only  $n-m$  evaluations of the constraint gradients, while a full Hessian evaluation would require  $n$  evaluations. The estimation of the reduced Hessian is performed as follows:

$$(\mathbf{e}_i^T \mathbf{Z}^T \nabla_x^2 L) = \frac{\nabla_x L(x + \gamma \mathbf{e}_i^T \mathbf{Z}) - \nabla_x L(x)}{\gamma} \quad i = 1, \dots, n-m \quad (4.10a)$$

where  $\gamma$  is the perturbation size in the finite difference scheme and  $\mathbf{e}_i$  are vectors of the canonical basis of  $\mathfrak{R}^{n-m}$ . Similarly  $\nabla_{x\epsilon}^2 L$  is calculated by:

$$\left(\mathbf{e}_i^T \mathbf{Z}^T \nabla_{x\epsilon}^2 L\right) = \frac{\nabla_{\epsilon} L(x + \gamma \mathbf{e}_i^T \mathbf{Z}) - \nabla_{\epsilon} L(x)}{\gamma} \quad i = 1, \dots, n - m \quad (4.10b)$$

Matrices  $\mathbf{Z}^T \nabla_x^2 L \mathbf{Z}$  and  $\mathbf{Z}^T \nabla_x^2 L \mathbf{Y}$  in Equation (4.9b) can then be easily calculated by multiplying with the proper matrix. Calculation of the sensitivities of the Lagrange multipliers,  $\nabla_{\epsilon} \Lambda^*$ , requires the computation of matrix  $\mathbf{Y}^T \nabla_x^2 L \mathbf{Y}$ , which leads to  $m$  additional evaluations of the constraint gradients.

### 4.2.3 Parameter Rank Ordering in Sensitivity Analysis

The number of parameters in a process model is usually large as is the number of process variables, thus the dimensionality of the sensitivity matrix,  $\mathbf{X} = \nabla_{\epsilon} x$ , may become very large. Inspection of all the individual entries of the sensitivity matrix to determine the effects of the model parameters to the optimal solution may become a very tedious procedure. In addition, combined parameter variations may increase the severity of change in the optimal solution. The determination of those parameter directions that can cause a large change in the optimal solution may not be possible by a simple inspection of the sensitivity matrix. The relative importance of each parameter may be estimated by calculating its contribution to the major directions in the parameter space that cause the largest variability in the variable space.

Usually the process measurements do not contain sufficient information in order to update the values of all the model parameters in the parameter estimation stage of the real-time optimization loop. Rank ordering the significance of each parameter in affecting the optimal solution will determine those parameters for which a more accurate estimate of their actual value is required.

The direction in the multi-dimensional parameter space that causes the largest change, in the 2-norm sense, in the set of state variables, that consist the solution of a set of ordinary differential equations, is defined by the eigenvector that corresponds to the

largest in magnitude eigenvalue of  $\mathbf{X}^T\mathbf{X}$  (Hearne, 1985). A similar conclusion may be derived for the optimal solution of (P4.1) as shown in Appendix C. By analogy, the eigenvector that corresponds to the eigenvalue second largest in magnitude eigenvalue, defines the direction in the parameter space, that causes the second largest variability in the optimal variable values and so on for subsequent eigenvectors. A similar procedure is used in the analysis of measurement data in order to investigate the correlation and variability structure between different measured variables (Wold et al., 1987).

The evaluation of the eigenvectors of  $\mathbf{X}^T\mathbf{X}$  can be easily performed using a singular value decomposition of the  $\mathbf{X}$  matrix. A singular value decomposition (SVD) of the  $\mathbf{X}$  ( $n \times p$ ) matrix results in two unitary matrices  $\mathbf{U}$  ( $n \times n$ ) and  $\mathbf{V}$  ( $p \times p$ ) and a matrix  $\mathbf{D}$  ( $n \times p$ ) with the singular values of  $\mathbf{X}$  in the diagonal and the remaining elements equal to zero. Given that matrix  $\mathbf{X}$  is of rank  $r$ , then  $\mathbf{D} = \text{diag}\{\sigma_1, \dots, \sigma_r, 0, \dots, 0\}$  with the singular values arranged in descending order. The columns of  $\mathbf{U}$  and  $\mathbf{V}$  are the normalized eigenvectors of  $\mathbf{X}\mathbf{X}^T$  and  $\mathbf{X}^T\mathbf{X}$  respectively. The first  $r$  eigenvectors correspond to the nonzero singular values. The decomposition has the form:

$$\mathbf{X} = \mathbf{U}\mathbf{D}\mathbf{V}^T \quad (4.11)$$

The normalized eigenvector  $\mathbf{v}_1$  that corresponds to the largest singular value can be interpreted as the direction in the parameter space in which the largest variability in the variable space exists. The individual entries in  $\mathbf{v}_1$  indicate the weight of each parameter in this direction. The corresponding  $\sigma_1\mathbf{u}_1$  can be interpreted as the coordinates of the variables in the axis defined by  $\mathbf{v}_1$  (Bratchell, 1989). Relatively large entries indicate that the particular optimal variable value varies significantly for simultaneous parameter perturbations along the given direction. The eigenvector  $\mathbf{v}_2$  that corresponds to the second largest singular value determines the direction in which the second largest variability in the entries of matrix  $\mathbf{X}$  exists and so forth.

A plot of the entries of the first two  $\sigma_i \mathbf{u}_i$  may reveal possible similarities in the behaviour of groups of optimal variable values for perturbations along the corresponding directions  $\mathbf{v}_i$ . For example, variables with entries in the first two  $\sigma_i \mathbf{u}_i$  close to zero are almost unaffected by changes along the corresponding eigenvector directions. Since the eigenvectors  $\mathbf{v}_i$  are orthogonal to each other, every direction explains a unique mode of variation in the variable space.

The sensitivities of the optimal objective function value (4.5) may be included as an additional row in the sensitivity matrix, so that the changes in the objective function are taken into account in the calculation of the major directions of variation. The augmented sensitivity matrix  $\mathbf{X}_A$ , of dimension  $(n+1 \times p)$ , has the following form:

$$\mathbf{X}_A = \begin{bmatrix} \mathbf{X} \\ \nabla_{\varepsilon} f^* \end{bmatrix} \quad (4.12)$$

Singular value decomposition is scale dependent; therefore careful scaling of the variable and parameter values is necessary for meaningful results. It is generally recommended that the variables and parameters be scaled before optimization. Another way to scale the entries of the sensitivity matrix is as follows (Tilden et al., 1981):

$$\frac{\partial x_i}{\partial \varepsilon_j} \frac{\varepsilon_j^*}{x_i^*} \quad i = 1, \dots, n \quad j = 1, \dots, p \quad (4.13)$$

The scaling uses the relative change of the process variables with respect to relative changes in the model parameters and may inflate the sensitivities of variables that have very small values at the optimum (e.g. composition of nonkey components in distillation columns).

In addition to this scaling procedure, engineering knowledge may be used so that the sensitivities of the most important variables, such as output variables, setpoints and product specifications, have a greater impact on the scaled sensitivity matrix. The

procedure can be viewed as discarding the least important variables from consideration in a SVD of the sensitivity matrix.

## 4.3 Nonlinear Parametric Programming

### 4.3.1 Literature Review

In Section 4.2 the main local sensitivity results for the parametric NLP (P4.1) were presented. The method provides the local gradients of the optimal solution with respect to the model parameters that are only valid for infinitesimal variations around the reference optimal point  $(x^*, \varepsilon^*)$ . However, a local sensitivity approach cannot provide any information about either the behaviour of the optimal solution to parameter variations of finite magnitude or the interaction effects from simultaneous changes in the parameter estimates. Finite parameter variations may cause the active constraint set to vary while optimality is maintained. Ganesh and Biegler (1987) and Wolbert et al. (1994) formulated a quadratic program for every parameter in order to determine possible changes in the active set for individual parameter changes.

Nonlinear parametric programming (NLPP) attempts to determine the behaviour and characteristics of the optimal solution for multiple simultaneous parameter value changes of arbitrary magnitude. The philosophy of NLPP is to trace the parameterized first-order optimality conditions for varying parameter estimates.

Kojima and Hirabayashi (1984) developed the theoretical background for the study of the continuous deformation of the optimal solution due to perturbations of one free parameter. The behaviour of the optimal solution path around singular points was studied by Jongen et al. (1986). Jongen and coworkers classified the singular points into five types and investigated the characteristics of the stationary points near the singular points. Tiahr and Poore (1986) analyzed the behaviour of the optimal path near a singular point using bifurcation theory. Jongen and Weber (1990) summarized the main

theoretical results of the parametric analysis of nonlinear programs. Guddat et al. (1990) and Lundberg and Poore (1993) proposed efficient pathfollowing algorithms that are able to handle singularities in the solution path of the NLPP using continuation methods. Hirabayashi et al. (1993) studied the structure of the KKT solution set with two free parameters.

Continuation methods (Rheinboldt, 1986) may be used for the pathfollowing of the optimal solution set. These methods have been used extensively for the solution of nonlinear equation sets by parameterizing the original system in terms of an artificial parameter, namely the *homotopy* parameter. At the initial value (usually equal to zero) of the homotopy parameter the system takes a simplified form whose solution is known. Then the solution path is traced until a target value for the homotopy parameter (typically equal to unity) is reached, where the parameterized system takes its original form. This point represents a solution to the original equation system. Seider et al. (1991) reviewed procedures based on homotopy-continuation methods that are used for the solution of NLP problems. A number of applications of the homotopy-continuation methods are available including: process design (Wayburn and Seader, 1987), heterogeneous azeotropic distillation (Kovach and Seider, 1987), continuous reactors (Seader et al., 1990), countercurrent separation processes (Salgovic et al., 1981), optimization (Kernez et al., 1990), multi-objective optimization (Rakowska et al., 1991) and global optimization (Sun and Seider, 1991).

#### **4.3.2 Parameterized Karush-Kuhn-Tucker Set**

The parametric NLP (P4.1) with the first-order Karush-Kuhn-Tucker conditions for a local minimizer (4.2) is considered. The stationary conditions (4.2a, b), combined with the feasibility relations (4.2d), form a set of parameterized nonlinear equations.

$$F_p(x, \lambda, \mu, \varepsilon) = \begin{bmatrix} \nabla_x^T L(x, \lambda, \mu, \varepsilon) \\ h_i(x, \varepsilon) \\ \mu_j g_j(x, \varepsilon) \end{bmatrix} = 0 \quad i \in I, j \in J \quad (4.14)$$

A point  $z_0 = (x_0, \lambda_0, \mu_0)$ , that is a solution of (4.14) for a fixed set of parameter values  $\varepsilon_0$ , is called a generalized critical point. When (4.14), LICQ and (4.2c) are satisfied then the point is called a *critical* and KKT point. A point  $z$  which satisfies (4.14) and has a nonsingular Jacobian of  $F_p$  with respect to  $z$  ( $\nabla_z F_p$ ) is called a *regular* point of  $F_p$ . If  $\nabla_z F_p$  is singular, then the point is called a *singular* point of  $F_p$ .

An active set index strategy that eliminates inactive inequality constraints is used to reduce the size of the system. Since the Lagrange multipliers that correspond to the inactive inequalities are equal to zero then the equation set takes the following form:

$$F(x, \lambda, \mu, \varepsilon) = \begin{bmatrix} \nabla_x^T L(x, \lambda, \mu, \varepsilon) \\ h_i(x, \varepsilon) \\ g_j(x, \varepsilon) \end{bmatrix} = 0 \quad i \in I, j \in J_0 \quad (4.15)$$

The number of equations is equal to  $(n+m_1+m_3)$ , where  $m_3 \leq m_2$  is the number of the active inequality constraints, including  $(n+m_1+m_3+p)$  unknowns. Thus the system has  $p$  degrees of freedom, equal to the dimension of the parameter space.

Since the parameter variations are of finite magnitude, the active constraint set,  $J_0$ , may be altered. The changes in the active set can be easily detected by the changes in the sign of the Lagrange multipliers,  $\mu$ . The set of KKT points for (P4.1) for different values of the parameter vector is obtained by solving (4.15) with the addition of the strict complementarity condition (4.2c), that requires positive Lagrange multipliers which correspond to the active inequality constraints.

An alternative formulation would be to include the strict complementarity relations (Equation 4.2b) into the equation system as in (4.14). Such a formulation is

used for the solution of NLP using continuation for fixed parameter values (Seider et al., 1991). However, the strict complementarity relations are not differentiable when there is a change in the active set. Mangasarian (1976) proposed an equivalent formulation to the strict complementarity problem, that consists of a set of continuous once differentiable nonlinear equations. Such a formulation includes all the inequalities in the equation set, but only a few of them may be active at any given optimal point.

The implicit function theorem (Fiacco, 1983) states that the solution of (4.15),  $(z_0, \varepsilon_0)$ , can be parameterized by means of the parameter  $\varepsilon$  in a neighbourhood of  $(z_0, \varepsilon_0)$  provided that the Jacobian of system (4.15) with respect to  $z$  is nonsingular at the point  $(z_0, \varepsilon_0)$ . More specifically there exists a once continuously differentiable function  $\varphi(\varepsilon)$  such that  $F(\varphi(\varepsilon), \varepsilon) = 0$  for all  $\varepsilon$  near  $\varepsilon_0$  and  $\varphi(\varepsilon_0) = z_0$ . The solution set of system (4.15) is a  $p$ -dimensional manifold.

The entire analysis of the behaviour of the optimal solution path as the parameter vector  $\varepsilon$  varies is based upon the following theorem.

---

Theorem 4.2 (McCormick, 1978; Tiahn and Poore, 1986)

Let  $(z_0, \varepsilon_0)$  be a solution of (4.14) and assume that  $f, h, g$  are twice continuously differentiable in a neighbourhood of  $(x_0, \varepsilon_0)$ . Then a necessary and sufficient condition that  $\nabla_x F$  is nonsingular is that each of the following three conditions hold:

C1. Strict complementarity condition (SC);  $\mu_{0j} > 0$  for all  $j \in J_0$ .

C2.  $\{\nabla_x h_i(x_0, \varepsilon_0), i \in I \cup \nabla_x g_j(x_0, \varepsilon_0), j \in J_0\}$  is a set of linearly independent vectors.

C3. The reduced Hessian of the Lagrangian  $Z^T \nabla_x^2 L Z$  is nonsingular at  $(z_0, \varepsilon_0)$ , where  $Z$  is a matrix whose columns form a basis for the null space of the gradients of the active constraints.

---

A direct corollary of Theorem 4.1 is that the characteristic features of a stationary point may change only when a singular point is crossed in the optimal path trajectory

(Guddat et al., 1990). Kojima and Hirabayashi (1984) and Guddat et al. (1990) introduced indices in order to fully describe the characteristics of a stationary point (local minimum, local maximum, saddle point). Guddat et al. (1990) used the linear index (linear co-index) as the number of the negative (positive) Lagrange multipliers  $\mu_j$  that correspond to the active inequality constraints ( $j \in J_0$ ) and the quadratic index (quadratic co-index) which denotes the number of the negative (positive) eigenvalues of the reduced Hessian of the Lagrangian. For instance, a local minimum has the linear and quadratic indices equal to zero (all  $\mu_j$  are positive and the reduced Hessian is positive definite) and a local maximum has the linear and quadratic co-indices equal to zero. The local characteristics of the optimal solution can be fully determined by these four indices and they are invariant under parameter variations until a singular point is reached. The type of singularity in the optimal solution path, which depends upon the violated conditions stated in Theorem 4.1, defines the way that the indices will be altered (Jongen et al., 1986; Poore and Tiaht, 1990). A detailed analysis of the solution curve around singular points is presented in Section 4.5.

### 4.3.3 Simple Variable Bounds

Variable bounds are the simplest form of inequality constraints. Since variable bounds are present in most practical applications in chemical engineering they will be examined separately. The standard form of an NLP with equality constraints and simple variable bounds will be:

$$\begin{aligned}
 & \text{Min}_x \quad f(x, \varepsilon) \\
 & \text{s.t.} \quad h_i(x, \varepsilon) = 0 \quad i \in I, \quad I = \{1, \dots, m\} \\
 & \quad \quad x_k - x_k^u(\varepsilon) \leq 0 \quad k \in K, \quad K = \{1, \dots, n\} \\
 & \quad \quad x_k^l(\varepsilon) - x_k \leq 0
 \end{aligned} \tag{P4.3}$$

where  $x^u(\varepsilon)$  and  $x^l(\varepsilon)$  are the parameter dependent vectors of the upper and lower bounds of the state variables.

The first order stationary condition is then expressed by the relation:

$$\nabla_x L = \nabla_x f(x, \varepsilon) + \sum_{i \in I} \lambda_i \nabla_x h_i(x, \varepsilon) + \sum_{j \in U_0} (\kappa_u)_j - \sum_{j \in L_0} (\kappa_l)_j \quad (4.16)$$

where  $\kappa_u$  and  $\kappa_l$  are the Lagrange multipliers that correspond to the active variables' upper and lower bounds respectively.  $\kappa_u$  and  $\kappa_l$  obey the SC condition and they are equal to zero if the corresponding bounds are not active.  $U_0$  and  $L_0$  are the index sets that contain the indices of those variables which are at their upper or lower bound, respectively. The set of nonlinear equations that is used, after eliminating the inactive constraints, for the pathfollowing of the KKT points of (P4.3) is given by:

$$\begin{bmatrix} \nabla_x^T L(x, \lambda, \kappa_u, \kappa_l, \varepsilon) \\ h_i(x, \varepsilon) \\ x_j - x_j^u(\varepsilon) \\ x_k'(\varepsilon) - x_k \end{bmatrix} = 0 \quad i \in I, j \in U_0, k \in L_0 \quad (4.17)$$

#### 4.3.4 Multiple Parameter Perturbations

The parameter vector  $\varepsilon$  may contain a large number of physical parameters of the process model. The sensitivity of the optimal solution to multiple parameter perturbations usually differs from the sum of the effects of individual parameter variations due to nonlinearities in the process model. Most numerical continuation algorithms can handle problems with only one degree of freedom; i.e. one independently varying parameter. However, the equation system can be modified to accommodate the requirement for multiple parameter changes.

A new scalar parameter ( $\zeta$ ) is introduced which varies between zero and any defined target value (positive or negative). Additional equations are introduced that express the functional relation between the changes of the physical model parameters and the variation of the free parameter  $\zeta$ . Then the value of each model parameter at a certain point in the optimal solution curve satisfies the following relation:

$$\Delta\varepsilon(\varepsilon, \zeta)_i = \frac{(\varepsilon_{new} - \varepsilon_{ref})_i}{(\varepsilon_{ref})_i} - \theta_i, \zeta = 0 \quad i = 1, \dots, p \quad (4.18)$$

where  $\varepsilon_{ref}$  and  $\varepsilon_{new}$  are the reference (initial) and the current parameter values vectors, respectively. The first term corresponds to the relative change of the  $i$ -th parameter at the current point. The relative rate of change is chosen for scaling purposes. The vector  $\theta$  represents a direction of perturbation in the parameter space which can be selected, by utilizing engineering knowledge about the most frequently occurring variations, by using the correlation between the parameters, or by using the major directions of variation for the reference point as calculated in Section 4.2.3. The error associated with the estimate of every parameter may be incorporated in the assignment of the value for  $\theta$ . The product  $\theta_i \zeta$  at the final point, where  $\zeta$  is at its target value, reflects the final relative change of the  $i$ -th parameter from the initial point. Therefore, large values of  $\theta_i$  denote large final relative change for the  $i$ -th parameter. Figure 4.1 shows the relation between the relative changes for two simultaneously varying parameter values. The slope of the line is equal to the ratio of the individual entries of vector  $\theta$  for the given parameters.

Equation (4.18) implies that the parameter values vary linearly between an initial and final value as a function of the perturbation size  $\zeta$ . However, relation (4.18) may take the form of any nonlinear function that describes the change in the parameters (e.g. catalyst deactivation curve with time, kinetic parameter changes with temperature) as follows:

$$\Delta\varepsilon(\varepsilon, \zeta)_i = \left( \frac{\varepsilon_{new} - \varepsilon_{ref}}{\varepsilon_{ref}} \right)_i - d(\zeta) \quad i = 1, \dots, p \quad (4.19)$$

where  $d(\zeta)$  is a nonlinear function that relates the perturbation size with the relative change of the  $i$ -th parameter. An example of a nonlinear behaviour for two model parameters is shown in Figure 4.1.

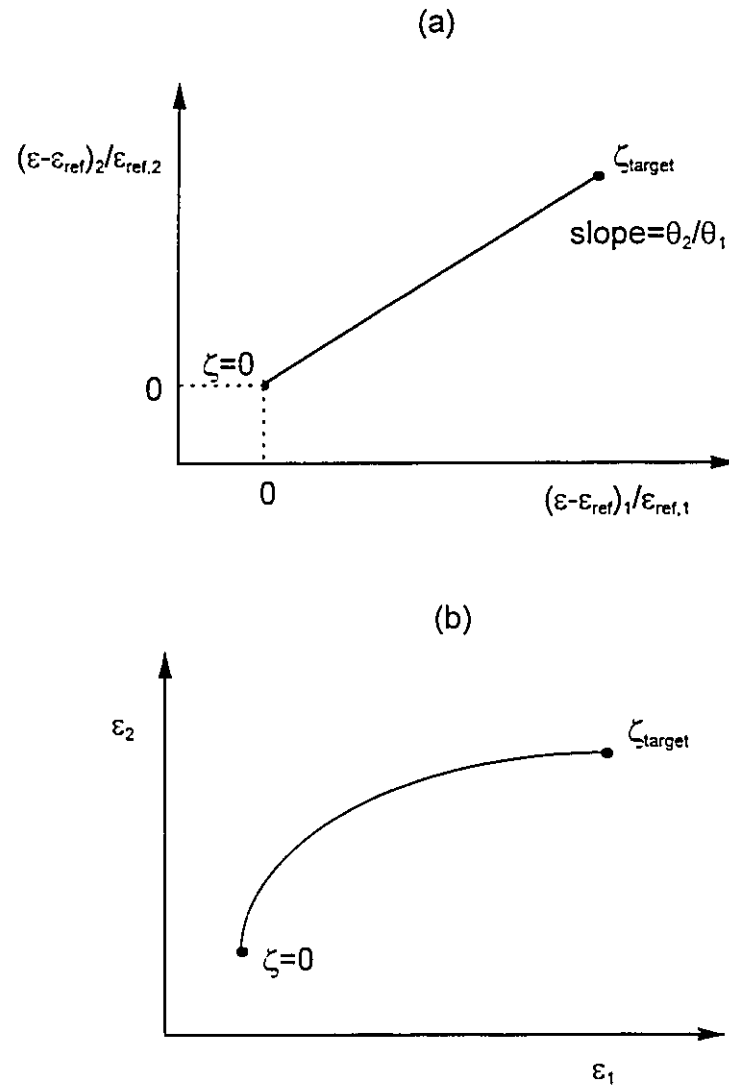


Figure 4.1 Relation between the relative changes of parameters for multiple model parameter variations, (a) linear relation (Equation 4.18), (b) nonlinear relation (Equation 4.19).

#### 4.4 Continuation Methods for the Pathfollowing of the Optimal Solution

The solution of the parameterized equation set (4.15), with the addition of the relations that govern the variation of the physical parameters of the process model, (4.18)-(4.19), is obtained by continuation methods. Allgower and Georg (1990) reviewed a large variety of algorithms for continuation methods which can be classified into two types: predictor-corrector methods (Rheinboldt, 1986) and piecewise linear methods that approximate the solution curve by a sequence of linear segments. Conjugate gradient methods are used to handle pathfollowing of large-scale systems. Continuation methods are able to trace the solution path past bifurcation points, where two solution branches intersect, but however, in the usual form cannot determine all the solution branches. Morgan (1987) proposed a numerical procedure to examine the behaviour of the solution set of polynomials under parametric variations. An algorithm for calculating the zeros of a homotopy map, HOMPACK, was proposed by Watson et al. (1987).

##### 4.4.1 Description of PITCON

In the present work, a predictor-corrector continuation method is used as implemented in PITCON (Rheinboldt and Burkardt, 1983 a, b). PITCON allows one parameter to be varied independently.

The equation system that is to be solved, allows multiple model parameters to vary as a function of the independent parameter  $\zeta$  and has the form

$$F_{MP}(x, \lambda, \mu, \varepsilon, \zeta) = \begin{bmatrix} \nabla_x^T L(x, \lambda, \mu, \varepsilon) \\ h_i(x, \varepsilon) \\ g_j(x, \varepsilon) \\ \Delta \varepsilon_k(\varepsilon, \zeta) \end{bmatrix} = 0 \quad i \in I, j \in J_0, k = 1, \dots, p \quad (4.20)$$

System  $F_{MP}$  has  $n+m_1+m_3+p$  equations with  $n+m_1+m_3+p+1$  unknowns.

The predictor stage evaluates the tangent vector to the optimal solution path by solving the following augmented system of equations which has a unique solution:

$$\begin{bmatrix} \nabla_w F_{MP} \\ \mathbf{e}_i^T \end{bmatrix} v = \mathbf{e}_i, \quad T(w) = \sigma_T \frac{v}{\|v\|_2} \quad (4.21)$$

The symbol  $w$  denotes the set  $(x, \lambda, \mu, \varepsilon, \zeta)$ ,  $t$  the total number of the unknowns,  $T(w)$  is the tangent vector at the solution curve at point  $w$  and  $\mathbf{e}_i$  is the  $i$ -th vector of the canonical basis of  $\mathfrak{R}^t$ . The term  $\sigma_T$  defines the sign of the tangent vector and is determined by

$$\sigma_T = \text{sign}(v^T \mathbf{e}_i) \text{sign} \left( \det \begin{bmatrix} \nabla_w F_{MP} \\ \mathbf{e}_i^T \end{bmatrix} \right) \quad (4.22)$$

The term  $\sigma_T$  is used to prevent taking the wrong direction when two components of the solution's manifold cross each other (Rheinboldt, 1986). Such a situation may occur when there is a bifurcation point in the optimal solution manifold. Variable  $i$  acts as the continuation variable in the augmented system (4.21). In order to provide faster convergence to the next point in PITCON the variable that has the largest component in the tangent vector is chosen as the continuation variable for the next predictor step. However, when a variable value approaches a limit point where its tangent entry changes sign then PITCON selects this variable as the continuation variable. The user also has option to defines the continuation variable.

The predictor step continues by taking a step along the tangent direction with a step-length ( $\delta_k$ ) to determine the prediction point,  $\hat{w}^{k+1}$ .

$$\hat{w}^{k+1} = w^k + \delta_k T(w^k) \quad (4.23)$$

The size of the step-length is calculated by estimating the distance of the prediction point to the solution manifold. Starting from the prediction point  $\hat{w}^{k+1}$  a corrector action is taken by solving the following system.

$$\hat{F}_{MP} = \left[ \begin{array}{c} F_{MP} \\ (\mathbf{e}_i)^T (w - \hat{w}^{k+1}) \end{array} \right] = 0 \quad (4.24)$$

The solution to this system is obtained by an iterative method based on the modified Newton's formula:

$$u^{j+1} = u^j - \nabla_z F_{MP}(\hat{w}^{k+1})^{-1} F_{MP}(u^j) \quad j = 0, 1, \dots \quad u^0 = \hat{w}^{k+1} \quad (4.25)$$

where the Jacobian of  $F_{MP}$  is evaluated numerically at the beginning of every continuation step. In large-scale mildly nonlinear problems, the Jacobian may be updated only at the continuation steps that the corrector stage fails to converge. Then the predictor and the corrector stages are repeated using the updated Jacobian. A schematic of the predictor-corrector procedure is shown in Figure 4.2.

The solution of the linear system (4.21) is performed by block elimination using the LINPACK package (Dongarra et al., 1979). The system of equations that appears during the course of the continuation method includes the Jacobian of  $F_{MP}$ , (4.21), which has the following form:

$$\nabla_w F_{MP} = \left[ \begin{array}{cccc} \nabla_x^2 L & \nabla_x \mathbf{H}^T & \nabla_{x,c}^2 L & 0 \\ \nabla_x \mathbf{H} & 0 & \nabla_c \mathbf{H}^T & 0 \\ 0 & 0 & \mathbf{I} & \varepsilon_{ref} \end{array} \right] \quad (4.26)$$

where  $\mathbf{I}$  is the  $(p \times p)$  identity matrix and  $\varepsilon_{ref}$  is a  $(p \times 1)$  column vector made up of the reference values of the parameters. The matrix in (4.26) contains the full Hessian of the Lagrangian function which is evaluated numerically; a procedure that requires great computational effort. Null space decomposition techniques can be incorporated in order to invert or factor the Hessian of the Lagrangian for large-scale systems. In cases where the reduced Hessian becomes singular as the optimal solution path reaches a singular point specialized factorizations for indefinite matrices should be used (Lundberg and Poore, 1993). However, in the present work, the full Hessian of the Lagrangian as it

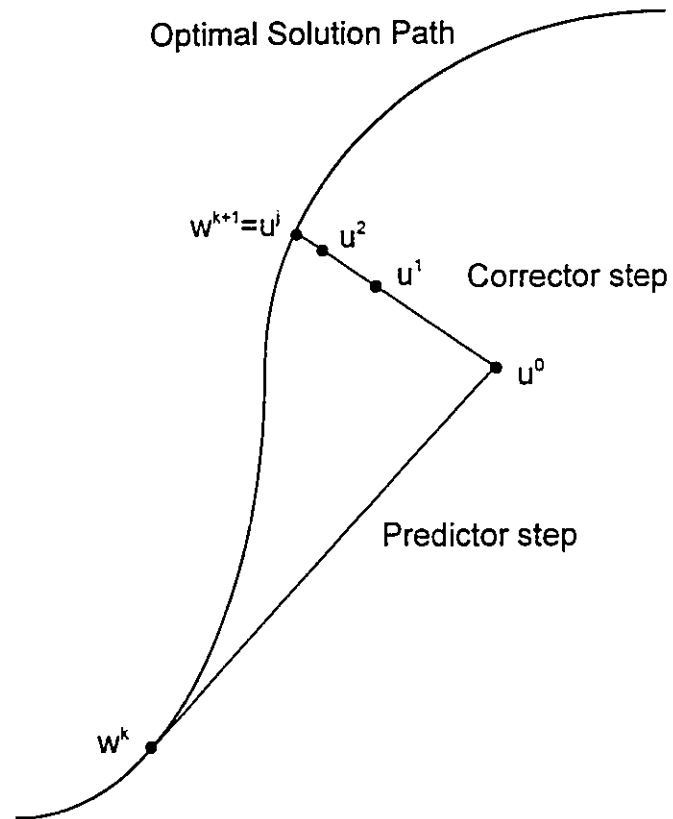


Figure 4.2 Schematic of the predictor-corrector procedure in PITCON

appears in Equation (4.26) is evaluated numerically at the continuation points that the corrector step fails to converge.

## 4.5 Singularities in the Optimal Solution Path

In this section the discussion involves the detection and study of the behaviour of the optimal solution path around singular points. Without any loss of generality, the analysis is performed for system  $F$ , equation (4.15), and it is assumed that  $\epsilon$  is one-dimensional. The extension of the results to system  $F_{MP}$ , with  $\epsilon$  being the free parameter, is straightforward.

### 4.5.1 Violation of the Strict Complementarity (SC) Condition

In this case, the SC condition is violated at point  $(z_0, \lambda_0)$  causing  $\nabla_z F$  to become singular. It is assumed that both linear independence and second-order optimality conditions hold. There are two distinct cases for violation of the SC condition. The first case involves the situation where one multiplier which corresponds to an active inequality crosses zero (SC violation). The second case occurs when one of the inactive inequality becomes infeasible (feasibility loss). In the first case, the corresponding inequality is removed from the set of binding constraints and the pathfollowing continues on the modified set of equations. In the latter case, the opposite action is taken by adding the constraint that became infeasible to the equation set.

Jongen et al. (1986), Guddat et al. (1990) and Tiaht and Poore (1990) studied extensively the behaviour of the characteristic indices around a singular point where SC is violated. Tiaht and Poore (1990) allowed multiple violations of the SC condition at the same point and showed that under certain conditions there exists at least one branch of solutions for  $\epsilon < \epsilon_0$  and one for  $\epsilon > \epsilon_0$  that is comprised of local minimizers.

The check of the satisfaction of the strict complementarity and the feasibility conditions is carried out at the end of every continuation step before advancing to the

calculation of the new point. The algorithm detects changes in the active constraint set and then modifies the nonlinear set of equations involved in the continuation stage accordingly.

Strict complementarity at the  $k$ -th continuation point is expressed in the form  $\mu_j > 0$  for all  $j \in J_0^k$  and feasibility is expressed as  $g_j(x, \varepsilon) < 0$  for all  $j \in J \setminus J_0^k$ . At every point in the optimal solution path (continuation point) the Lagrange multipliers of the active inequality constraints are examined if they are positive and the inactive inequalities are checked for feasibility. If both tests are successful, then the active set index remains the same and the algorithm proceeds for the computation of the next continuation point.

Let  $j_q \in J$  be an index, for which either the strict complementarity or feasibility conditions are violated and the active set index must be modified. In the case where  $j_q \in J_0^k$  ( $\mu_{j_q} \leq 0$ ; SC violation) then the corresponding constraint is removed from the basis and the active set index for the next continuation point will be  $J_0^{k+1} = J_0^k \setminus \{j_q\}$ ; the previous active set index without  $j_q$ . In the case where  $j_q \in J \setminus J_0^k$  ( $g_{j_q}(x, \varepsilon) > 0$ ; infeasible point) then the corresponding constraint is added to the equation set and the active set index used in the calculation of the next point will be  $J_0^{k+1} = J_0^k \cup \{j_q\}$ .

A simple example illustrates the behaviour of the optimal solution path around a singular point of this kind. The parametric NLP is taken from Fiacco (1983).

$$\begin{aligned} \text{Min} \quad & f(x_1, x_2) = (x_1 - \varepsilon)^2 + (x_2 + 1)^2 \\ \text{s.t.} \quad & g_1(x_1, x_2) = x_1 - x_2 \leq 0 \\ & g_2(x_1, x_2) = -x_1 - x_2 \leq 0 \end{aligned} \tag{P4.4}$$

The objective function is the minimization of the distance from the feasible region to point  $(\varepsilon, -1)$ . For  $\varepsilon = -2.0$  (point A in Figure 4.3), constraint  $g_2$  is active. At point B where

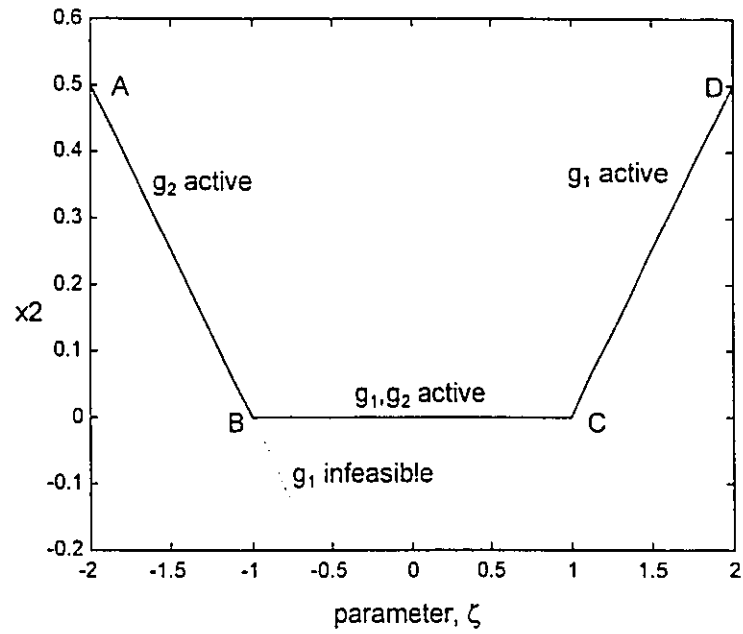


Figure 4.3 Optimal solution path for problem (P4.4).

$\varepsilon = -1.0$ , constraint  $g_1$  becomes active and the active set is properly modified. Continuation on the dashed curve causes  $g_1$  to be infeasible. In the segment B-C both inequality constraints are active at the solution with both  $x_1$  and  $x_2$  equal to zero. At point C ( $\varepsilon = 1.0$ ) the Lagrange multiplier that corresponds to  $g_2$  becomes equal to zero which results in a SC violation case. The constraint is removed from the active set and the optimal solution path is traced until point D ( $\varepsilon = 2.0$ ).

The tests for the violation of SC and feasibility are performed after the evaluation of every continuation point on all the inequality constraints. In the case of SC loss, for only one active inequality, the continuation direction is reversed temporarily to calculate the point where the respective Lagrange multiplier is equal to zero. Then the corresponding constraint is removed from the equation set and the continuation algorithm proceeds on the modified set. This procedure is followed in order to calculate as close as possible the point in the optimal solution path at which the SC condition is violated. In the case of feasibility loss, the inequality constraint that becomes infeasible is included in the equation set with its associated Lagrange multiplier. The continuation algorithm performs a corrector step to adjust the point so that the Lagrange multiplier of the added constraint is equal to zero. Then, the continuation procedure begins on the altered set of equations.

Usually the calculated continuation point at which multiple violations are detected, does not coincide with the exact point where the active set has to be altered. In a situation, where multiple violations of SC and feasibility are encountered, the last continuation step is performed again using a smaller step-length in the predictor stage. The objective is to identify the set of constraints that first violated the conditions. If there are any constraints that violate any of the SC or feasibility conditions at the exact same point in the optimal solution curve then the corresponding constraints are removed or added into the equation system (4.15) accordingly. The continuation method proceeds on

the modified equation set. There may be bifurcation points where different active set selections result in branches consisting of local minimizers for problem (P4.1).

#### 4.5.2 Linear Independence Loss

Let  $(z_0, \varepsilon_0)$  be a solution of  $F=0$  and the rank of  $\nabla_x \mathbf{H}$  at that point is equal to  $(m-1)$ , where  $m=m_1+m_3$ , while around this point the rank of  $\nabla_x \mathbf{H}$  is  $m$ . Then  $\nabla_x F$  is singular at  $(z_0, \varepsilon_0)$ . It is also assumed that the rank of  $\nabla_{(x,\varepsilon)} F$  is equal to  $n+m$ , which implies that  $\nabla_x F$  does not belong to the range space of  $\nabla_x F$ . It can then be shown that the optimal solution path of (P4.1) exhibits a quadratic turning point (Jongen et al., 1986; Keller, 1987).

Lagrange multipliers, that correspond to the constraints that cause the rank deficiency, tend to infinity when the LI condition is violated. As a consequence, the optimal solution path cannot be calculated using the described continuation method near the singular point. Guddat et al. (1990) suggested that a constraint should be imposed on the magnitude of the multipliers in order to approach the singularity. The stationary conditions are thus modified by introducing a multiplier for the gradient of the objective function.

$$\nabla_x L(x, \lambda, \mu, \varepsilon) = \nu \nabla_x f(x, \varepsilon) + \sum_{i \in I} \lambda_i \nabla_x h_i(x, \varepsilon) + \sum_{j \in J_0} \mu_j \nabla_x g_j(x, \varepsilon) = 0 \quad (4.27)$$

At KKT points,  $\nu$  is assumed to be equal to 1. The imposed constraint has the following form:

$$\nu^2 + \lambda^T \lambda + \mu^T \mu = \beta^2 \quad (4.28)$$

The term  $\beta^2$  is a constant scalar that is equal to the sum of squares of the Lagrange multipliers including  $\nu^2$  at the point where  $\nu$  is to be introduced. In a case of LI loss, as some of the Lagrange multipliers approach infinity the value of  $\nu$  decreases, so that Equation (4.28) is satisfied, and eventually for some parameter values will cross zero.

The system, for which the solution set is to be calculated, thus becomes:

$$F_{\mu}(x, \nu, \lambda, \mu, \varepsilon) = \begin{bmatrix} \nabla_x L(x, \nu, \lambda, \mu, \varepsilon) \\ h_i(x, \varepsilon) \\ g_j(x, \varepsilon) \\ \nu^2 + \lambda^T \lambda + \mu^T \mu - \beta^2 \end{bmatrix} = 0 \quad i \in I, j \in J_0 \quad (4.29)$$

The solution of system (4.29) is equivalent to the solution set of (4.15) with the Lagrange multipliers given by  $\hat{\lambda}_i = \frac{\lambda_i}{\nu}$   $i \in I$ , and  $\hat{\mu}_j = \frac{\mu_j}{\nu}$   $j \in J_0$  (Guddat et al., 1990). As  $\nu$  approaches zero, then  $\hat{\lambda}$  and  $\hat{\mu} \rightarrow \infty$ .

If  $\nu=0$ , then the matrix  $\nabla_x H$  is rank deficient (the Lagrangian becomes  $\sum_{i \in I} \lambda_i \nabla_x h_i + \sum_{j \in J_0} \mu_j \nabla_x g_j = 0$  with nonzero multipliers). If  $\nabla_x H$  is full rank then  $\nu \neq 0$  (because if  $\nu=0$ , then  $\nabla_x H$  would be singular). This simple test is used to detect the LI violation in the optimal solution path.  $\nu$  is normalized by dividing the stationary conditions by the numerical value of  $\nu$ , after it crosses zero and takes negative values. The variables  $x$  will remain unchanged but all the Lagrange multipliers will reverse sign and so will the eigenvalues of the reduced Hessian (Tiarht and Poore, 1990). A direct consequence will be that a path consisting of local minimizers will become a path consisting of local maximizers when a singular point due to LI loss is crossed. The branch of the local maximizers can be traced numerically using continuation but in the opposite direction. In practical applications LI loss may occur when the varying parameters appear in the set of nonlinear constraints.

An example of LI loss is given by considering the following simple minimization problem (Guddat et al., 1990).

$$\begin{aligned} \text{Min} \quad & f(x) = (x-3)^2 \\ \text{s.t.} \quad & h(x) = \frac{1}{3}x^3 - \frac{1}{2}x^2 - 2x + 5 - 3.5\varepsilon \end{aligned} \quad (P4.5)$$

$\varepsilon$  varies from 1 to 0. For  $\varepsilon = 1$  the minimum is at  $x=3$  (Figure 4.4). The Lagrange multiplier for  $h$  approaches infinity at  $x=2$  and  $\varepsilon=0.48$ , since the gradient of the constraint becomes zero at that point. This is a case that the LI condition does not hold, the optimal solution path exhibits a quadratic turning point and the local minima branch turns to a local maxima branch. At  $x=-1$  the gradient of the constraint becomes zero again and there is another turning point in the solution path with the characteristics of the optimal solution changing to those of a local minimum. Figure 4.4 shows the case of multiple minima for the same parameter value which are calculated by the continuation method.

### 4.5.3 Special Case of LI Loss

In many practical applications of NLPP, where inequality constraints are involved, it is possible that the total number of active constraints (equality + binding inequality constraints) exceeds the number of process variables. Such a situation may occur when the solution of a fully determined system hits another process constraint due to variation in the model parameters. More specifically, the case where  $m_1+m_3=n+1$  will be examined based on the work by Jongen et al. (1986) and Guddat et al. (1990).

The analysis requires that the number of active constraints is  $n+1$  with  $m_1 \geq 2$  and  $\nabla_{\varepsilon} \mathbf{H}$  does not belong to the range space of  $\nabla_x \mathbf{H}$ , which implies that  $\left\{ \nabla_{(x,\varepsilon)} h_i, i \in I, \nabla_{(x,\varepsilon)} g_j, j \in J_0 \right\}$  is a set of linearly independent vectors ( $\nabla_{(x,\varepsilon)} \mathbf{H}$  has rank equal to  $n+1$ ). Since LI does not hold, then the set of Lagrange multipliers do not have a unique set of values.

A weaker constraint qualification than the LICQ was introduced by Mangasarian and Fromowitz (1967) denoted as *Mangasarian-Fromowitz constraint qualification* (MFCQ) which requires that

- i.  $\nabla_x h_i, i \in I$  is a set of linearly independent vectors and
- ii.  $\exists \mathbf{w} \in \mathcal{R}^n$  such that  $\nabla_x h_i \mathbf{w} = 0, i \in I, \nabla_x g_j \mathbf{w} < 0, j \in J_0$

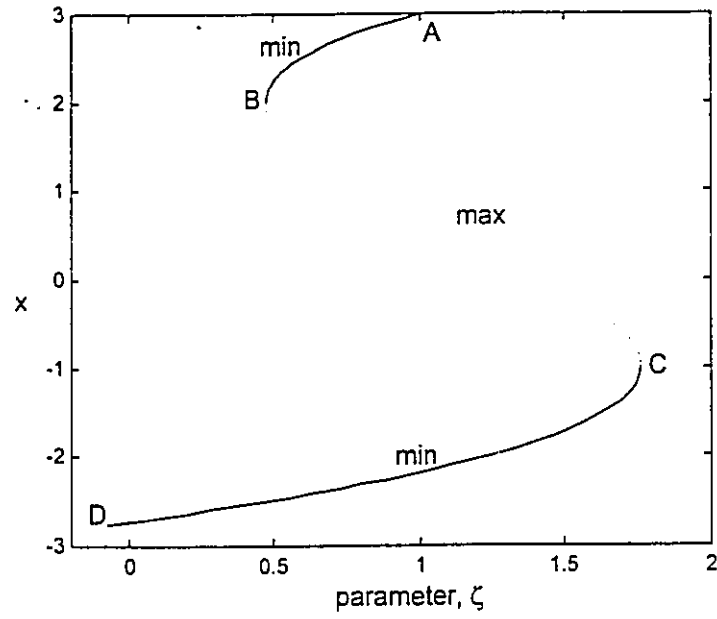


Figure 4.4 Optimal solution path for problem (P4.5).

The Lagrange multipliers are bounded and unique up to a common multiple when the MFCQ is satisfied (Kojima and Hirabayashi, 1984).

The system of equations (4.15) is feasible only at one point  $(z_0, \varepsilon_0)$ , when  $n+1$  active constraints are present. In the neighborhood of the point  $(z_0, \varepsilon_0)$ , the stationary conditions are satisfied if one of the active inequalities is removed. The set of generalized critical points will consist of the union of solution branches that correspond to the different problems in which one active inequality has been removed from the basis (Figure 4.5). However, not all of these branches will necessarily be comprised of local minimizers. Jongen et al. (1986) proved that if MFCQ hold at point  $(z_0, \varepsilon_0)$  then there is a solution branch consisting of local minimizers for  $\varepsilon > \varepsilon_0$ . In contrast, if MFCQ does not hold at  $(z_0, \varepsilon_0)$  then this point is a boundary point for the KKT set. This implies that there are no local minimizers for  $\varepsilon > \varepsilon_0$ , thus defining the boundary of the feasible region for problem (P4.1). The boundary point will determine the range of parameter changes for which the system has no feasible solution. In such a situation the Lagrange multipliers of the active inequalities will tend to infinity since MFCQ does not hold at  $(z_0, \varepsilon_0)$ .

The tracking of the optimal solution around a point where a special case of LI loss occurs is handled similarly to the procedure described in Section 4.5.2. When the number of active constraints exceed the number of state variables then the modified system (4.29) is used. If at point  $(z_0, \varepsilon_0)$  MFCQ holds, then a SC violation occurs, which is detected by the sign of the Lagrange multipliers, and the corresponding constraint is removed from the active set. The pathfollowing switches back to the original system (4.15). If however, MFCQ does not hold, then a LI loss case occurs at point  $(z_0, \varepsilon_0)$  and the same procedure described in Section 4.5.2 is followed.

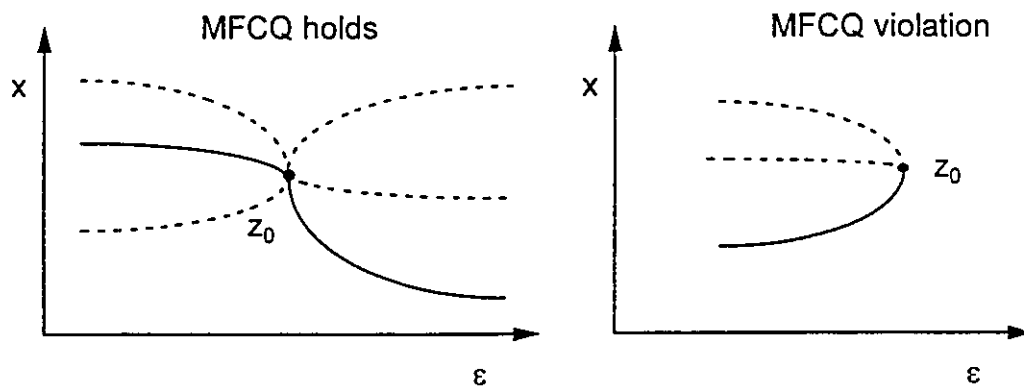


Figure 4.5 Optimal solution path around a point where a special case of LI occurs (solid curves: local minimizers, dashed curves: generalized critical points).

#### 4.5.4 Singularity of the reduced Hessian

In this section it is assumed that SC and LI conditions hold and exactly one eigenvalue of the reduced Hessian of the Lagrangian vanishes at point  $(z_0, \varepsilon_0)$ . The optimal solution path exhibits a quadratic turning point at  $(z_0, \varepsilon_0)$  with one eigenvalue of the reduced Hessian changing sign (Jongen et al., 1987). Therefore a solution branch that consists of a sequence of local minimizers will turn to a branch of saddle points. This is equivalent to loss of the second-order optimality condition. The active set remains unchanged and so does the linear index when the optimal solution path crosses such a point. Consider the following one-dimensional problem:

$$\text{Min } f(x) = \frac{1}{5}x^5 - \frac{1}{4}\varepsilon x^4 - \frac{1}{3}\varepsilon(x-2)^3 \quad (\text{P4.6})$$

Figure 4.6 shows the optimal solution path as the parameter  $\varepsilon$  varies from 1 to 0. At  $\varepsilon=0$  the second derivative of the objective becomes zero and the second-order optimality condition is violated. The optimal solution has a turning point and the second derivative changes sign and becomes negative, which results in a branch consisting of local maxima.

The presence of this kind of singular point can be detected by inspection of the sign of the eigenvalues of the reduced Hessian  $(\mathbf{Z}^T \nabla_x^2 L \mathbf{Z})$ . Matrix  $\mathbf{Z}$  has size  $n \times (n - m_1 - m_2)$  and columns that form a basis for the null space of  $\nabla_x \mathbf{H}$ .  $\mathbf{Z}$  can be easily calculated by performing a QR decomposition of  $\nabla_x \mathbf{H}$  (Equation 4.6). However, a QR decomposition is computationally intensive for a large-scale problem. An alternative way to evaluate  $\mathbf{Z}$  would be to find a matrix that is orthogonal to  $\nabla_x \mathbf{H}$ . If

$\mathbf{Z} = \begin{bmatrix} I \\ -(\nabla_{x_{dep}} \mathbf{H})^{-1} (\nabla_{x_{ind}} \mathbf{H}) \end{bmatrix}$ , the requirement that  $\nabla_x \mathbf{H} \mathbf{Z} = 0$  is satisfied for the partition of the variables into independent ( $x_{ind}$ ) and dependent ( $x_{dep}$ ).

The reduced Hessian is then calculated numerically by perturbing simultaneously all the variables along the directions defined by the columns of  $\mathbf{Z}$  (Equation 4.10). In

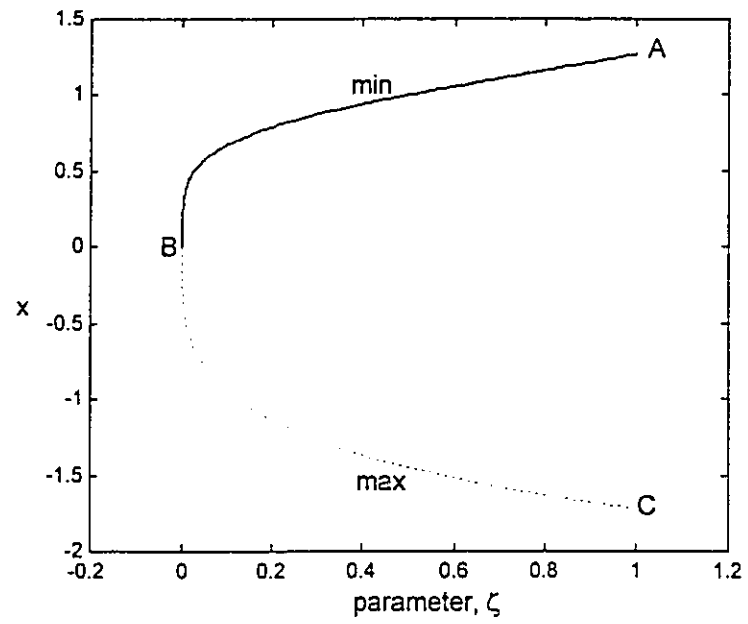


Figure 4.6 Optimal solution path for problem (P4.6).

cases where the number of active constraints is equal to the number of variables (no degrees of freedom) the reduced Hessian cannot be defined since the null space of  $\nabla_x \mathbf{H}$  has dimension equal to zero.

PITCON has the ability to trace solution curves that exhibit turning points (limit points) in some of the variables. A limit point for a variable occurs when the tangent element that corresponds to this variable changes sign. A simple inspection of the tangent elements in the predictor stage will detect such a situation. The eigenvalues of the reduced Hessian do not change unless a singular point is encountered. Hence the reduced Hessian will be examined for positive definiteness only when the optimal solution path crosses singular points. Such situations can be detected when there is a limit point in the perturbation parameter  $\zeta$  and when any of the SC or LI conditions is violated.

#### 4.6 Algorithm for the Pathfollowing of the Optimal Solution

The tests for the detection of singularities in the optimal solution and the actions that are taken in order to trace the optimal solution around singular points are embedded into the pathfollowing algorithm. The block diagram of the algorithm is shown in Figure 4.7. The conditions and tests that are given correspond to that for a local minimizer, but can be easily transformed to accommodate a local maximizer.

A series of tests is performed for a given continuation point  $(x^k, \lambda^k, \mu^k, \epsilon^k, \zeta^k)$  and an active index set  $J_0^k$ . First variations in the active set are examined. If either the SC or the feasibility conditions are violated, then the active set that will be used in the next continuation point is modified by proper addition or removal of constraints. The next step involves the LI condition. If LI loss is suspected, because some of the Lagrange multipliers tend to infinity for very small changes in the perturbation size  $\zeta$ , or an overconstrained case is encountered (where special case of LI loss occurs), then the

pathfollowing switches to the equation system  $F_{Li}$  (4.29). When the continuation is performed in system  $F_{Li}$ , then the value of  $\nu$  is also checked. If  $\nu$  crosses zero then the LI does not hold at the point where  $\nu$  is equal to zero. Then the procedure continues on the set of local maximizers of the original system by normalizing the value of  $\nu$ . The second-order optimality conditions are checked whenever a turning point is detected or a singular point due to violation of another condition is crossed by examining the signs of the eigenvalues of the reduced Hessian. Upon violation of the second-order optimality condition (at least one eigenvalue becomes negative), PITCON performs a limit point calculation. The final test examines if the perturbation size has reached the specified target point. If not, then the pathfollowing continues on the equation set taking in account the modifications dictated by any violating conditions.

The proposed algorithm can handle multiple violations of the conditions stated in Theorem 4.2. The procedure described in Section 4.5.1 for multiple active set changes is extended to accommodate simultaneous violations of more than one test in the algorithm flowsheet shown in Figure 4.7. The last continuation step is repeated with smaller predictor step-length. A sufficiently small step-length will permit the determination of the condition(s) that cause failure and the exact point where these violations occurred. Proper action, as described in Sections 4.5.1-4.5.4, will be then taken depending on the violated condition.

## 4.7 Chapter Summary

The relative significance of each parameter and combination of parameter variations in affecting the optimal solution is determined by evaluation of the eigenvectors of matrix  $\mathbf{X}^T\mathbf{X}$ . The eigenvector that corresponds to the largest eigenvalue of  $\mathbf{X}^T\mathbf{X}$  can be interpreted as the direction in the parameter space that causes the largest changes in the optimal variable values around the reference point. The contribution of

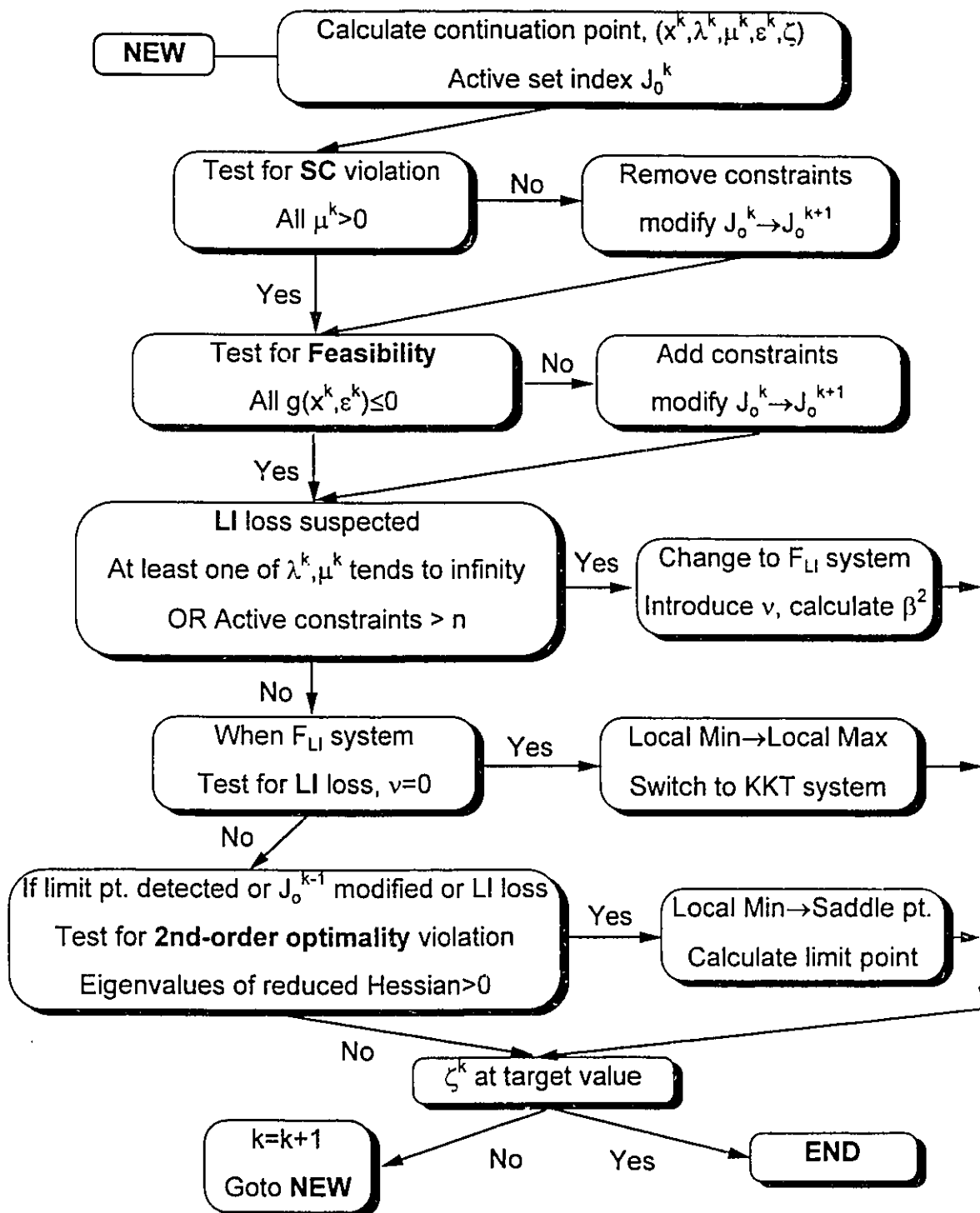


Figure 4.7 Flowsheet of the optimal solution pathfollowing algorithm.

each model parameter to the major directions of perturbation defines the parameter's relative importance in the optimal solution at the given optimal point.

A sensitivity analysis methodology of nonlinear programs that allows multiple simultaneous changes along specified directions of arbitrary magnitude in the model parameters is proposed. The method is based on the pathfollowing of the solution of the parameterized first-order optimality conditions for different parameter values. The parameter variations studied are of deterministic type. The solution method that is used is based on a predictor-corrector type of continuation technique as implemented in PITCON.

The methodology can handle variations in the active constraint set by examining the sign of the Lagrange multipliers of the binding inequalities and the inactive constraints for feasibility at every point in the optimal solution path. At a point of the optimal solution path where a LI loss is suspected, the equation system is modified by imposing a constraint on the values of the Lagrange multipliers. The solution set can then be traced around the point where LI loss occurred. The second-order optimality condition is checked whenever there is either a turning point in the optimal solution path or when a singularity due to violation of either the SC or LI condition is encountered. The eigenvalues of the reduced-Hessian are evaluated using a null space decomposition that requires the process variables to be partitioned into independent and dependent variables.

## 5. Parametric Sensitivity Analysis for Chemical Processes

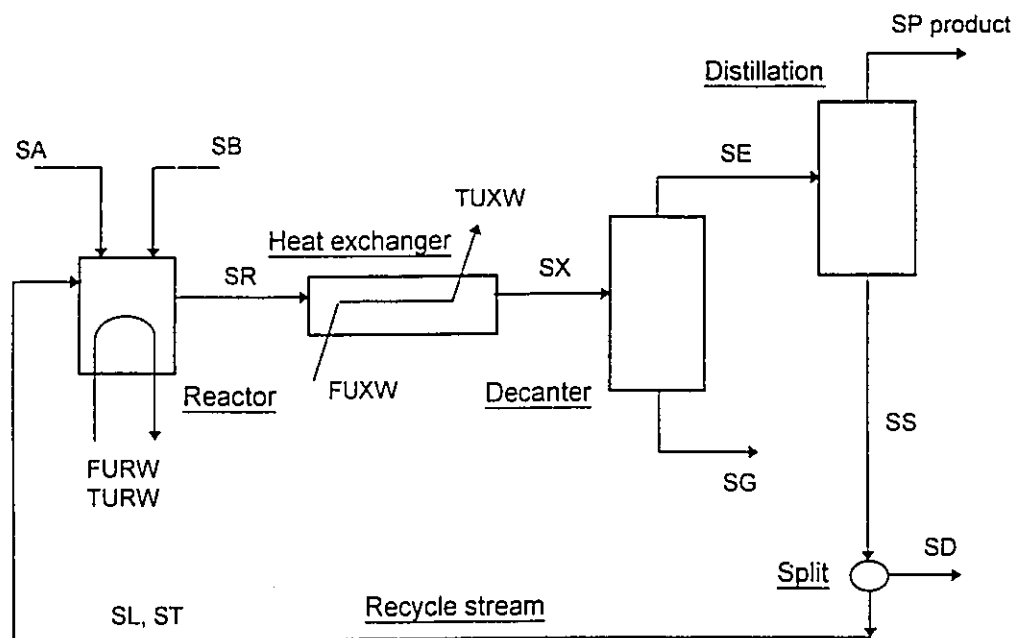
### 5.1 Williams-Otto Plant

The optimal solution path of the Williams-Otto plant shown is calculated for model parameter variations along specified directions. The combined effects of multiple parameter changes in the optimal solution are investigated. The Williams-Otto plant shown in Figure 5.1 consists of a continuous stirred tank reactor, a heat exchanger, a decanter and a distillation column (Williams and Otto, 1960). A three reaction model (Figure 5.1) is used in the reactor, where component 'p' is the product and component 'g' is the undesirable by-product. Pure components 'a' and 'b' (streams SA and SB) and a recycle stream (SL) are fed into the reactor, which is assumed to be perfectly mixed. All three reactions are exothermic with Arrhenius temperature dependent kinetic parameters. There is a heat removal system from the reactor, and the reactor's effluent is further cooled at a target temperature in the heat exchanger. A logarithmic mean temperature difference (LMTD) is used for the heat exchanger's energy balance. There is no constraint imposed on the temperature of the heat exchanger's outlet stream. The decanter removes all the amount of component 'g' from the system. The distillation column is modeled as a simple split with the overhead product consisted of pure product 'p'. The reference model parameter values are given in Table 5.1.

The objective function to be maximized is:

$$\% \text{ return} = \sum_{i=1}^{nstr} (\text{price}_i \text{ FLOW}_i) - C_A (\text{FUXW} + \text{FURW}) - C_B (\text{TURW} - T_w)^2 \quad (5.1)$$

$\text{FLOW}_i$  denotes the flow rate of the  $i$ -th stream, FUXW and FURW are the heat exchanger and the reactor cooling water flow rates, TURW is the outlet temperature of the reactor's cooling water flow rate,  $T_w$  is a reference temperature for the cooling water



Reactions

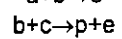
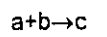


Figure 5.1 Williams-Otto plant flowsheet.

Table 5.1 Model parameter values and directions of perturbation for the Williams-Otto plant.

Model parameter	Reference Value	$\theta$ in 1st eigenvector direction	$\theta$ in 2nd eigenvector direction	$\theta$ in scenario 2 direction
Reactor cooling jacket heat transfer coefficient, $\text{kJ}/(\text{m}^2 \text{ s K})$	$2.6 \cdot 10^{-5}$	-0.1885	-0.2584	-
Heat exchanger heat transfer coefficient, $\text{kJ}/(\text{s K})$	$4.457 \cdot 10^{-4}$	-0.0674	0.0108	-
Arrhenius gain in reaction 1, $(\text{s wt frac})^{-1}$	2.7778	0.0015	0.0027	-
Arrhenius gain in reaction 2, $(\text{s wt frac})^{-1}$	4.1667	0.0004	-0.0002	-
Arrhenius gain in reaction 3, $(\text{s wt frac})^{-1}$	5.5556	-0.0003	0.0003	-
Arrhenius exponent in reaction 1, $(\Delta E/R_g)$ , K	6,666.7	-0.0066	-0.0130	0.5773
Arrhenius exponent in reaction 2, $(\Delta E/R_g)$ , K	8,333.3	-0.0005	0.0013	-0.5773
Arrhenius exponent in reaction 3, $(\Delta E/R_g)$ , K	11,111.1	0.0004	-0.0016	0.5773
Heat of reaction 1, $\text{kJ}/\text{kg}$	0.523	0.2868	0.3869	-
Heat of reaction 2, $\text{kJ}/\text{kg}$	0.209	0.3431	0.4603	-
Heat of reaction 3, $\text{kJ}/\text{kg}$	0.599	0.0592	0.0742	-
Reactor cooling water inlet temperature, $^{\circ}\text{C}$	15.7	0.0441	0.0635	-
Heat exchanger cooling water inlet temperature, $^{\circ}\text{C}$	15.7	0.5807	-0.0916	-
Flow rate of stream SA (reactant a), $\text{kg}/\text{s}$	1.827	0.2144	0.2045	-
Temperature of stream SA, $^{\circ}\text{C}$	21.3	0.0938	0.1348	-
Temperature of stream SB, $^{\circ}\text{C}$	21.3	0.1880	0.2524	-
Temperature of stream SL, $^{\circ}\text{C}$	38.0	0.5719	0.6555	-
Mass holdup of the CSTR reactor, $\text{kg}$	2,104.7	0.0003	0.0006	-

outlet temperature,  $price_i$  is the value per kg of each stream (negative for feed streams, positive for product streams, zero for intermediate streams),  $C_A$  is the cost factor for the cooling water requirements and  $C_B$  is the cost factor for the temperature deviation of the reactor's cooling water from the reference temperature. The values of the economic factors appearing in the objective function are given in Appendix B.

The values of the decision variables and the model parameters are scaled so that their values lie between zero and one.

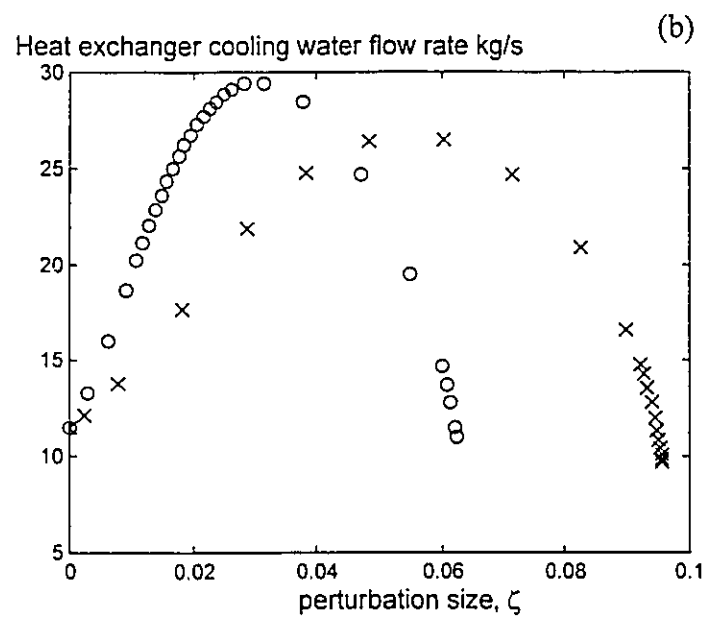
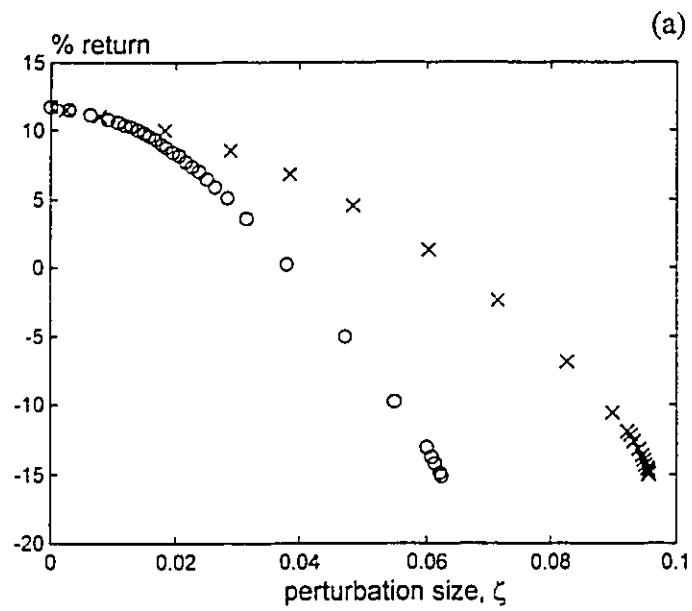
### 5.1.1 Parameter Variation along Eigenvector Directions

The optimal solution is obtained using MINOS 5.3 for the reference parameter values as given in Table 5.1. There are three independent variables at the optimal solution, after a degree of freedom analysis of the active constraint set. A local sensitivity analysis using the reduced space approach is performed for the 18 parameters of Table 5.1 at the optimal solution. An inspection of the absolute values of the individual entries of the sensitivity matrix, reveals that the most sensitive variable is the heat exchanger's cooling water flow rate (FUXW). In order to determine the significance of each parameter and combination of parameters on the optimal solution a singular value decomposition of the sensitivity matrix is performed. The individual entries of the first and second eigenvector directions in the parameter space are shown in Table 5.1. The relative importance of the model parameters to the optimal solution may be assessed by the contribution of each parameter to the eigenvector directions. However, the results are only valid at the reference optimal point because the eigenvectors are calculated using local sensitivity information.

Inspection of the magnitude of the individual entries of vector  $\sigma_1 \mathbf{u}_1$  reveals that parameter perturbation along the first eigenvector direction will cause the largest change in variable FUXW. Similarly, perturbation along the second eigenvector direction will mainly influence the process stream flow rates (streams SL, SR, SX, SE, SS and ST).

Such a conclusion does not imply that parameter variation along each of the eigenvector directions will not affect the remaining process variables. However, each parameter combination, as defined by the eigenvectors, affects the most, in a 2-norm sense, a specific group of process variables. The individual entries of the first eigenvector directions (Table 5.1) indicate that the heat exchanger's cooling water inlet temperature, the target temperature of the heat exchanger's outlet process stream (equal to the temperature of stream SL) and the heat of the first and second reactions have the largest contribution in the first eigenvector direction. Similarly the temperature of stream SL and the heat of reaction for the first and second reactions have the strongest impact on the second eigenvector direction.

The optimal solution path is traced for changes along the first and second eigenvector directions. This will provide useful insight about the behaviour of the system under an extreme situation. There are 150 unknowns (67 process variables, 64 Lagrange multipliers, 18 model parameters and the perturbation size  $\zeta$ ) and 149 equations (67 gradients of the Lagrangian function, 64 equality constraints and 18 relations for the parameter moves, Equation 4.18). The optimal solution paths for the objective function value, the heat exchanger's cooling water flow rate, the reactor's temperature and the flow rate of the reactant 'b' are shown in Figures 5.2a-d, respectively. The cooling water flow rate rapidly increases as the perturbation size increases until it reaches a maximum value at  $\zeta=0.03$  and  $0.054$  for the first and second eigenvector direction respectively; then decreases due to quenching of the reaction. The pathfollowing sensitivity analysis reveals that a 1.7% increase in the heat exchanger's cooling water inlet temperature and in the target temperature for stream SL. when combined with smaller variations in the values of the remaining parameters, may cause FUXW to triple (Figure 5.2b), if optimality is to be preserved. The profit decreases for perturbations in both eigenvector directions but in the first case the slope is steeper. The marginal parameter values for which the plant remains profitable can be determined from Figure 5.2a. This may be



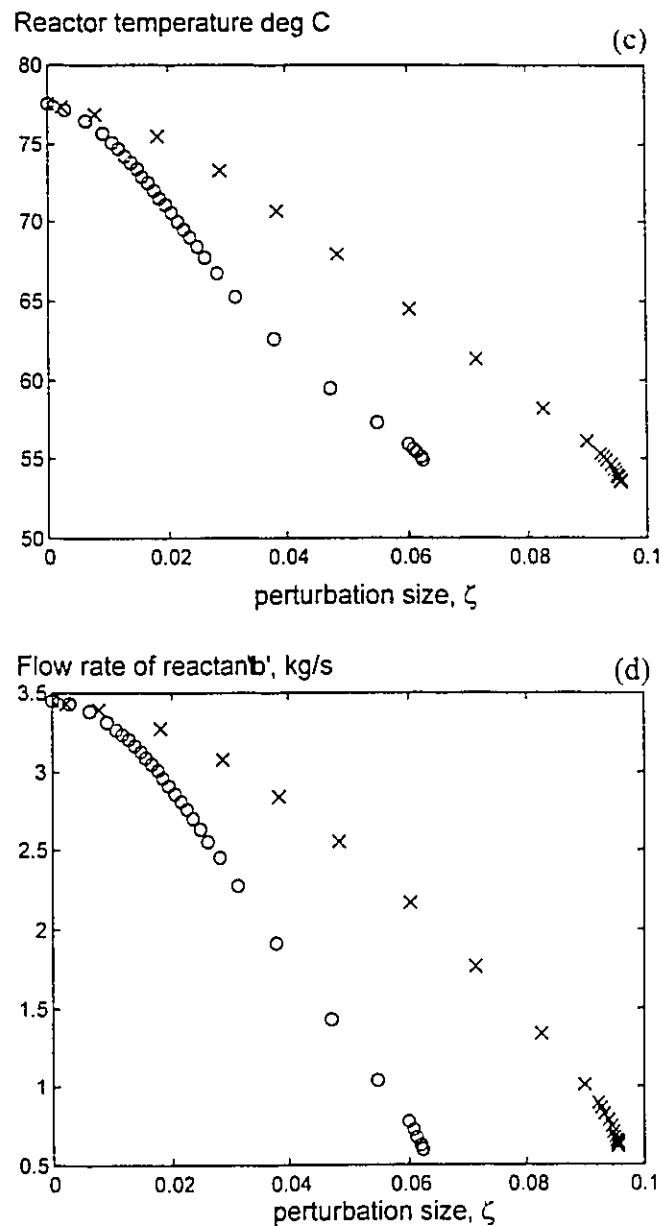


Figure 5.2 Optimal solution path of the (a) objective function value, (b) heat exchanger cooling water flow rate, (c) reactor temperature and (d) flow rate of reactant 'b' for the Williams-Otto plant (° perturbation along the first eigenvector direction, x perturbation along the second eigenvector direction).

more beneficial in a case where the perturbed parameters are cost terms or market values in the objective function. The inlet temperature of reactor's and heat exchanger's cooling water vary differently. The proposed sensitivity analysis method is capable of examining the nonlinear effects arising from multiple parameter changes that cannot be predicted by a local sensitivity analysis.

The optimal solution path obtained by PITCON is compared with the optimal solution calculated by MINOS 5.3 for the same parameter values at every continuation point. Both MINOS and the continuation method give identical solutions for the same parameter values. Each case in MINOS used the previous basis and variable values as a starting point. The main advantage of the continuation method over the case study approach for sensitivity calculations is that it systematizes the procedure by adaptively controlling the step size, so that convergence is facilitated. The continuation approach identifies the parameter values at the points where the active set varies or a singularity occurs. Furthermore, continuation allows the pathfollowing on branches that do not correspond to KKT points. Hence, the characteristics of the solution set can be identified and possible multiple KKT points can be calculated for the same parameter values in the same connected path. In the case study approach to sensitivity analysis, the sampling points are chosen arbitrarily and this may result in failure of the optimizer to converge. Consider the following example to support this statement. The optimal solution path, between the initial and final values of  $\zeta$ , is divided into equispaced intervals with respect to the perturbation size  $\zeta$  and the optimal solution is calculated by MINOS for the parameter values that correspond to these sampling points. The starting point for MINOS is the optimal solution obtained in the previous sampling point. For the case of 10 intervals, MINOS converges to a different optimal solution, that may belong to another branch of local minimizers, after the 7th interval. A different set of variable bounds is active at the solution. For a partition of the range of interest into less than 10 intervals, MINOS fails to converge at some of the selected sampling points.

### 5.1.2 Kinetic Parameter Variations

The optimal solution path of the Williams-Otto plant is calculated for changes in the activation energy estimates of the three reactions. It is assumed that there is a negative bias for the activation energy of the first and third reaction and a positive bias for the activation energy of the second reaction. The values of the  $\theta$  coefficient, shown in Table 5.1, are equal for all three activation energies which imply that the absolute relative change for every parameter is the same at every point in the optimal solution curve.

The optimal solution curve for the reactor and cooling water in the heat exchanger temperatures are shown in Figure 5.3. As the kinetic parameter estimates change, the reactor's optimal temperature decreases in order to favor the desired second reaction that produces the valuable component 'p'. For a perturbation size of -0.232 (13.4% relative change, positive for the second and negative for the first and third reaction, in the kinetic parameter estimates) the temperature difference at the two sides of the counter-current heat exchanger become equal (40°C), which causes the logarithmic mean temperature difference model for the heat exchanger to fail. In order to avoid numerical instabilities an approximation to the logarithmic mean temperature difference is used as suggested by Prasad (1988). The use of the approximate LMTD allows the continuation method to trace the curve around the turning point at  $\zeta = -0.232$  ( $AE1/R_p = 5773$  K,  $AE2/R_p = 9450$  K,  $AE3/R_p = 9622$  K). A calculation of the (3×3) reduced Hessian reveals that one of the eigenvalues vanishes at this point. This results in a transition from a branch of local maximizers to a branch of saddle points. The direction of the predictor step in the continuation procedure is reversed and the solution curve is traced until the temperature of the reactor and the heat exchanger cooling water approach to the same value which results in an infeasible situation.

The sensitivity analysis reveals some significant aspects of the solution curve of the stationary conditions. The magnitude of variation of the activation energies in the specified direction is determined for which the system loses its optimality due to the

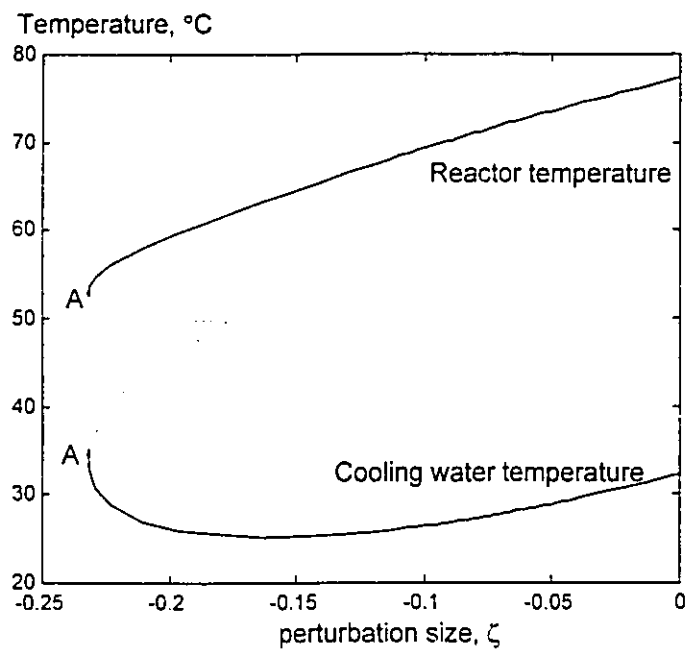


Figure 5.3 Optimal solution path for changes in the activation energy estimates of the reactions in the Williams-Otto plant (solid curves: local minimizers, dashed curves: saddle points).

violation of the second-order optimality condition. Multiple solutions of the stationary conditions for the same set of parameter values are calculated, but not all of them correspond to local optima.

## 5.2 Multicomponent Distillation Units

### 5.2.1 Deisobutanizer (DIB) with a Tray Efficiency Model

This example involves the study of the optimal solution path under feed composition variations for a single multicomponent distillation column. The efficiency of the methodology to handle active set changes on the optimal solution path of the column is examined. Active set variations alter drastically the behaviour of the process variables to parameter changes. The range of feed composition variation for which no feasible optimal solution exist is determined.

A tray-by-tray model based on the MESH equations, as described in Chapter 2, is used to model the DIB column. The thermodynamic properties of the components and the phase equilibrium data are computed by regressed equations (2.16, 2.17 and 2.19). A model based on the Hughmark correlations (Lockett, 1988) is used to estimate the Murphree tray efficiencies. The size of the model is 374 equality constraints with 372 process variables. The objective function to be minimized is the total cost for the separation, which includes the utility costs and the differential product cost for the  $iC_4$  and  $nC_4$  lost in the bottoms and overhead product streams respectively as given by (2.46). The setpoints for the control system are the  $iC_4$  and  $nC_4$  purity levels in the two product streams (Bailey, 1991).

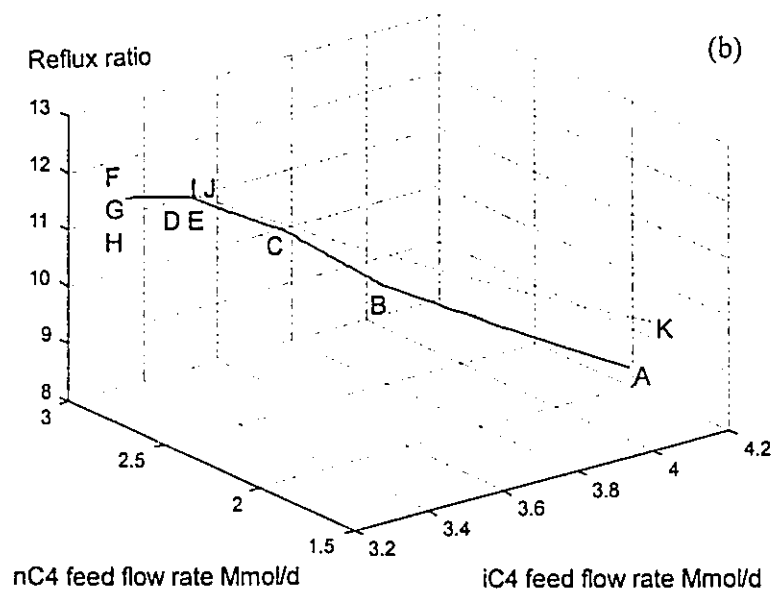
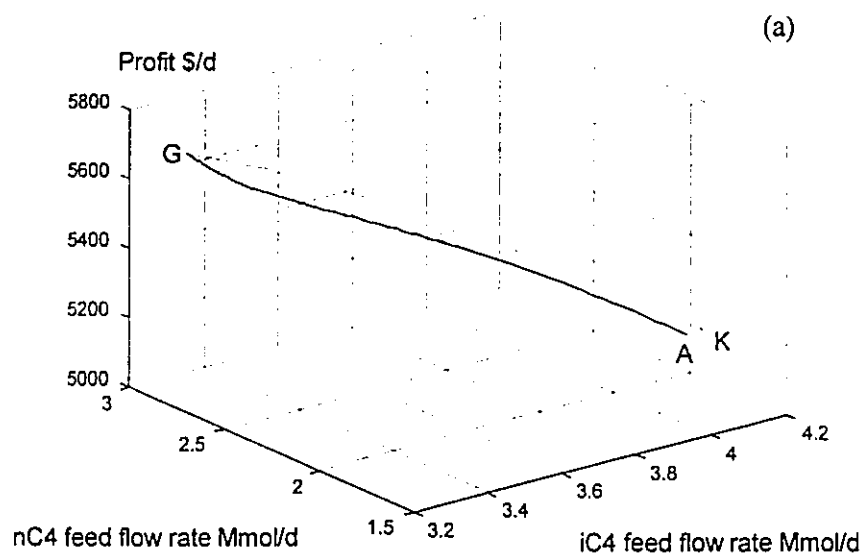
The base optimal solution is obtained for  $iC_4=4.09594$  Mmol/d and  $nC_4=1.81285$  Mmol/d with MINOS 5.3, which has two degrees of freedom and none of the variables are at their upper or lower bounds. The optimal solution path is traced for a disturbance in the feed composition. The feed flow rate of  $iC_4$  (light key) decreases linearly from its

reference value to a final value, but the feed flow rate for  $nC_4$  is changing in such a way, so that the total feed to the column is kept constant. The parameterized set of optimality conditions has 747 equations which includes the relation that governs the variation of the feed composition of the key components. The upper and lower bounds imposed on some of the variable values are shown in Table 5.2. For the remaining variables (component and total flow rates and tray temperatures) a lower bound equal to zero is imposed.

Figures 5.4a-d show the optimal solution path for the objective function value, the reflux ratio, the reboiler heat duty and the  $iC_4$  molar fraction in the bottoms product and Table 5.3 provides information about the type of singularity encountered in the optimal solution path. Starting from the base case (point A) with the feed composition estimates varying linearly as described in the previous paragraph, the reflux ratio and the reboiler's heat duty are increasing in order to anticipate for the increased losses of  $nC_4$  in the overhead product that are penalized in the objective function. At point B of the optimal solution path (relative change in feed flow rates,  $iC_4=-10.4\%$  and  $nC_4=+23.6\%$ ), the upper purity level of the overhead product (3.5% mole in  $nC_4$ ) is reached and one degree of freedom is removed from the optimal solution. Beyond point B, the reflux ratio and the reboiler heat duty increase at a higher rate, because of the lost degree of freedom, in order to anticipate for the continuing change in the feed composition. At point C ( $iC_4=-15.0\%$  and  $nC_4=+33.9\%$ ), the reboiler reaches its highest heat duty level (800 MJ/d) resulting in a system with no degrees of freedom. The optimal solution at this point is simply the solution of the fully determined set of the nonlinear equations (with two fixed variables,  $nC_4$  mole fraction in overhead and reboiler's heat duty) for different values of the feed composition. As the pathfollowing procedure progresses, the increasing reflux ratio violates its maximum allowable level of 12.0 at point D in the optimal solution path ( $iC_4=-19.1\%$  and  $nC_4=+43.2\%$ ). The value of the reflux ratio is fixed at its upper level which results in an overconstrained problem with 3 fixed variables. Therefore the system can be satisfied only for a unique feed composition. This is a situation where the path encounters a point that a special case of LI loss occurs. The Lagrange multipliers

Table 5.2 Variable bounds for the DIB.

	Upper Bound	Lower Bound
Bottoms product flow rate, B (Mmol/d)	3.0	1.5
Overhead product flow rate, D (Mmol/d)	5.2	3.0
Reflux ratio, RF	12.0	8.0
Reboiler heat duty, $Q_B$ (MJ/d)	800.0	700.0
Condenser heat duty, $Q_D$ (MJ/d)	-650.0	-800.0
iC <sub>4</sub> molar fraction in bottoms product, $x_B(iC_4)$	0.040	0.0
nC <sub>4</sub> molar fraction in overhead product, $x_D(nC_4)$	0.035	0.0



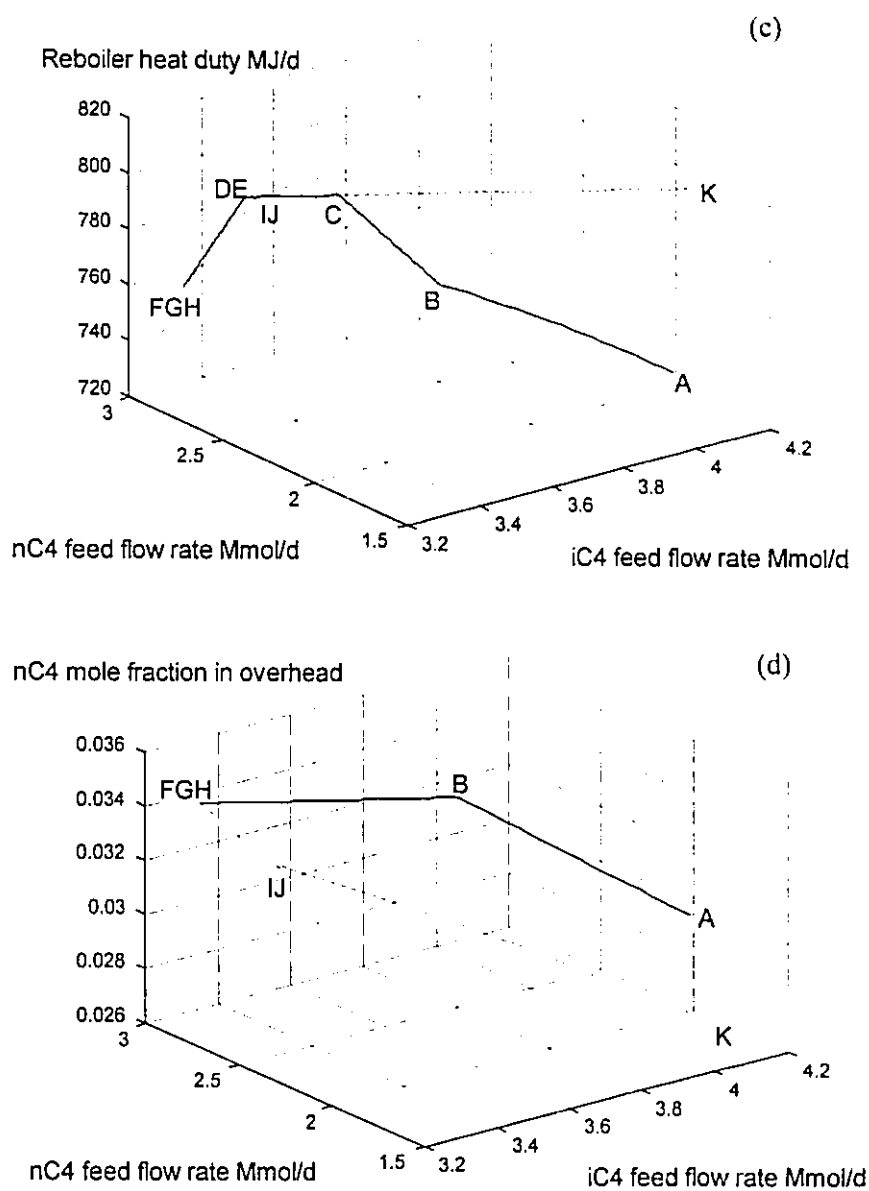


Figure 5.4 Optimal solution path for changes in the feed composition estimates of the DIB: (a) objective function value, (b) reflux ratio, (c) reboiler heat duty and (d)  $iC_4$  molar fraction in bottoms product (solid curves: local minimizers, dashed curves: local maximizers).

Table 5.3 Singularities in the optimal solution path for the DIB.

		$iC_4$ feed flow rate (Mmol/d)	$nC_4$ feed flow rate (Mmol/d)	Continuation points	Singular point type	Active set Upper level
A	min	4.0959	1.8129		Starting point	$\emptyset$
B	min	3.6687	2.2401	21	Upper bound violation for $x_D(nC_4)=0.035$	$\{x_D(nC_4)\}$
C	min	3.4816	2.4272	24	Upper bound violation for $Q_B=800$ MJ/d	$\{x_D(nC_4), Q_B\}$
D	min	3.3133	2.5955	45	Upper bound violation for reflux $RF=12.0$	$\{x_D(nC_4), Q_B, RF\}$
E	min	3.3133	2.5955	4	SC violation for $Q_{Bul}$	$\{x_D(nC_4), RF\}$
F	min	3.2015	2.7073	74	Upper bound violation for $x_B(iC_4)=0.040$	$\{x_D(nC_4), RF, x_B(iC_4)\}$
G		3.2015	2.7073	109	Linear Independence loss Transition min $\rightarrow$ max	$\{x_D(nC_4), RF, x_B(iC_4)\}$
H	max	3.2015	2.7073	183	SC violation for $x_D(nC_4)_{ul}$	$\{RF, x_B(iC_4)\}$
I	max	3.3351	2.5737	9	Upper bound violation for $Q_B=800$ MJ/d	$\{RF, x_B(iC_4), Q_B\}$
J	max	3.3351	2.5737	3	SC violation for $RF_{ul}$	$\{x_B(iC_4), Q_B\}$
K	max	4.1088	1.8000	31	Target point reached	$\{x_B(iC_4), Q_B\}$

associated with the active inequalities are changing dramatically for infinitesimal perturbations in the feed stream. According to the analysis described in Section 4.5.3 the stationary condition system is augmented as in (4.29), so that the multipliers are bounded and allow for possible LI violations to be detected. At point E, which coincides with point D (same values for the feed composition estimates), the Lagrange multiplier associated with the active upper bound on the reboiler's heat duty crosses zero, violating the SC condition, which implies that MFCQ is satisfied at this point. The constraint that sets the reboiler's heat duty to be at its upper bound is removed from the basis thus leaving two fixed variables in the optimal solution.

At point F ( $iC_4 = -21.8\%$  and  $nC_4 = +49.3\%$ ) the upper bound for the purity level in the bottoms product (4.0% mole of  $iC_4$ ) is reached. When the corresponding constraint, that fixes the bottoms purity level at its upper bound, is added to the basis all the Lagrange multipliers of the binding inequalities increase rapidly for infinitesimal changes in the feed composition. The augmented system (4.29) is used again and allows the continuation method to calculate the solution very close to point G where  $\nu = 0$  and the LI condition does not hold. This point also defines the boundary of the feasible region for the column for the given parameter variation. No optimal solution can be obtained for any feed composition change beyond this point. At point G, the direction that the continuation method traverses the optimal solution path has to be reversed. The pathfollowing continues for negative values of  $\nu$  in order to avoid division by zero and then switches back to system (4.20) (point G). The transition from system (4.29) to (4.20) is achieved by dividing the optimality conditions by the current value of  $\nu$ , thus normalizing  $\nu$  and switching back to the KKT conditions. The optimal solution path is comprised by local maximizers since all Lagrange multipliers and all eigenvalues of the reduced Hessian change sign ( $\nu$  is negative). The local maximizers do not have any practical application (path of maximum costs) in this case but the path is traced to show the optimal solution type change.

At the local maximizer branch-points H, I and J, different types of singularities are encountered that are explained in detail in Table 5.3. The calculation is terminated at point K where the reboiler's heat duty and the  $iC_4$  molar fraction in the bottoms product are the active constraints which actually represent the operating conditions that result in the greatest cost for the given process constraints.

Figure 5.4a shows the variation of the optimal objective function value given the change in the feed composition estimates. It is of interest to calculate the difference between the optimal solution path as shown in Figures 5.4a-d and the solution of the process model with fixed setpoints as determined by the optimizer at the reference point (A), under the same variation in the feed composition estimates. The difference between the objective function values at the two points will indicate the necessity for the calculation of a new optimal solution at the updated parameter estimates.

Such a case is examined for the DIB. The setpoints are the purity levels in the two product streams and are fixed at the values determined by the optimizer for the reference values of the feed composition. The system is solved using the pathfollowing methodology for varying feed composition. It should be noted that with the two purity levels fixed the column does not have any degrees of freedom. The solution path for the objective function value and the reflux ratio are shown in Figures 5.5a-b. At point Z in Figures 5.5a-b, that corresponds to a 10% relative change in the  $iC_4$  feed flow rate, the upper level for the condenser's heat duty (-820 MJ/d) is reached. Point Z is equivalent to a point where a special case of LI loss occurs. The simulation shows that there is no solution that satisfies the system of equations for larger parameter estimate variations. If the change in the feed composition estimates is greater than 10% in the  $iC_4$  feed flow rate, then there is going to be a steady-state offset from the setpoint values of the reference case for the column and the difference in the cost will be larger between the two curves.

However, one can observe that for small changes in the feed composition, there is no substantial difference between the 'ideal' curve (if the parameter values were known at

every point and a new optimal solution was obtained) and the actual curve (for fixed setpoints and some model mismatch) in the value of the objective function (Figure 5.5a). Changes in the manipulated variables, such as the reflux ratio, may be more severe than in the 'ideal' case (Figure 5.5b).

### 5.2.2 Column Train Example

This example involves the simultaneous optimization of three multicomponent stagewise distillation columns in series (Figure 5.6). The behaviour of the optimal solution path is studied for variations in the feed composition estimates. It is of great interest to investigate the interaction between the different units under the influence of simultaneous parameter variations.

The feed to the column train is a 12 component mixture of hydrocarbons. The debutanizer (DB) separates pentane and heavier components from the mixture which are used as fuel gas. The  $C_3$ - $C_4$  splitter (SP) separates propane and lighter components, with the overhead product priced as pure propane. The overhead and bottoms products from the deisobutanizer (DIB) are priced as pure  $iC_4$  and  $nC_4$  respectively. The economic data are taken from Bailey et al. (1993). The columns are modeled using tray-by-tray models and the thermodynamic properties are calculated using regressed equations (Bailey, 1991). The system originally has six degrees of freedom and the setpoints to the multivariable controller are:

- a) The reflux to feed flow rate ratio in the DB
- b) The  $nC_4$  molar fraction in the bottoms product in the DB
- c) The  $iC_4$  molar fraction in the overhead product in the SP
- d) The  $C_3$  molar fraction in the bottoms product in the SP
- e) The  $nC_4$  molar fraction in the overhead product in the DIB
- f) The  $iC_4$  molar fraction in the bottoms product in the DIB

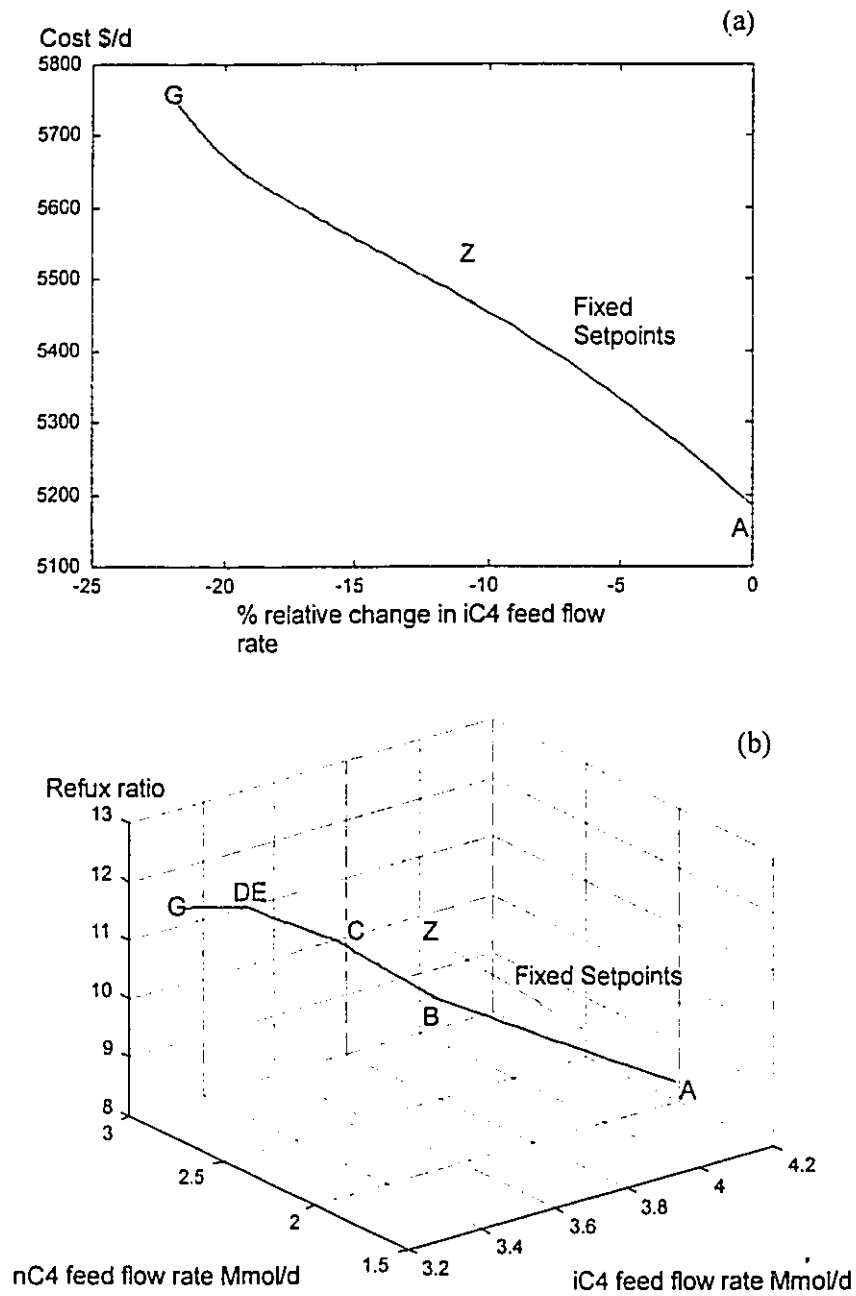


Figure 5.5 Comparison between the optimal solution path and the trajectory of the solution with the setpoints fixed at the values obtained in the nominal case (point A): (a) objective function value, (b) reflux ratio.

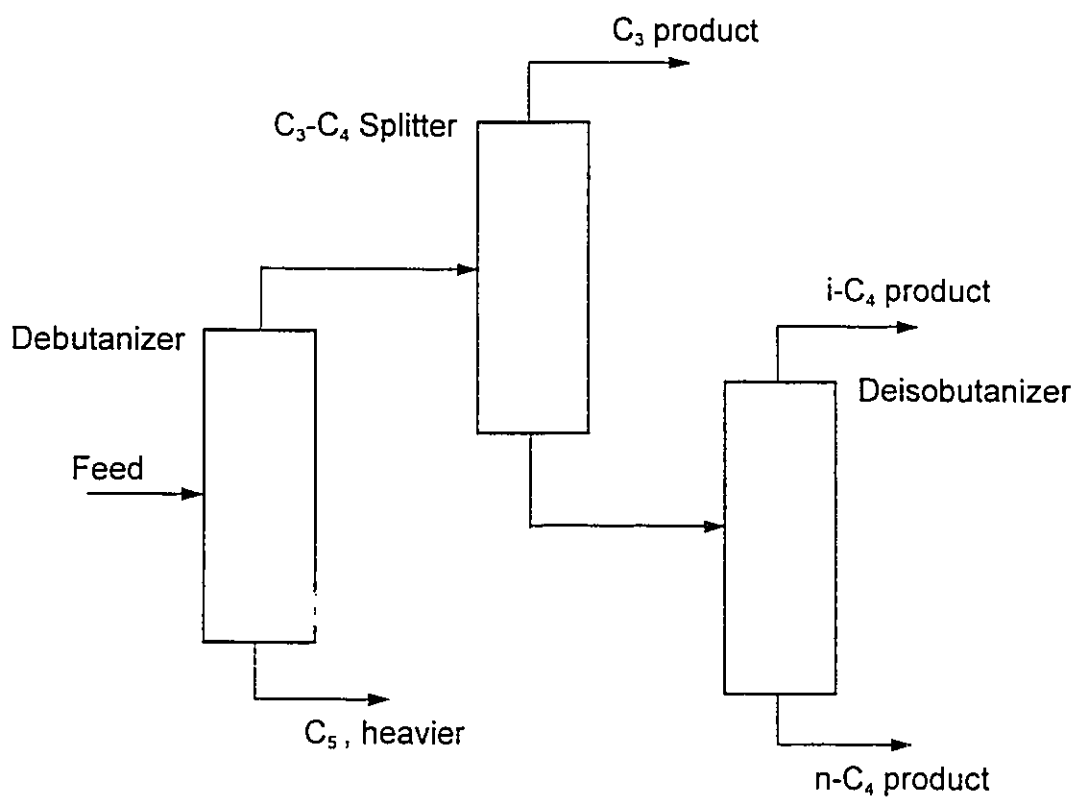


Figure 5.6 Schematic of the distillation column train

In this case, the  $iC_4$  molar flow rate in the feed increases from a base case value of 3.975 Mmol/d to an upper estimate of 4.3 Mmol/d linearly, while the  $nC_4$  decreases at the same rate from 1.7559 Mmol/d to 1.4322 Mmol/d, so that the total feed flow rate in the system is kept constant. The upper and lower bounds for the variables are shown in Table 5.4. The optimal solution for the initial values of the feed composition ( $iC_4=3.975$ ,  $nC_4=1.7559$  Mmol/d), which is obtained using MINOS 5.3, has two degrees of freedom with four independent variables found at their bounds. The total number of equality constraints in the model are 855 and the equation set (4.20) has 1715 equations.

The light and heavy keys for the DIB are the  $iC_4$  and  $nC_4$  respectively. As a result, the main effects of the variation in the feed composition are initially noticed in the DIB where the bottoms flow rate reaches its lower bound and the bottoms purity level its upper bound for very small changes in the feed composition (0.2% increase in  $iC_4$ ). The system at this point has no degrees of freedom with the DIB overconstrained (3 active variable bounds). In order to compensate for any changes in the feed quality estimate, the active bound on the upper level of the bottoms flow rate in the DB becomes inactive. The profit starts to decrease since the DB bottoms product stream whose flow rate decreases has the highest molar value. As a result heavier components (mainly pentanes) are sent into the SP and DIB so that the level of the  $iC_4$  in the DIB bottoms could satisfy the product specification. The DIB column is sensitive to this particular kind of feed composition disturbance and forces the degrees of freedom in the other columns to adjust so that the entire system remains feasible.

At point K, that corresponds to a relative change for  $iC_4$  equal to +8.1% and for  $nC_4$  equal to -18.4%, the upper bound on the molar fraction of pentanes and higher components in the DIB bottoms product is reached. The system could not absorb any further changes in the feed stream composition and there is a sequence of active set changes for infinitesimal changes in the feed.

Table 5.4 Variable bounds for the distillation column train.

<b>Debutanizer (DB)</b>	<b>Upper Bound</b>	<b>Lower Bound</b>
Bottoms product flow rate (Mmol/d)	1.50	0.90
Reflux ratio	1.050	0.90
Reflux to Feed ratio	1.20	0.80
Reboiler heat duty (MJ/d)	90.0	74.0
Condenser heat duty (MJ/d)	-130.0	-170.0
iC <sub>4</sub> molar fraction in bottoms product	0.011	0.0
nC <sub>4</sub> molar fraction in bottoms product	0.022	0.0
<b>C<sub>3</sub>-C<sub>4</sub> Splitter (SP)</b>		
Overhead product flow rate (Mmol/d)	2.00	1.00
Reflux ratio	8.0	11.0
Reboiler heat duty (MJ/d)	260.0	210.0
Condenser heat duty (MJ/d)	-180.0	-220.0
iC <sub>4</sub> molar fraction in overhead product	0.015	0.0
C <sub>3</sub> molar fraction in bottoms product	0.015	0.0
<b>Deisobutanizer (DIB)</b>		
Bottoms product flow rate (Mmol/d)	2.30	1.70
Reflux ratio	10.0	8.0
Reboiler heat duty (MJ/d)	840.0	680.0
Condenser heat duty (MJ/d)	-630.0	-790.0
nC <sub>4</sub> molar fraction in overhead product	0.027	0.0
iC <sub>4</sub> molar fraction in bottoms product	0.032	0.0
iC <sub>5</sub> +nC <sub>5</sub> +C <sub>6</sub> molar fraction in bottoms product	0.170	0.0

Table 5.5 shows the details of the type of singularities encountered in the optimal solution path for the column train. Figures 5.7a-e show the optimal solution path for the profit, the bottoms product flow rate and the reflux to feed flow rate ratio in the DB, the reflux ratio in the DIB and the  $iC_4$  molar fraction in the overhead product of the SP, respectively.

### 5.2.3 Comparison of Parametric Sensitivity Results between Tray-by-tray and OCFE Models

One of the requirements for the adequacy of a simplified process model to represent the full-order model in process optimization is that both the simplified and the full-order models should have the same sensitivity with respect to the major model parameters at the optimal solution (Biegler et al., 1985; Forbes and Marlin, 1994). In Chapter 2 OCFE models for stagewise distillation units that provide the same optimal solution as the full-order, tray-by-tray model, have been developed. In this section the pathfollowing methodology will be used to study the parametric sensitivity of the OCFE model and compare it to the tray-by-tray sensitivity results.

Variations in the feed composition estimates and the column pressure estimates are investigated separately. The OCFE model for the DIB column in Chapter 2 is considered with the nonlinear objective function (2.46). The error in the feed stream composition estimates affects the two key components in the column in a similar fashion as in section 5.2.1. Table 5.6 presents the singular points and the active set in the solution path for the OCFE and the tray-by-tray models. Both models show an almost identical behaviour for this type of disturbance.

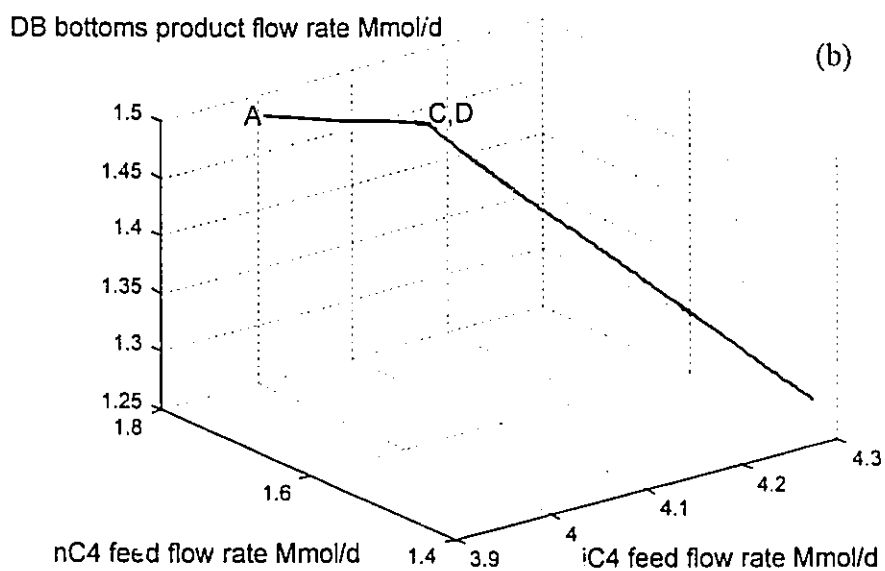
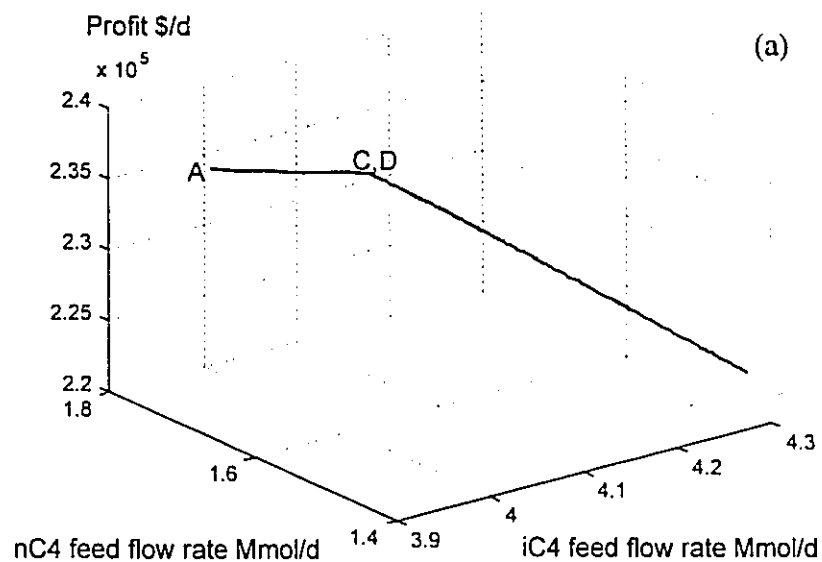
A second scenario involves a variation in the pressure estimates of the column. Given a total pressure drop for the column, the pressure estimate in the condenser is subject to positive variation. The results obtained using both tray-by-tray and OCFE

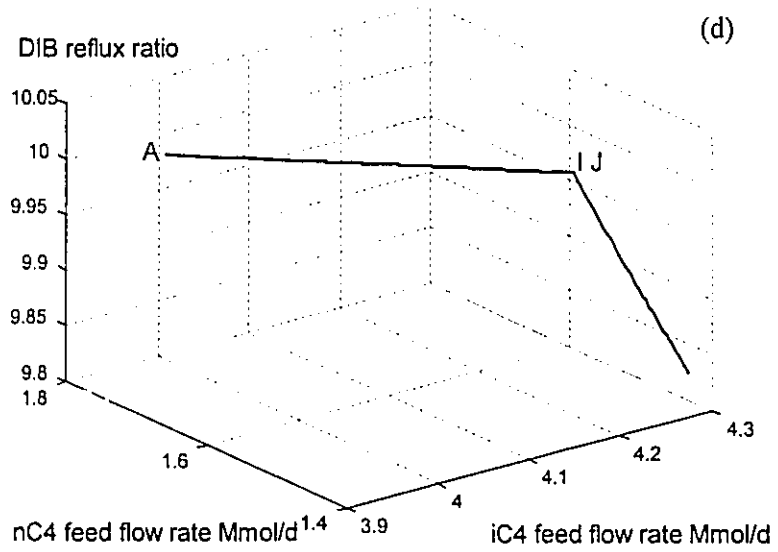
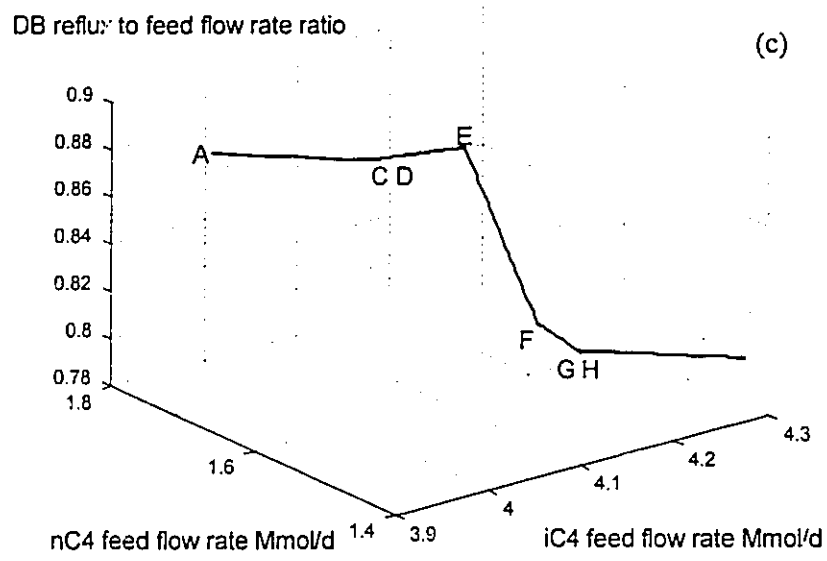
Table 5.5a Singularities in the optimal solution path for the distillation column train.

	DOF	iC <sub>4</sub> feed flow rate (Mmol/d)	nC <sub>4</sub> feed flow rate (Mmol/d)	Singular point type	Active set
A	2	3.9750	1.7559	Starting point	{1, 2, 3, 4}
B	2	4.0634	1.6675	Lower bound violation for bottoms product flow rate in DIB (1.7 Mmol/d)	{1, 2, 3, 4, 5}
C	1	4.0713	1.6594	Upper bound violation for purity level in DIB bottoms product ( $x_B=0.032$ )	{1, 2, 3, 4, 5, 6}
D	0	4.0715	1.6594	SC violation for bottoms product flow rate upper bound in DB	{2, 3, 4, 5, 6}
E	1	4.1284	1.6025	SC violation for reflux ratio upper bound in DB	{3, 4, 5, 6}
F	2	4.1744	1.5565	Lower bound violation for reboiler heat duty in DB (74.0 MJ/d)	{3, 4, 5, 6, 7}
G	1	4.1984	1.5325	Lower bound violation for reflux to feed ratio in DB (0.80)	{3, 4, 5, 6, 7, 8}
H	0	4.1984	1.5325	SC violation for reboiler heat duty lower bound in DB	{3, 4, 5, 6, 8}
I	1	4.2234	1.5075	Upper bound violation for reboiler heat duty in DIB (840.0 MJ/d)	{3, 4, 5, 6, 8, 9}
J	0	4.2234	1.4322	SC violation for reflux ratio upper bound in DIB	{3, 5, 6, 8, 9}
K	1	4.2987	1.4322	Upper bound violation for pentane and heavier in DIB bottoms product (0.17)	{3, 5, 6, 8, 9, 10}
L	0	4.2987	1.4322	Upper bound violation for iC <sub>4</sub> molar fraction in SP overhead product (0.015)	{3, 5, 6, 8, 9, 10, 11}
M	-	4.2987	1.4322	Special case of LI loss SC violation for reflux to feed ratio lower bound in DB	{3, 5, 6, 9, 10, 11}
N	0	4.2987	1.4322	Upper bound violation for reboiler heat duty in DB (90.0 MJ/d)	{3, 5, 6, 9, 10, 11, 12}

Table 5.5b Constraint numbers for Table 5.5a.

Constraint No	Description	Numerical Value
1	Upper bound on bottoms product flow rate in DB	1.50 Mmol/d
2	Upper bound on reflux ratio in DB	1.05
3	Upper bound on reboiler heat duty in SP	260.0 MJ/d
4	Upper bound on reflux ratio in DIB	10.0
5	Lower bound on bottoms product flow rate in DIB	1.70 Mmol/d
6	Upper bound on $iC_4$ molar fraction in DIB's bottom product	0.032
7	Lower bound on reboiler heat duty in DB	74.0 MJ/d
8	Lower bound on reflux to feed ratio in DB	0.80
9	Upper bound on reboiler heat duty in DIB	840.0 MJ/d
10	Upper bound on molar fraction of pentanes and heavier in DIB's bottoms product	0.17
11	Upper bound on $iC_4$ molar fraction in SP's overhead product	0.015
12	Upper bound on reboiler heat duty in DB	90.0 MJ/d





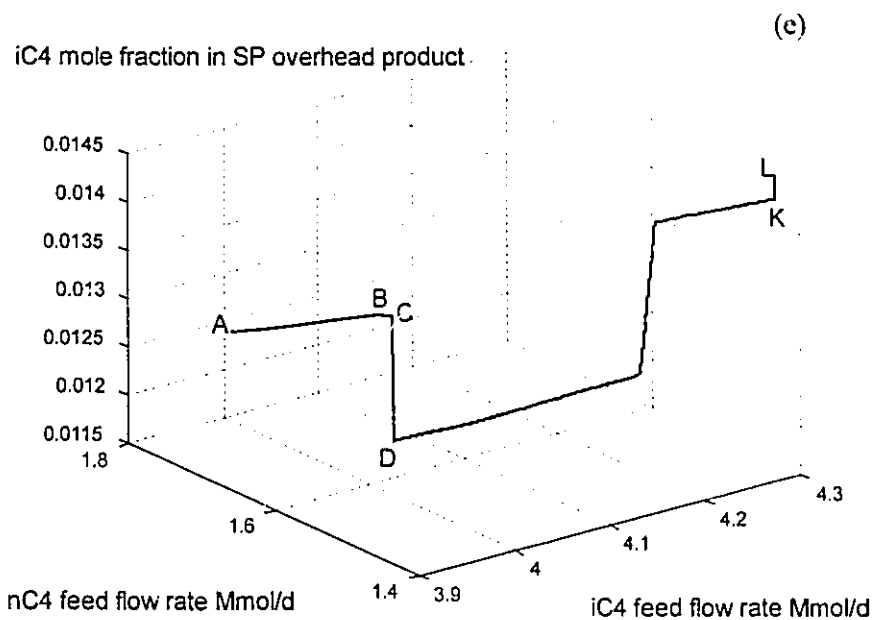


Figure 5.7 Optimal solution path for changes in the feed composition estimates in the column train: (a) profit, (b) DB bottoms product flow rate, (c) DB reflux to feed flow rate ratio, (d) DIB reflux ratio and (e) iC<sub>4</sub> molar fraction in SP overhead product.

models are shown in Table 5.7. The element partition in the OCFE model remains unchanged during the continuation procedure.

The results in Tables 5.6 and 5.7 show that both tray-by-tray and OCFE models have similar behaviour in the optimal solution under variations in the estimates of the feed composition and column pressure. The same active set changes occur for the same set of parameter values. The results suggest that the OCFE model represents accurately the tray-by-tray optimal solution for a range of model parameter values.

#### **5.2.4 Optimal Solution Sensitivity to Element Partition Variations for OCFE Models**

In Chapter 3 the effect of the finite element partition on the OCFE optimal solution has been examined and a method for the adaptive placement of the element breakpoints, to minimize the approximation error has been developed. A conclusion that was drawn from experience with the adaptive placement methodology was that there may be a wide range of element partitions that satisfy the imposed residual equidistribution criterion. As mentioned in Chapter 3, the simultaneous economic optimization and residual equidistribution problem may become ill-conditioned if too many element breakpoints are allowed to vary.

In this Section the sensitivity information obtained by the pathfollowing methodology is utilized in order to identify the finite element lengths that have the greatest impact on the economic optimal solution. Based on this result, the effort for the optimal distribution of the element breakpoints would be concentrated in the most sensitive elements in the model. Sensitivity analysis using continuation will be used to determine the range for the element size variations for which the economic optimization problem remains feasible.

Furthermore, sensitivity analysis with respect to the element partition may provide an indication about the sufficiency of the total number of collocation points in the

Table 5.6 Singular points in the optimal solution paths obtained by tray-by-tray and OCFE models for variation in the feed composition estimate.

		Tray-by-tray	OCFE		
		$iC_4$ feed flow rate (Mmol/d)	$iC_4$ feed flow rate (Mmol/d)	Singular point type	Active set Upper or Lower level
A	min	4.096	4.096	Starting point	$\emptyset$
B	min	3.982	3.981	Lower bound violation for $Q_D = -820.0$ MJ/d	$\{Q_{D,L}\}$
C	min	3.671	3.672	Upper bound violation for $x_D(nC_4) = 0.025$	$\{Q_{D,L}, x_D(nC_4)_U\}$
D	min	3.454	3.454	Upper bound violation for reflux $RF = 12.0$	$\{Q_{D,L}, x_D(nC_4)_U, RF_U\}$
E	min	3.454	3.454	SC violation for $Q_{D,L}$	$\{x_D(nC_4)_U, RF_U\}$
F	min	3.369	3.369	Upper bound violation for $x_3(iC_4) = 0.030$	$\{x_D(nC_4)_U, RF_U, x_3(iC_4)_U\}$
G		3.369	3.369	Linear Independence loss Transition min $\rightarrow$ max	$\{x_D(nC_4)_U, RF_U, x_3(iC_4)_U\}$

OCFE model: 3 elements per column section, 2 collocation points per element in rectifying section, 3 collocation points in the stripping section

Notation: subscripts U and L denote that the variable is at its upper or lower bound, respectively.

Table 5.7 Singular points in the optimal solution paths obtained by tray-by-tray and OCFE models for variation in the column pressure estimate.

		Tray-by-tray	OCFE		
		Condenser Pressure (kPa)	Condenser Pressure (kPa)	Singular point type	Active set Upper or Lower level
A	min	479.90	479.90	Starting point	$\emptyset$
B	min	499.97	500.07	Lower bound violation for $Q_D = -820.0$ MJ/d	$\{Q_{D,L}\}$
C	min	542.69	543.05	Upper bound violation for $x_B(iC_4) = 0.030$	$\{Q_{D,L}, x_B(iC_4)_U\}$
D	min	554.50	554.50	Upper bound violation for $x_D(nC_4) = 0.025$	$\{Q_{D,L}, x_B(iC_4)_U, x_D(nC_4)_U\}$
E		554.50	554.50	Linear Independence loss Transition min $\rightarrow$ max	$\{Q_{D,L}, x_B(iC_4)_U, x_D(nC_4)_U\}$

OCFE model: 3 elements per column section, 2 collocation points per element in rectifying section, 3 collocation points in the stripping section

Notation: subscripts U and L denote that the variable is at its upper or lower bound, respectively.

OCFE model. More specifically, an element whose element size variations have a large effect on the optimal solution, even for small variations, may be considered as a candidate for a collocation point addition. If the opposite is true, a collocation point may be removed from the given element. The redistribution of the collocation points may be performed in such a way so that the resulting OCFE model becomes less sensitive to the element partition.

The DIB column as described in Chapter 2 is considered with the nonlinear objective function (2.46). The OCFE model that has 3 elements in each column section is partitioned using the residual-based approach as follows: element lengths 3.900, 3.900, 4.200 in the rectifying section and 5.230, 4.903, 7.867 in the stripping section. The first set of simulations involve the variation of the element partition at the rectifying section while keeping the stripping section partition fixed. The first element's length in the rectifying section increases linearly with respect to the perturbation parameter  $\zeta$ , while the second and third element lengths decrease at half the rate of increase in the first element length. The changes in element lengths are defined in such a way so that the sum of the lengths of the elements in each section is constant.

The change in the economic optimal solution does not seem to be significant until the first element length reaches the value of 4.283. At this point, the flow rate for pentane (nonkey component), at the first collocation point of the first element becomes equal to zero. For larger values of the first element length, the pentane flow rate becomes negative leading to an infeasible problem. Pathfollowing continues on the modified system of equations that include the additional active bound constraint for the pentane flow rate. For values of the first element length greater than 4.283, the accuracy of the optimal solution starts deteriorating and the composition profile becomes unrealistic. The behaviour of the optimal reflux ratio and the cost are shown in Figures 5.8a-b. According to the sensitivity results there is an upper bound for the first element length, given the

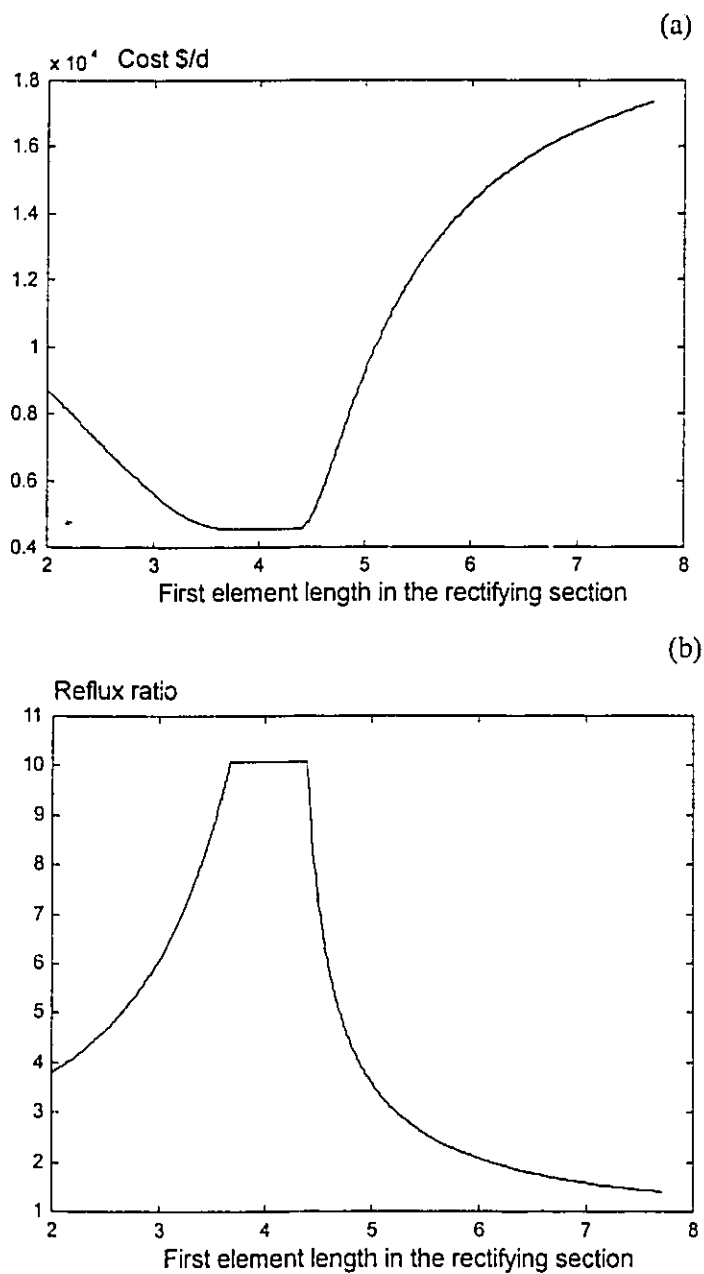


Figure 5.8 Optimal solution path for an OCFE DIB model for variations in the element partition of the rectifying section: (a) objective function value, (b) reflux ratio.

order of the interpolation polynomial used in the element, for which an accurate solution is achieved.

A similar situation is examined by decreasing the length of the first element while increasing the lengths of the other two elements in the section by half the rate of decrease in the first element. At an element partition of the rectifying section at points 3.666, 4.017 and 4.317, the pentane flow rate in the first collocation point of the third element reaches its lower bound. This implies that the element partition cannot provide an accurate optimal solution composition profile for pentane.

The reason for the inaccuracy of the OCFE model for some element partitions is that the model fails to predict the behaviour of the nonkey components. The predicted profiles may provide unrealistic values at small component compositions due to inadequate model resolution.

A similar case is examined for the partition of the stripping section. The pathfollowing on the KKT set shows that the length of the third stripping section does not cause any significant changes in the optimal solution or undesirable behaviour in the composition profile of the nonkey components. The second element's length could not be increased above the value of 5.058 because the propane flow rate becomes negative.

The information regarding the sensitivity of the optimal solution to the element partition is utilized in order to:

- a. Determine if a smaller OCFE model can be obtained by removing collocation points from those elements, whose length variation does not affect the optimal solution.
- b. Decide about a proper distribution of the collocation points among the elements, by relocating the collocation points, thus changing the order of the approximation polynomials within each element, from the least sensitive elements to the most sensitive.

Different scenarios are examined for the DIB column. In the first scenario, a collocation point is added in the second element of the rectifying section, in order to improve the robustness of the optimal solution to changes in the element partition of the rectifying section. The additional collocation point allows the element length to be larger, thus making the other two elements smaller in size. The result is an improved model resolution, since the density of collocation points is increased in the rectifying section. The optimal solution of OCFE 2 shown in Table 5.8 is closer to the tray-by-tray solution than the original OCFE 1 model.

In the second scenario, a collocation point is removed from the third element of the stripping section because of the robustness of the optimal solution to variations in its length. A new element partition is obtained using the residual-based approach and a new optimal solution is calculated. Table 5.8 shows the new optimal solution for OCFE 3 model, that converges faster than the original OCFE 1 model but the approximation error has slightly increased. Moreover, the sensitivity of the optimal solution has increased for changes in the length of the third element as shown in Figure 5.9.

A third scenario considers the relocation of the removed collocation point from the third element (second scenario) to the second element of the stripping section. Thus the interpolating polynomial in the second element becomes fifth-order. The optimal solution obtained by OCFE 4 model is shown in Table 5.8. The accuracy of the optimal solution is slightly reduced compared to OCFE 1 model and so is the solution time. However, the optimal solution becomes more insensitive to changes in the second element's length.

The sensitivity results may be utilized to understand the effects of the element partition in OCFE models for distillation units on the economic optimal solution. Determination the sections in the column where the approximation model is the most sensitive to partition changes allows the selection of a more robust collocation scheme.

Table 5.8 Comparison of the optimal solution of different OCFE models

	Tray-by-tray	OCFE 1	OCFE 2	OCFE 3	OCFE 4
Reflux ratio	10.078	10.077	10.078	10.057	10.066
Condenser heat duty (MJ/d)	-810.458	-810.409	-810.458	-808.610	-809.465
Reboiler heat duty (MJ/d)	831.339	831.292	831.341	829.477	830.340
nC <sub>4</sub> % mole in overhead	2.142	2.143	2.142	2.143	2.143
iC <sub>4</sub> % mole in bottoms	2.720	2.718	2.718	2.759	2.740
Cost \$/d	4560.3	4560.2	4560.2	4568.4	4565.0
RS/6000 355, CPU time (s)	18.7	9.0	10.0	7.8	8.4
OCFE models					
Collocation points per element					
Rectifying section	-	2, 2, 2	2, 3, 2	2, 2, 2	2, 2, 2
Stripping section	-	3, 3, 3	3, 3, 3	3, 3, 2	3, 4, 2

All OCFE models: 3 elements per column section.

Element partition:

OCFE 1: 3.900, 3.900, 4.200 rectifying section, 5.230, 4.903, 7.867 stripping section

OCFE 2: 3.800, 4.100, 4.100 rectifying section, 5.230, 4.903, 7.867 stripping section.

OCFE 3: 3.900, 3.900, 4.200 rectifying section, 5.230, 6.403, 6.367 stripping section

OCFE 4: 3.900, 3.900, 4.200 rectifying section, 5.430, 5.303, 7.267 stripping section

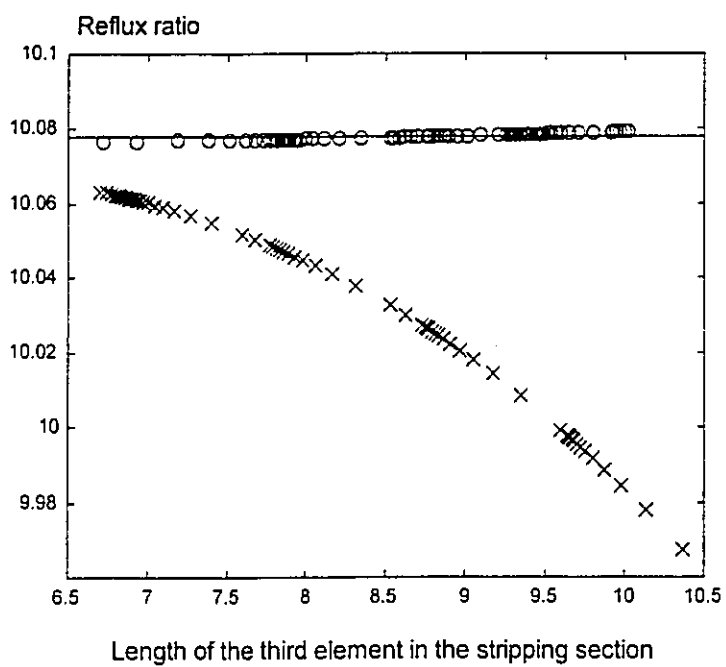


Figure 5.9 Optimal solution path for the reflux ratio for variations in the length of the third element in the stripping section, (o) fourth-order polynomial approximation, (x) third-order polynomial approximation.

The choice of the structure of the OCFE model will have to compromise between solution speed and prediction accuracy.

### 5.3 Ammonia Synthesis Reactor

#### 5.3.1 Parametric Sensitivity Analysis

Sensitivity analysis of system described by differential/algebraic equations has been studied by Caracotsios and Stewart (1985) and Leis and Kramer (1985). They proposed efficient algorithms for the estimation of the local sensitivities of such systems simultaneously with the calculation of the trajectory of the state variables. In this example the parametric sensitivity of an OCFE model that describes the behaviour of a differential/algebraic system is examined.

The sensitivity analysis method using continuation will be implemented in a ammonia synthesis reactor system described by Murase et al. (1970) and Vasantharajan and Biegler (1990). The production of ammonia is performed in a Haber-Bosch catalytic reactor that operates at high pressure. The reaction that takes place is:

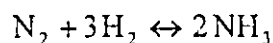


Figure 5.10 shows a schematic of the reactor, which is separated in to a reaction and a cooling tube zone. The reaction zone contains the catalyst with the cooling tubes inserted vertically through the reaction zone. The feed gas goes through a heat exchanger and then through the cooling tube, where it removes heat from the exothermic reaction. The removed heat brings the feed gas at the proper temperature to initiate the reaction in the catalyst zone and enhance the ammonia conversion. The feed gas changes direction of flow at the end of the cooling tube zone and enters the reaction zone. Murase et al. (1970) considered the optimization of the reactor in order to determine the optimal length of the reactor and the optimal heat transfer coefficient profile along the reactor.

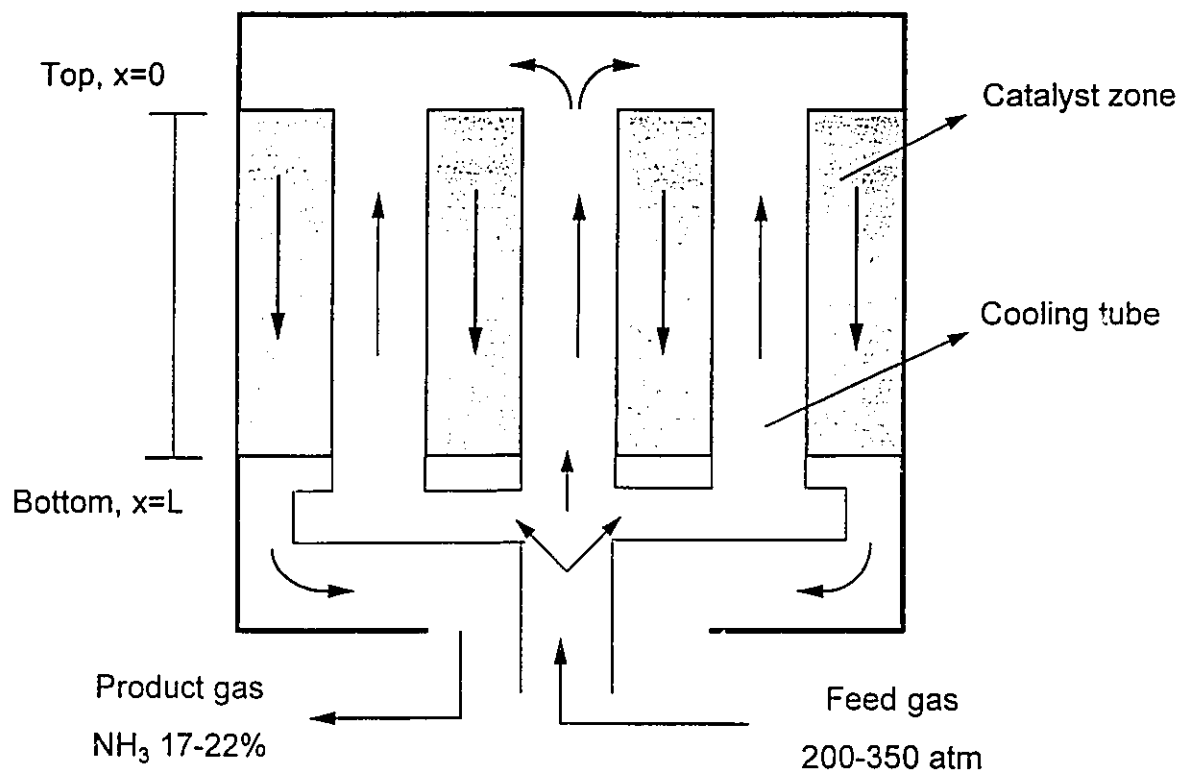


Figure 5.10 Schematic of the ammonia synthesis reactor.

Following the model formulation described in the mentioned references the system of differential equations that represent the ammonia synthesis are summarized below:

$$\frac{dX_1}{dX_0} = -K_1 U(X_2 - X_1) \quad (\text{a})$$

$$\frac{dX_2}{dX_0} = -K_2 U(X_2 - X_1) + K_3 R_C \quad (\text{b}) \quad (5.2)$$

$$\frac{dX_3}{dX_0} = -K_4 R_C \quad (\text{c})$$

where the following dimensionless variables are defined as:

$$X_0 = x_R / L_{\text{reac}} \in [0,1]$$

$$X_1 = T_f / T_{\text{ref}} \in [1,2]$$

$$X_2 = T_g / T_{\text{ref}} \geq 1$$

$$X_3 = N_{N_2} / G \in [0,1]$$

and the parameters  $K_1$ ,  $K_2$ ,  $K_3$  and  $K_4$  given by:

$$K_1 = (S_1 L_{\text{reac}}) / (W_{\text{tot}} C_{pf})$$

$$K_2 = (S_1 L_{\text{reac}}) / (W_{\text{tot}} C_{pg})$$

$$K_3 = (-\Delta H S_2) / (W_{\text{tot}} C_{pf}) (L_{\text{reac}} / T_{\text{ref}})$$

$$K_4 = L_{\text{reac}} / G$$

Table 5.9 provides the nomenclature and the values of the parameters for the system equations. The reaction rate expression is given by:

$$R_C = F_C \left( k_1 \frac{P_{N_2} (P_{H_2})^{1.5}}{P_{NH_3}} - r_2 \frac{P_{NH_3}}{(P_{H_2})^{1.5}} \right) \quad (5.3)$$

The partial pressures of each component are evaluated using the stoichiometry of the reaction as:

Table 5.9 Notation and data for the ammonia synthesis reactor

	Independent and dependent variables
$x_R =$	Total reactor length, m
$x_1 =$	Length of the first reactor section, m
$N_{N_2} =$	Molar flow rate of $N_2$ per unit area catalyst, $\text{kg mol hr}^{-1} \text{m}^{-2}$
$T_f =$	Temperature of feed gas, K
$T_g =$	Temperature of reacting gas, K
	Parameters
$C_{pf} =$	Heat capacity of feed gas = $0.707 \text{ kcal kgr}^{-1} \text{K}^{-1}$
$C_{pg} =$	Heat capacity of reacting gas = $0.719 \text{ kcal kgr}^{-1} \text{K}^{-1}$
$R_g =$	Ideal gas constant = $1.987 \text{ kcal kmol}^{-1} \text{K}^{-1}$
$k_1 =$	Rate constant 1 = $1.78954 \times 10^4 \exp[-20,800 / (R T_g)]$
$k_2 =$	Rate constant 2 = $2.5714 \times 10^{16} \exp[-47,400 / (R T_g)]$
$F_C =$	Catalyst activity = 1
$\Delta H =$	Heat of reaction = $-26,600 \text{ kcal kmol}^{-1} N_2$
$N_{i-}$	Molar flow rate of $i$ th-component through catalyst zone
$P_{i-}$	Partial pressure of $i$ th-component, atm
$P_{tot-}$	Total reactor pressure = 286 atm
$S_1 =$	Surface area of catalyst tubes per unit reactor length = 52 m
$S_2 =$	Cross-sectional area of catalyst zone = $0.78 \text{ m}^2$
$T_{ref-}$	Reference temperature = $127 \text{ }^\circ\text{C} = 400.15 \text{ K}$
$L_{reac-}$	Reference length = 10 m
$U =$	Overall heat transfer coefficient = $100 \text{ kcal m}^{-2} \text{hr}^{-1} \text{K}^{-1}$
$W =$	Total mass flow rate = $26,400 \text{ kgr hr}^{-1}$
$\rho_f =$	Density of feed gas = $10.5 \text{ kgr kmol}^{-1}$
$G =$	Total molar flow rate = $3,223.44 \text{ kmol hr}^{-1} \text{m}^{-2}$
$\Phi =$	Profit objective function, $\text{\$ yr}^{-1}$

$$P_i = P_{tot} \left( \frac{N_i}{G - 2\xi_R} \right) \quad i = N_2, H_2, NH_3 \quad (5.4)$$

where  $\xi_R$  is the extent of the reaction, which is calculated as:

$$\xi_R = N_{N_2}^0 - N_{N_2} \quad (5.5)$$

The molar flow rates for the components are given by the following relations:

$$N_{H_2} = N_{H_2}^0 - 3\xi_R \quad (a)$$

$$N_{NH_3} = N_{NH_3}^0 + 2\xi_R \quad (b) \quad (5.6)$$

with  $N_i^0$  ( $i=N_2, H_2$  and  $NH_3$ ) being the molar flow rate of each component at the feed gas stream. The mole fraction for  $N_2, H_2$  and  $NH_3$  are 0.2175, 0.6525 and 0.05 respectively. The integration along the length of the reactor begins from the top of the reactor to the bottom, with initial conditions for the dimensionless variables,  $X_1=1.0, X_2=1.0$  and  $X_3=0.2175$ .

The heat transfer coefficient,  $U$ , is allowed to vary along the reactor which is divided into two subsections as proposed by the work of Murase et al. (1970). The first section operates at a constant heat transfer coefficient, set at a maximum value,  $U_{max}$ . In the second section  $U$  decreases monotonically in a quadratic manner ( $U=ax^2+bx+c$ ), as shown in Figure 5.11, until the end of the reactor. This type of profile is proposed by Murase and coworkers to be the optimal selection.

The independent variables are the lengths of the two reactor subsections and the coefficients in the quadratic relation for  $U$  in the second section. The profit objective function that is minimized is given by (Murase et al., 1970):

$$\begin{aligned} \Phi(\times 10^6) = & -0.27981 X_1 + 0.28174 X_2 - 55.070 X_3 - \\ & 10^{-6} (3.4566 \cdot 10^7 + 1.9837 \cdot 10^9 X_0)^{0.5} + 13.3543 \end{aligned} \quad (5.7)$$

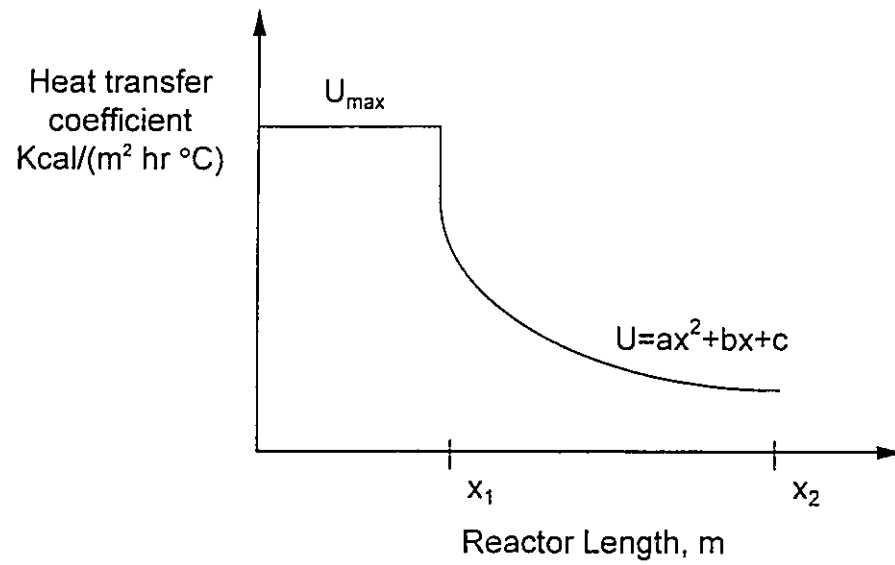


Figure 5.11 Typical optimal heat transfer coefficient profile for the ammonia reactor.

An OCFE model consisting of three elements in the first section and two elements in the second section with fifth-order Lagrange interpolating polynomials in each element is used. An element breakpoint is placed at the boundary point between the two reactor sections due to the discontinuity in the heat transfer coefficient profile at this point. For the nominal case with  $U_{\max}=100$  kcal/(m<sup>2</sup> hr K) the optimal values for the two reactor subsections are 4.01 and 5.99 m, respectively, which yields a 23.96% ammonia conversion at the exit of the reactor. The variable profiles at the optimal solution are shown in Figure 5.12 and are compared with the profiles obtained using a 4th-5th order Runge-Kutta integration method evaluated at the optimal values for the independent variables. The profiles recommend that the OCFE model predicts accurately the profiles in the reactor.

The parametric sensitivity studies using continuation involve the variation of the  $U_{\max}$  value in the first section of the reactor. Initially, the optimal solution path is traced for increasing values of  $U_{\max}$ . For a  $U_{\max}$  value of 157.5 kcal/(m<sup>2</sup> hr K) (point B), the optimal solution path exhibits a turning point due to violation of the second-order optimality condition. More specifically, one eigenvalue of the reduced Hessian vanishes at this point and the solution points turn to saddle points. The continuation direction is reversed and the value of  $U_{\max}$  starts decreasing. At point C, where  $U_{\max}=146.3$  kcal/(m<sup>2</sup> hr K), the restriction on the size of  $U$  at the boundary between the two sections, that does not allow the heat transfer coefficient in the second section to be greater than the value of  $U_{\max}$ , is reached. The active bound is then included in the equation set. However, the addition of the new active constraint, causes the reduced Hessian to become negative-definite and hence the points correspond to local maximizers. The pathfollowing continues for decreasing values of  $U_{\max}$  until point D.

From point E in the optimal solution that corresponds to  $U_{\max}=200$  kcal/(m<sup>2</sup> hr K) the optimal solution path is calculated for decreasing values of  $U_{\max}$ . At point F where  $U_{\max}=168.75$  kcal/(m<sup>2</sup> hr K) the upper bound for the value of  $U$  at the section boundary is

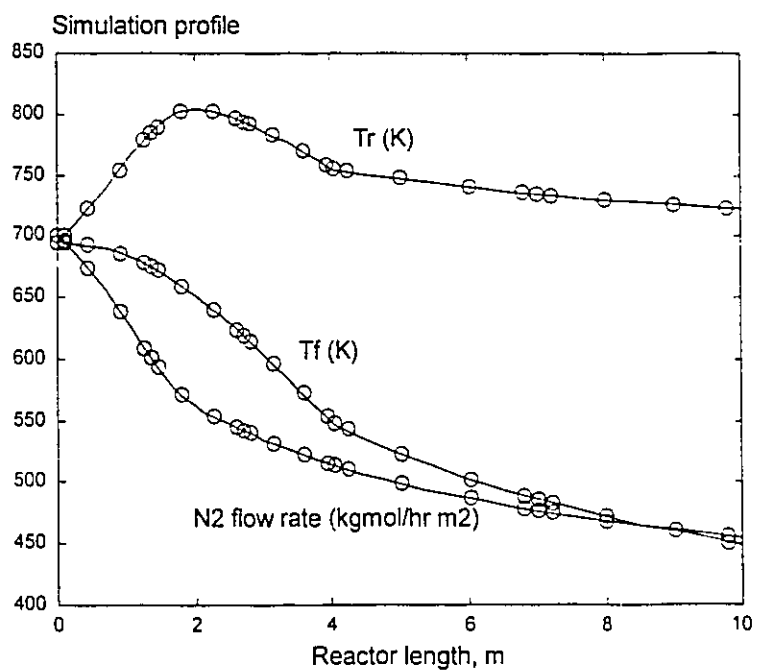


Figure 5.12 Comparison of the simulation profiles in the ammonia reactor between an orthogonal collocation solution (o) and a Runge-Kutta integration solution (solid lines).

reached. The pathfollowing continues and at point C the optimal solution path coincides with the one calculated starting from point A. The optimal solution paths for the length of the first reactor section and the profit are shown in Figures 5.13a-b.

If the restriction on the value of  $U$  at the section boundary had been raised, then the optimal solution path for the length of the first reactor section would have been as shown in Figure 5.14. We observe that the optimal solution path consists of two disconnected branches of solutions. There are more than one solution to the stationary conditions for the same value of  $U_{\max}$ , however not all of them correspond to a local maximizer as shown in Figure 5.14. Since it is not possible to calculate both solution branches starting from the same nominal point using the continuation methodology as described, MINOS 5.3 is used to find a solution point in the second branch.

Parametric sensitivity using continuation provides insight about the characteristics of the optimal solution path and can identify multiple solution points to the stationary conditions in the same connected path.

## 5.4 Chapter Summary

The pathfollowing methodology for the sensitivity analysis of parametric NLPs is applied to a number of problems, that involve single and multiple process units.

Multiple parameter variations will reveal the nonlinear effects on the optimal solution. The range of the parameter variation is determined for which the active set remains unchanged. Active set changes will identify the limiting constraints under different types of parameter estimate variations. The magnitude of the parameter perturbation can be evaluated for which the system remains feasible. In such a situation a special case of LI loss is detected, and the singular point is a boundary point of the KKT set. In cases where the optimization of multiple unit processes is involved sensitivity analysis can provide information about the interaction of the different units under the influence of disturbances so that optimality is maintained. Multiple solutions to the

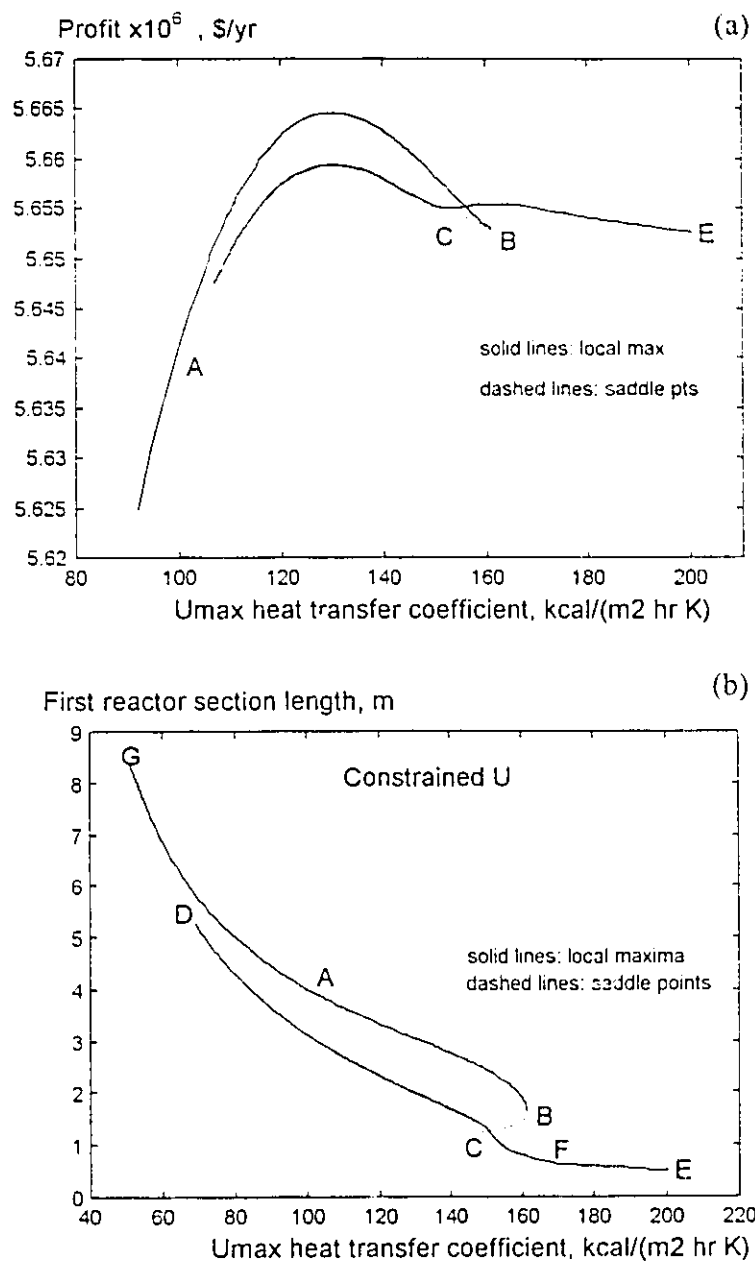


Figure 5.13 Optimal solution path for parametric variation in the  $U_{max}$  for the ammonia reactor (constrained case): (a) profit function, (b) first reactor section length.

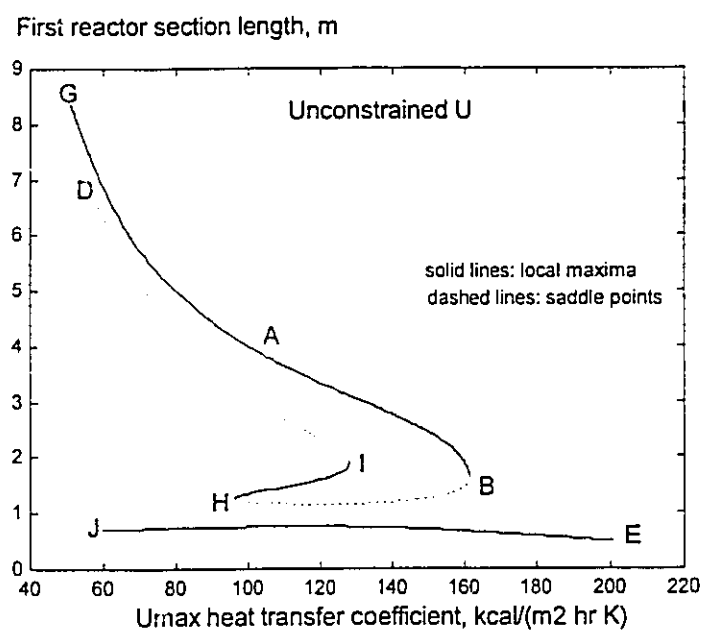


Figure 5.14 Optimal solution path for parametric variation in the  $U_{\max}$  for the ammonia reactor (unconstrained case).

stationary conditions, that are in the same connected path, can be calculated and the characteristics of the solution points can be explicitly determined.

The pathfollowing method can be used to calculate the difference between the optimal solution with all the independent variables varying and the solution of the system constraints with the setpoints fixed at the values determined at the reference point for changes in the parameter estimates. The difference between the two points can be used to determine the margins for the parameter changes for which a new optimal solution is necessary.

The sensitivity of the optimal solution of OCFE models for distillation units to different element partitions is investigated. The results can be utilized to define a structure for the OCFE model, so that an accurate and robust to element partition changes solution is obtained.

## 6. Conclusions

This thesis involves contributions in two different subjects that are tied under the RTO framework. The first subject focuses in the refinement and enhancement of the collocation models for the steady-state optimization of stagewise distillation units.

In Chapter 2, a number of modifications in the formulation of existing OCFE models for distillation columns have been introduced, thus improving the performance of the OCFE models in the steady-state optimization of distillation units:

- a) Finite elements are used within each column section in order to track irregularities in the column profiles.
- b) All stages in the column that have intermediate feed or product streams entering or leaving the column are modeled as discrete equilibrium stages. Such a formulation allows a more accurate representation of the column behaviour compared to existing models.
- c) An extension to the previous statement is that depending on the allowable level of model size reduction, some sections of the column may be modeled using OCFE while other sections using tray-by-tray formulation.

Based on observations from a number of simulated examples involving multicomponent distillation columns the following conclusions were drawn:

- a) The OCFE models recognize the same optimal solution and have similar sensitivity with respect to major model parameters, such as feed composition and column pressure, as the rigorous tray-by-tray model.
- b) The optimal solution for the OCFE model is obtained in less time than the tray-by-tray model.

- c) OCFE models have a wider range of starting points for which convergence to the optimal solution is possible compared with the tray-by-tray models, which results in improved robustness of the OCFE models to the initial variable values.
- d) The OCFE modeling alternative is beneficial for columns that have large sections with flat composition and temperature profiles, but is not generally recommended for multicomponent columns with multiple sidestreams or a small number of equilibrium stages.

The quality of the optimal solution obtained by the OCFE model is enhanced by adaptively placing the element breakpoint so that the approximation error for the distillation column is minimized (Chapter 3).

- a) A new method for the estimation of the error is introduced based on the residuals of the material and energy balances around envelopes that include certain parts of the distillation column. The magnitude of the residuals around different envelopes is equidistributed throughout the column.
- b) An approach that aims to determine the optimal economic operating conditions for the column and the optimal element partition simultaneously is developed.
- c) The residual equidistribution method results in element partitions that an economic optimal solution of improved accuracy is achieved for a given number of collocation points and elements. However, the procedure may converge to multiple element partitions. The optimization problem may become ill-conditioned if too many element breakpoints are allowed to move.
- d) Derivative equidistribution method does not always result in an element partition for which an accurate economic optimal solution exists.

The second part of the thesis involves the study of the sensitivity analysis in model-based process optimization. A sequence of KKT points of a parametric nonlinear

program is traced for varying parameter values using a continuation method as implemented in PITCON.

- a) Based on local sensitivity results the directions in the parameter space that cause the largest variability in the state variable space are determined, by performing a singular value decomposition on the sensitivity matrix. The relative significance of each individual parameter and combinations of parameters on the optimal solution can be evaluated.
- b) Multiple parameter perturbations of finite magnitude along any selected direction are implemented for the pathfollowing of the optimal solution. The procedure allows only deterministic type of variation in the parameters.
- c) Modification of the continuation algorithm so that the optimal solution path is calculated around singular points. Simple tests are implemented for the detection of the type of singularity encountered.

Sensitivity analysis is performed in chemical processes with respect to multiple simultaneous parameter changes of arbitrary magnitude along a specified direction, that can explicitly handle active set changes, linear independence constraint qualification loss and second-order optimality condition violation. The approach allows the study of nonlinear behaviour and the combined effects of group of parameters in the sensitivity of the optimal solution. A large variety of sensitivity analysis applications have been examined in Chapter 5.

- a) Determine the range of model parameter variations for which a feasible optimal solution exists.
- b) Determine the range of model parameter variations for which the active constraint set remains unchanged.
- c) Study the optimal solution behaviour of more than one unit under the influence of model parameter variations.

- d) Sensitivity analysis of the optimal solution of OCFE models for distillation units with respect to changes in the element partition. The result may provide information to determine the most sensitive elements in the model.
- e) Parametric sensitivity analysis of systems described by differential and algebraic equations using OCFE models.

### 6.1 Recommendations for Future Work

The ability of the adaptive OCFE models to accurately predict the optimal solution of the tray-by-tray model with less computational effort can be utilized in the size reduction of more detailed distillation models. Nonequilibrium stage models (Krishnamurthy and Taylor, 1985) and packed column models based on mass and energy transfer equations are of increasing interest in the modelling of distillation processes. However, the complexity of the model increases significantly with the inclusion of the mass and energy transfer relations for the calculation of the bulk liquid and vapour phase compositions. The multicomponent diffusive mass transfer coefficients require the solution of the Maxwell-Stefan equations at every stage. An OCFE approach would require the solution of the model equations at fewer points than the actual number of stages leading to considerable savings. Due to the complexity of the model, the OCFE model would probably need better tuning through the selection of the variables to be approximated and selection of the order of the approximation polynomials within each element.

The parametric sensitivity analysis examines the behaviour of the optimal solution for parameter variation along a unique direction in the parameter space. The parameter variations in a real plant, however, may cover a large range of directions. The information acquired by the pathfollowing of the optimal solution can be utilized to construct a response surface for the optimal solution. A low-dimensional space can be selected that is spanned by the dominant directions of parameter variation. These

dominant directions of variation can be the eigenvector directions of the sensitivity matrix as derived in Chapter 5. The behaviour of the optimal solution can be easily examined using the pathfollowing methodology for variations along the dominant directions or linear combinations of the dominant directions. The objective would be to construct a function that would approximate the behaviour of the optimal solution in the reduced space of the dominant eigenvector directions. The response surface information can be utilized in order to operate the plant in conditions less sensitive to parameter variations.

The stochastic behaviour of the model parameter estimates would be of great interest to incorporate in the proposed sensitivity analysis methodology. Parameters with relatively low sensitivity may cause large uncertainty in the optimal values of the decision variables if the parameter is associated with large uncertainty. The problem becomes even more complicated when multiple parameters are considered. The approximation of the stochastic distribution of the parameter estimates using some deterministic equivalent model (DiNaro et al., 1994) will allow the study of the behaviour of the optimal solution under the presence of stochastic type of variation.

In terms of applications in real-time systems, the pathfollowing methodology can be utilized in deciding an optimal policy under parameter variations. In large systems with multiple units and a large number of degrees of freedom, the pathfollowing sensitivity analysis method provides an optimal path for the entire plant by adjusting the degrees of freedom in order to compensate for the effects of the parameter variations.

## 7. Bibliography

- Allgower, E. L., and K. Georg, *Numerical Continuation Methods*, Springer-Verlag, New York, 1990.
- Armacost, R. L., and A. V. Fiacco, "Computational Experience in Sensitivity Analysis for Nonlinear Programming", *Math. Program.*, **6**, 301-326 (1974).
- Ascher, U., J. Christiansen, and Russell, R. D., "A Collocation Solver for Mixed Order Systems of Boundary Value Problems", *Math. Comput.*, **33**, 659-679 (1979).
- Askey, R., "Continuous Hahn Polynomials", *J. Phys. A:Math. Gen.*, **18**, L1017-1019 (1985).
- Bailey, J. K., A. N. Hrymak, S. S. Treiber, and R. B. Hawkins, "Nonlinear Optimization of a Hydrocracker Fractionation Plant", *Comput. Chem. Eng.*, **17**, 123-138 (1993).
- Bailey, J. K., *Nonlinear Optimization of a Hydrocracker Fractionation Plant*, M. Eng. Thesis, McMaster University, Canada, 1991.
- Benallou, A., D. E. Seborg, and D. A. Mellichamp, "Dynamic Compartmental Models for Separation Processes", *AIChE J.*, **32**(7), 1067-1078 (1986).
- Bequette, B. W., and T. F. Edgar, "Non-Interacting Control System Design Methods in Distillation", *Comput. Chem. Eng.*, **13**(6), 641-650 (1989).
- Biegler, L. T., I. E. Grossmann, and A. W. Westerberg, "A Note on Approximation Techniques used for Process Optimization", *Comput. Chem. Eng.*, **9**(2), 201-206 (1985).
- Boston, J. F., and S. L. Sullivan Jr, "A New Class of Solution Methods for Multicomponent, Multistage Separation Processes", *Can. J. Chem. Eng.*, **52**, 52-63 (1974).

- Bratchell, N., "Multivariate Response Surface Modelling by PCA", *J. Chemometrics*, **3**, 579-588 (1989).
- Buzzi Ferraris, G., "Interlinked, Multistaged Separators with Nonstandard Specifications Solved by the Newton-Raphson Method", *AIChE J.*, **27**(1), 163-166 (1981).
- Caracotsios, M., and W. E. Stewart, "Sensitivity Analysis of Initial Value Problems with Mixed ODEs and Algebraic Equations", *Comput. Chem. Eng.*, **9**(4), 359-365 (1985).
- Carey, C. F. and Finlayson, B. A., "Orthogonal Collocation on Finite Elements", *Chem. Eng. Sci.*, **30**, 587-596 (1975).
- Carta, R., G. Tola, A. Servida, and M. Mordibelli, "Error Analysis for Collocation Models for Steady-State Multistage Separation Units", *Comput. Chem. Eng.*, **19**(1), 123-127 (1995).
- Cho, Y. S., and B. Joseph, "Reduced Order Models for Separation Columns-III. Application to Columns with Multiple Feeds and Sidestreams", *Comput. Chem. Eng.*, **8**(2), 81-90 (1984).
- Cho, Y. S., and B. Joseph, "Reduced Order Steady-State and Dynamic Models for Separation Processes. Part I. Development of the Model Reduction Procedure", *AIChE J.*, **29**(2), 261-269 (1983a).
- Cho, Y. S., and B. Joseph, "Reduced Order Steady-State and Dynamic Models for Separation Processes. Part II. Application to Nonlinear Multicomponent Systems", *AIChE J.*, **29**(2), 270-276 (1983b).
- Coleman, T. F., and J. J. Moré, "Estimation of Sparse Hessian Matrices and Graph Coloring Problems", *Math. Program.*, **28**, 243-270 (1984).
- Cuthrell, J. E., and L. T. Biegler, "On the Optimization of Differential-Algebraic Process Systems", *AIChE J.*, **33**(8), 1257-1270 (1987).

- Darby, M. L., and D. C. White, "On-Line Optimization of Complex Process Units", *Chem. Eng. Progr.*, October, 51-59 (1988).
- De Boor, C. and Swartz, B., "Collocation at Gaussian Points", *SIAM J. Num. Anal.*, **10**(4), 582-606 (1973).
- De Boor, C., "Good Approximation by Splines with Variable Knots II", *Dundee Conf. on Numerical Solution of Differential Equations, Lecture Notes in Mathematics No 363*, pp. 12-19, Springer-Verlag, New York, 1974.
- De Boor, C., *Practical Guide to Splines*, Springer-Verlag, New York, 1978.
- DiNaro, J., B. Phenix, M. Tatang, J. W. Tester, and J. B. Howard, "Application of Uncertainty Analysis to SCWO Kinetic Mechanism", paper presented at the Annual AIChE Meeting, San Francisco, 1994.
- Dongarra, J. J., J. R. Bunch, C. B. Moler, and G. W. Stewart, *LINPACK User's Guide*, Society for Industrial and Applied Mathematics, Philadelphia, 1979.
- Drozdowicz, B. and Martinez, E., "Reduced Models for Separation Processes in Real-Time Simulators", *Comput. Chem. Eng.*, **12**(6), 547-560 (1988).
- Eduljee, H. E., "Equations replace Gilliland Plot", *Hydroc. Proc.*, September, 120-122 (1975).
- España, M., and I. D. Landau, "Reduced Order Bilinear Models for Distillation Columns", *Automatica-J. IFAC*, **14**, 345-355 (1978).
- Ferguson, N. B. and Finlayson, B. A., "Error Bounds for Approximate Solutions to Nonlinear Ordinary Differential Equations", *AIChE J.*, **18**(5), 1053-1059 (1972).
- Fiacco, A. V., "Sensitivity Analysis for Nonlinear Programming using Penalty Methods", *Math. Program.*, **10**(3), 287-311 (1976).
- Fiacco, A. V., *Introduction to Sensitivity and Stability Analysis in Nonlinear Programming*, Academic Press, New York, 1983.

- Finlayson, B. A., *Nonlinear Analysis in Chemical Engineering*. McGraw-Hill Inc., New York, 1980.
- Fletcher, R., *Practical Methods of Optimization*, 2nd Ed., J. Wiley & Sons, New York, 1987.
- Forbes, J. F., and T. E. Marlin, "Model Accuracy for Economic Optimizing Controllers: The Bias Update Case". *Ind. & Eng. Chem. Res.*, **33**, 1919-1929 (1994).
- Forbes, J. F., *Model Structure and Adjustable Parameter Selection for Operations Optimization*, Ph.D. Thesis, McMaster University, Canada, 1993.
- Gal, T., *Postoptimal Analysis, Parametric Programming, and Related Topics*, McGraw-Hill, New York, 1979.
- Ganesh, N., and L. T. Biegler, "A Reduced Hessian Strategy for Sensitivity Analysis of Optimal Flowsheets", *AIChE J.*, **33**(2), 282-296 (1987).
- Garcia, C. E., and M. Morari, "Optimal Operation of Integrated Processing Systems. Part I: Open-Loop On-Line Optimizing Control", *AIChE J.*, **27**(6), 960-968 (1981).
- Georgakis, C., and M. A. Stoeber, "Time Domain Order Reduction of Tridiagonal Dynamics of Staged Processes-I. Uniform Lumping", *Chem. Eng. Sci.*, **37**(5), 687-697 (1982).
- Gill, P. E., W. Murray, and M. H. Wright, *Practical Optimization*, Academic Press, New York, 1981.
- Glinos, K., and M. F. Malone, "Maximum Reflux, Product Distribution and Lumping Rules for Multicomponent Distillation", *Ind. & Eng. Chem. Process Des. Dev.*, **23**, 764-768 (1984).
- Guddat, J., F. G. Vasquez, and H. T. Jongen, *Parametric Optimization: Singularities, Pathfollowing and Jumps*, J. Wiley & Sons, 1990.

- Hearne, J. W., "Sensitivity Analysis of Parameter Combinations" *Appl. Math. Modelling*, **9**, 106-109 (1985).
- Hirabayashi, R., M. Shida, and S. Shindoh, "Manifold Structure of the Karush-Kuhn-Tucker Stationary Solution Set with Two Parameters". *SIAM J. Optim.*, **3**, 564-581 (1993).
- Holland, C. D., *Fundamentals of Multicomponent Distillation*, McGraw-Hill Inc., New York, 1981.
- Horton, R. R., B. W. Bequette, and T. F. Edgar, "Improvements in Dynamic Compartmental Modelling for Distillation", *Comput. Chem. Eng.*, **15**(3), 197-201 (1991).
- Huss, R. S., and A. W. Westerberg, "Collocation Methods for Distillation Design". presented at the AIChE Annual Meeting, San Francisco Ca., (1994).
- Hyprotech Ltd., *HYSIM User's Guide*. Version 1.51, Calgary, Alberta, Canada, 1991.
- Jongen, H. Th., G.-W. Weber, "On Parametric Nonlinear Programming", *Annals Operations Research*, **27**, 253-284 (1990).
- Jongen, H. Th., P. Jonker, and F. Twilt, "Critical Sets in Parametric Optimization", *Math. Program.*, **34**, 333-353 (1986).
- Keller, H. B., *Lectures on Numerical Methods in Bifurcation Problems*, Springer Verlag, 1987.
- Kernevez, J. P., Y. Liu, M. L. Seoane, and E. J. Doebel, "Optimization by Continuation", in *Continuation and Bifurcations: Numerical Techniques and Applications*, D. Roose et al. (Eds), Kluwer Academic Publishers, The Netherlands, 349-362, 1990.
- Kim, H. S., K. S. Lee, K. P. Yoo, W. H. Lee, and H. S. Park, "Two-Part Modular Reduced-Order Model for Multicomponent Multistage Distillation Columns", *J. Chem. Eng. Japan*, **22**(1), 41-47 (1989).

- King, C. J., *Separation Processes*. pp. 643-651, McGraw-Hill Inc., New York, 1980.
- Kisala, T. P., R. A. Trevino-Lozano, J. F. Boston, H. I. Britt, and L. B. Evans, "Sequential Modular and Simultaneous Modular Strategies for Process Flowsheet Optimization", *Comput. Chem. Eng.*, **11**(6), 567-579 (1987).
- Kojima, M., and R. Hirabayashi, "Continuous Deformation of Nonlinear Programs", *Math. Program. Study*, **21**, 150-198 (1984).
- Koninckx, J., *On-Line Optimization of Chemical Plants using Steady-State Models*. Ph.D. Thesis, University of Maryland, 1988.
- Koster, L. G., Gazi, E. and Seider, W. D., "Finite Elements for Near-Singular Systems: Application to Bacterial Chemotaxis" *Comput. Chem. Eng.*, **17**(5/6), 485-503 (1993).
- Kovach, III, J. W., and W. D. Seider, "Heterogeneous Azeotropic Distillation: Homotopy-Continuation Methods", *Comput. Chem. Eng.*, **11**, 593-605 (1987).
- Krishnamurthy, R., and R. Taylor, "A Nonequilibrium Stage Model of Multicomponent Separation Processes-Part I: Model Description and Method of Solution", *AIChE J.*, **31**(3), 449-456 (1985).
- Leis, J. R., and M. A. Kramer, "Sensitivity Analysis of Systems of Differential and Algebraic Equations", *Comput. Chem. Eng.*, **9**(1), 93-96 (1985).
- Leis, J. R., S. A. Gallagher, and M. A. Kramer, "Parametric Sensitivity Analysis of Complex Process Flowsheets using Sequential Modular Simulation", *Comput. Chem. Eng.*, **11**(4), 409-421 (1987).
- Lockett, M. J., *Distillation Tray Fundamentals*, Cambridge University Press, 1988.
- Lundberg, B. N., and A. B. Poore, "Numerical Continuation and Singularity Detection Methods for Parametric Nonlinear Programming", *SIAM J. Optim.*, **3**, 134-154 (1993).

- Mangasarian, O. L., "Equivalence of the Complementarity Problem to a system of Nonlinear Equations", *SIAM J. Appl. Math.*, **31**(1), 89-92 (1976).
- Mangasarian, O. L., and S. Fromovitz, "The Fritz-John Necessary Optimality Conditions in the Presence of Equality and Inequality Constraints", *J. Math. Anal. Appl.*, **17**, 37-47 (1967).
- McCormick, G. P., "Optimality Criteria in Nonlinear Programming", in *Nonlinear Programming* SIAM-AMS Proceeding vol. IX, 1976.
- McFarlane, R. C., and D. W. Bacon, "Empirical Strategies for Open-Loop On-Line Optimization", *Can. J. Chem. Eng.*, **67**(8), 665-677 (1989).
- Morgan, A. P., *Solving Polynomial Systems Using Continuation for Engineering and Scientific Problems*, Prentice-Hall, Englewood-Cliffs NJ, 1987.
- Murase, A., H. L. Roberts, and A. O. Converse, "Optimal Thermal Design of an Autothermal Ammonia Synthesis Reactor", *Ind. & Eng. Chem. Process Des. Dev.*, **9**(4), 503-512 (1970).
- Murtagh, B. A. and Saunders, M. A., *MINOS 5.3 User's Guide*. Technical Report SOL 83-20R, 1990.
- Naphtali, L. M., and D. P. Sandholm, "Multicomponent Separation Calculations by Linearization", *AIChE J.*, **17**(1), 148-153 (1971).
- Pereyra, V. and Sewell, E. G., "Mesh Selection for Discrete Solution for Boundary Problem in Ordinary Differential Equations", *Numer. Math.*, **23**, 261-268 (1975).
- Pinto, J. C., and E. C. Biscaia Jr, "Order Reduction Strategies for Models of Staged Separation Systems", *Comput. Chem. Eng.*, **12**(8), 821-831 (1988).
- Poore, A. B., and C. A. Tiaht, "Bifurcation Problems in Nonlinear Parametric Programming", *Math. Program.*, **39**, 189-205 (1987).

- Powell, M. J. D., and Ph. L. Toint, "On the Estimation of Sparse Hessian Matrices", *SIAM J Num. Anal.*, **16**(6), 1060-1074 (1979).
- Prasad, R., "An Improved Approximation for the log-mean temperature difference", *Chem. Eng.*, **95**(14), 110 (1988).
- Prett, D. M., and C. E. Garcia, *Fundamental Process Control*, Butterworths Pub., 1988.
- Rabitz, H., M. Kramer, and D. Dacol, "Sensitivity Analysis in Chemical Kinetics", *Ann. Rev. Phys. Chem.*, **34**, 419-461 (1983).
- Rakowska, J., R. T. Haftka, and L. T. Watson, "Tracing the Efficient Curve for Multi-Objective Control-Structure Optimization", *Computing Sys. Eng.*, **2**, 461-471 (1991).
- Renfro, J. G., *Computational Studies in the Optimization of Systems described by Differential/Algebraic Equations*, Ph.D. Thesis, University of Houston, Texas, 1986.
- Rheinboldt, W. C., and J. V. Burkardt, "A Locally Parameterized Continuation Process", *ACM Trans. Math. Software*, **9**, 215-235 (1983a).
- Rheinboldt, W. C., and J. V. Burkardt, "Algorithm 596. A Program for a Locally Parameterized Continuation Process", *ACM Trans. Math. Software*, **9**, 236-241 (1983a).
- Rheinboldt, W. C., *Methods for Solving Systems of Nonlinear Equations*, SIAM, Philadelphia Pa., 1984.
- Rheinboldt, W. C., *Numerical Analysis of Parametrized Nonlinear Equations*, J. Wiley & Sons Inc., 1986.
- Russell, R. A., "A Flexible and Reliable Method Solves Single-Tower and Crude-Distillation-Column Problems", *Chem. Eng.*, October, 53-59 (1983).

- Russell, R. D. and Christiansen, J., "Adaptive Mesh Selection Strategies for Solving Boundary Value Problems", *SIAM J. Num. Anal.*, **15**(1), 59-80 (1978).
- Salgovic, A., V. Hlavacek, and J. Ilavsky, "Global Simulation of Countercurrent Separation Processes via One-Parameter Imbedding Techniques", *Chem. Eng. Sci.*, **36**, 1599-1604 (1981).
- Schmid, C., and L. T. Biegler, "Quadratic Programming Methods for Reduced Hessian SQP", *Comput. Chem. Eng.*, **18**(9), 817-832 (1994).
- Seader, J. D., M. Kuno, W.-J. Lin, S. A. Johnson, K. Unsworth, and J. W. Wiskin, "Mapped Continuation Methods for Computing All Solutions to General Systems of Nonlinear Equations", *Comput. Chem. Eng.*, **14**, 71-85 (1990).
- Seider, W. D., D. D. Brengel, and S. Widagdo, "Nonlinear Analysis in Process Design", *AIChE J.*, **37**, 1-38 (1991).
- Shapiro, A., "Second Order Sensitivity Analysis and Asymptotic Theory of Parametrized Nonlinear Programs", *Math. Program.*, **33**, 280-299 (1985).
- Smith, B. D., and W. K. Brinkley, "General Short-cut Equation for Equilibrium Stage Processes", *AIChE J.*, **6**(3), 446-450 (1960).
- Srivastava, R. K., and B. Joseph, "Reduced Order Models for Separation Columns-V. Selection of Collocation Points", *Comput. Chem. Eng.*, **9**(6), 601-613 (1985).
- Srivastava, R. K., and B. Joseph, "Reduced Order Models for Separation Columns-IV. Treatment of Columns with Multiple Feeds and Sidestreams via Spline Fitting", *Comput. Chem. Eng.*, **11**(2), 159-164 (1987a).
- Srivastava, R. K., and B. Joseph, "Reduced Order Models for Staged Separation Columns-IV. Columns with Steep and Flat Composition Profiles", *Comput. Chem. Eng.*, **11**(2), 165-176 (1987b).

- Stewart, W. E., K. L. Levien, and M. Morari, "Simulation of Fractionation by Orthogonal Collocation", *Chem. Eng. Sci.*, **40**(3), 409-421 (1985).
- Stoever, M. A., and C. Georgakis, "Time Domain Order Reduction of Tridiagonal Dynamics of Staged Processes-II. Nonuniform Lumping", *Chem. Eng. Sci.*, **37**(5), 699-705 (1982).
- Sun, A. C., and W. D. Seider, "Homotopy Continuation Algorithm for Global Optimization", in *Recent Advances in Optimization*, C. A. Floudas and P. M. Pardalos (Eds). Princeton University Press, 561-592, 1991.
- Swartz, C. L. E., and W. E. Stewart, "A Collocation Approach to Distillation Column Design", *AIChE J.*, **32**(11), 1832-1838 (1986).
- Swartz, C. L. E., and W. E. Stewart, "Finite-Elements Steady State Simulation of Multiphase Distillation", *AIChE J.*, **33**(12), 1977-1985 (1987).
- Swartz, C. L. E., *Finite-Element Analysis of Staged Separation Processes*. PhD Thesis, University of Wisconsin-Madison, 1987.
- Tiaht, C. A., and A. B. Poore, "A Bifurcation Analysis of the Nonlinear Parametric Programming Problem", *Math. Program.*, **47**, 117-141 (1990).
- Tilden, J. W., V. Costanza, G. J. McRae, and J. H. Seinfeld, "Sensitivity Analysis of Chemically Reacting Systems", in *Modeling of Chemical Reaction Systems*, K. H. Ebert, P. Deuflhand, and W. Jager (Eds), Springer-Verlag, Berlin, 1981.
- Uber, J. G., and E. D. Brill Jr., "Design Optimization with Sensitivity Constraints", *Eng. Optim.*, **16**, 15-28 (1990).
- Vasantharajan, S. and Biegler, L. T., "Simultaneous Strategies for Optimization of Differential-Algebraic Systems with Enforcement of Error Criteria", *Comput. Chem. Eng.*, **14**, 1083-1100 (1990).

- Vickery, D. J., and R. Taylor, "Path-Following Approaches to the Solution of Multicomponent, Multistage Separation Process Problems", *AIChE J.*, **32**(4), 547-556 (1986).
- Vickery, D. J., J. J. Ferrari, and R. Taylor, "An "Efficient" Continuation Method for the Solution of Difficult Equilibrium Stage Separation Process Problems", *Comput. Chem. Eng.*, **12**(1), 99-103 (1988).
- Villadsen, J., and M. L. Michelsen, *Solution of Differential Equation Models by Polynomial Approximation*, Prentice-Hall Inc., Englewood-Cliffs NJ, 1978.
- Volin Y. M., and G. M. Ostrovskiy, "Sensitivity Calculation Methods for Complex Chemical Systems - 2: Comparison", *Comput. Chem. Eng.*, **5**, 31-40 (1981b).
- Volin Y. M., and G. M. Ostrovskiy, "Sensitivity Calculation Methods for Complex Chemical Systems - 1: Algorithmization", *Comput. Chem. Eng.*, **5**, 21-30 (1981a).
- Wang, J. C., and Y. L. Wang, "A Review of the Modeling and Simulation of Multi-Stage Separation Processes", in *Foundations of Computer-Aided Chemical Process Design*, vol II, R. S. H. Mah and W. D. Seider (Eds.), 121-170, 1981.
- Wardle, A. P., and H. Hapoglu, "On the Solution of Models of Binary and Multicomponent Packed Distillation Columns using Orthogonal Collocation on Finite Elements", *Trans. Inst. Chem. Eng.*, **72**(A), 551-564 (1994).
- Watson, L. T., S. C. Billups, and A. Morgan, "Algorithm 652. HOMPAC: A Suite of Codes for Globally Convergent Homotopy Algorithms", *ACM Trans. Math. Software*, **13**(3), 281-310 (1987).
- Wayburn, T. L., and J. D. Seader, "Homotopy Continuation Methods for Computer-Aided Process Design", *Comput. Chem. Eng.*, **11**, 7-25 (1987).
- White, Jr A. B., "On Selection of Equidistributing Meshes for Two-Point Boundary-Value Problems", *SIAM J. Num. Anal.*, **16**(3), 472-502 (1979).

- White, Jr A. B., "On the Numerical Solution of Initial/Boundary Value Problems in one Space Dimension", *SIAM J. Num. Anal.*, **19**(4), 683-697 (1982).
- Wolbert, D., X. Joulia, B. Koehret, and L. T. Biegler, "Flowsheet Optimization and Optimal Sensitivity Analysis using Analytical Derivatives", *Comput. Chem. Eng.*, **18**(11/12), 1083-1095 (1993).
- Wold. S., K. Esbensen, and P. Geladi, "Principal Component Analysis", *Chemometrics and Intelligent Laboratory Systems*, **2**, 37-52, (1987).
- Wong, K. T., and R. Luus, "Model Reduction of High-Order Multistage Systems by the Method of Orthogonal Collocation", *Can. J. Chem. Eng.*, **58**, 382-388 (1980).
- Wu, J.-S., and P. R. Bishnoi, "A Method for Steady-State Simulation of Multistage Separation Columns Involving Nonideal Systems", *Comput. Chem. Eng.*, **10**(4), 343-351 (1986).

### Appendix A: Coefficients for the regressed Equations 2.16, 2.17 and 2.19.

Table A1. Regression coefficients for K-values used in the C<sub>3</sub> splitter.

	$a_1$	$a_2$	$a_3$	$a_4$
propylene	8.020373e-1	-1.775595e-2	5.587970e-3	-4.647275e-4
propane	6.854639e+1	-4.326426e-1	6.837252e-4	-10.58095e-4

Table A2. Regression coefficients for K-values used in the Deisobutanizer (DIB).

	$a_1$	$a_2$	$a_3$	$a_4$
propane	-9.85809	5.45316e-2	-5.79078e-5	-1.39112e-3
i-butane	-8.67675	3.65983e-2	-2.08579e-5	-1.46492e-3
n-butane	-15.41127	7.80988e-2	-8.89839e-5	-1.17645e-3
i-pentane	-19.12111	9.46910e-1	-1.12866e-5	-9.97234e-4

Table A3. Regression coefficients for K-values used in the C<sub>3</sub>-C<sub>4</sub> splitter.

	$a_1$	$a_2$	$a_3$	$a_4$
ethane	-5.420597	3.48876e-2	-3.88490e-5	-5.09808e-4
propane	-13.133830	6.91381e-2	-8.13411e-5	-4.12676e-4
i-butane	-14.462916	6.88440e-2	-7.54950e-5	-3.41044e-4
n-butane	-17.345122	8.25619e-2	-9.32420e-5	-3.17356e-4
i-pentane	-20.023894	9.122537e-2	-1.01955e-4	-2.39818e-4
n-pentane	-22.205646	1.01407e-1	-1.114963e-4	-2.20114e-4

Table A4. Regression coefficients for K-values used in the EB/S column.

	$a_1$	$a_2$	$a_3$	$a_4$
ethyl-benzene	1.304356e+1	-7.516728e-2	1.086927e-4	-4.669269e-3
benzene	1.128412e+1	-6.600091e-2	9.513459e-5	-3.973728e-3

Table A5. Regression coefficients for liquid phase enthalpy used in the C<sub>3</sub> splitter.

	$b_1$	$b_2$	$b_3$	$b_4$
propane	-5.507860e+5	5.180234e+3	-1.673919e+1	1.845696e-2
propylene	-2.336810e+5	2.168266e+3	-7.086567	8.169412e-3

Table A6. Regression coefficients for vapour phase enthalpy used in the C<sub>3</sub> splitter.

	$c_1$	$c_2$	$c_3$	$c_4$	$c_5$	$c_6$
propane	-5.72554e+3	-5.10174e+3	-2.00812e+4	2.08929e+4	2.09357e+4	-1.15250e+3
propylene	-7.38623e+3	-7.98970e+3	-3.17627e+4	3.67828e+4	3.86803e+4	-1.26688e+4

Table A7. Regression coefficients for liquid phase enthalpy used in the Deisobutanizer (DIB) and the C<sub>3</sub>-C<sub>4</sub> splitter.

	$b_1$	$b_2$	$b_3$	$b_4$
propane	-4.114596e+5	3.948232e+3	-1.250259e+1	1.363845e-2
i-butane	-2.013476e+5	1.838203e+3	-5.425727	5.811588e-3
n-butane	-1.674945e+5	1.494509e+2	-4.259655	4.503788e-3
i-pentane	-9.877590e+4	8.301663e+2	-2.136380	2.317351e-3
n-pentane	-1.041395e+5	8.668001e+2	-2.195377	2.332018e-3

Table A8. Regression coefficients for vapour phase enthalpy used in the Deisobutanizer (DIB) and the C<sub>3</sub>-C<sub>4</sub> splitter.

	$c_1$	$c_2$	$c_3$	$c_4$	$c_5$	$c_6$
ethane	3.41889e+3	-1.13518e+4	1.24400e+4	-2.53216e+3	1.20954e+4	4.12111e+3
propane	1.87050e+4	-5.40087e+3	-5.92078e+3	5.58299e+3	5.24836e+3	1.30895e+4
i-butane	2.34751e+4	-6.88974e+3	-7.34538e+3	8.12559e+3	2.8715e+3	2.32235e+4
n-butane	2.75293e+4	-9.09605e+3	-6.53993e+3	9.38289e+3	-9.33633e+2	2.68593e+4
i-pentane	2.65374e+4	-7.98028e+3	-7.44774e+3	1.00612e+4	7.00015e+3	3.49152e+4
n-pentane	2.71551e+4	-7.97346e+3	-1.05076e+4	1.07723e+4	1.08482e+4	3.44538e+4

Table A9. Regression coefficients for liquid phase enthalpy used in the ES/B column.

	$b_1$	$b_2$	$b_3$	$b_4$
ethyl-benzene	-4.677991e+4	2.188577e+1	1.946613e-1	-
benzene	2.893203e+5	4.531152e+1	1.946613e-1	-

Table A10. Regression coefficients for vapour phase enthalpy used in the EB/S column.

	$c_1$	$c_2$	$c_3$	$c_4$	$c_5$	$c_6$
ethyl-benzene	1.477809e+3	-8.879201e+3	-2.475060e+3	0.0	5.635510e+3	7.734896e+4
styrene	3.315887e+5	2.318424e+4	7.618124e+3	-3.427691e+4	5.635510e+3	7.735896e+4

### Appendix B: Cost coefficients for Equations 2.45, 2.46 and 5.1

Table B1. Cost coefficients for objective functions 2.45 and 2.46.

	$C_3$ splitter	DIB	$C_3$ - $C_4$ splitter	EB/S
$C_B$	2.40	2.40	2.40	2.40
$C_D$	-0.40	-0.40	-0.40	-0.40
$C_{ht}$	80,000	15,000	0.0	15,000
$C_{lk}$	80,000	15,000	0.0	5,000

Table B2. Cost coefficients for objective function 5.1.

price							
SA	SB	SD	SG	SP	SR	$C_A$	$C_B$
-168.0	-252.0	50.04	-84.0	2207.52	-2.22	0.75	250

### Appendix C: Eigenvector directions for matrix $\mathbf{X}^T\mathbf{X}$

Let  $\mathbf{X}$  be the  $(n \times p)$  first-order sensitivity matrix at the reference point  $(x^*, \varepsilon^*)$  calculated by (4.4). The local behaviour of the optimal values for the process variables for variations in the parameter values can be approximated by the following expression:

$$x(\varepsilon) = x(\varepsilon^*) + \mathbf{X}(\varepsilon - \varepsilon^*) + O(\|\varepsilon\|) \quad (\text{C.1})$$

where  $O(\|\varepsilon\|)$  is the approximation error estimate which is proportional to the magnitude of variation in the parameter space. The change in the variable space can be defined as  $x(\varepsilon) - x(\varepsilon^*) = \Delta\varepsilon$ . Without any loss of generality it is assumed that  $\varepsilon^* = 0$  at the reference point.

The objective is to determine the direction in the parameter space that causes the greatest change in the optimal values of the process variables. A measure of variation in the variable space is defined to be the sum of squares of deviation from the optimal solution  $(x^*, \varepsilon^*)$ . More specifically the problem takes the following form:

$$\begin{aligned} \text{Max}_{\varepsilon} \quad & \Delta\varepsilon^T \Delta\varepsilon = \varepsilon^T \mathbf{X}^T \mathbf{X} \varepsilon \\ \text{s.t.} \quad & \varepsilon^T \varepsilon = 1 \end{aligned} \quad (\text{P.C1})$$

The constraint imposes a bound on the magnitude of the parameter perturbation. The solution to problem (P.C1) is given by forming the Lagrangian and setting its derivative with respect to  $\varepsilon$ , equal to zero.

$$\frac{d}{d\varepsilon} \left[ \varepsilon^T \mathbf{X}^T \mathbf{X} \varepsilon - \pi (\varepsilon^T \varepsilon - 1) \right] = 0 \quad (\text{C.2})$$

where  $\pi$  is the scalar Lagrange multiplier associated with the constraint. (C.2) results in:

$$\mathbf{X}^T \mathbf{X} \varepsilon - \pi \varepsilon = 0 \quad (\text{C.3})$$

The optimality conditions (C.3) for problem (P.C1) implies that  $\varepsilon$  is an eigenvector of matrix  $\mathbf{X}^T\mathbf{X}$  with  $\pi$  the corresponding eigenvalue. Hence, the maximum value for the objective function in (C.P1) is attained when  $\varepsilon$  is selected to be the eigenvector of  $\mathbf{X}^T\mathbf{X}$  that corresponds to the largest in magnitude eigenvalue.

### Appendix D: Conventions for vector differentiation

$\nabla_x f(x) = [\partial f / \partial x_1 \quad \cdots \quad \partial f / \partial x_n]$ , the gradient of the real-valued function  $f$  with respect to the  $n$ -dimensional vector  $x$ .

$$\nabla_{(x,\varepsilon)} f(x, \varepsilon) = [\nabla_x f(x, \varepsilon) \quad \nabla_\varepsilon f(x, \varepsilon)]$$

$\nabla_x h(x) = [\nabla_x h_1^T \quad \cdots \quad \nabla_x h_m^T]^T$ , the  $m \times n$  Jacobian of the  $m$ -dimensional vector  $h$ , with respect to the  $n$ -dimensional vector  $x$ .

$\nabla_x^2 f(x) = \nabla_x [\nabla_x f(x)^T]$ , is the  $n \times n$  Hessian matrix of a real-valued function  $f$  with  $ij$ -th element equal to  $\partial^2 f / \partial x_j \partial x_i$ .

$$\nabla_{\alpha\alpha}^2 f(x, \varepsilon) = \nabla_\varepsilon [\nabla_x f(x, \varepsilon)^T] = \begin{bmatrix} \nabla_\varepsilon (\partial f / \partial x_1) \\ \vdots \\ \nabla_\varepsilon (\partial f / \partial x_n) \end{bmatrix} = [\nabla_{x\varepsilon}^2 f(x, \varepsilon)]^T$$

Panagiotis Seferlis

1985-1990 Aristotle University of Thessaloniki, Greece Dipl. Chem. Eng.

1990-1995 McMaster University Ph.D. Chem. Eng.

Publications from the thesis

Seferlis, P., and A. N. Hrymak, "Optimization of Distillation Units using Collocation Models", *AIChE J.*, **40**(5), 813-825 (1994).

Seferlis, P., and A. N. Hrymak, "Adaptive Collocation on Finite Elements Models for the Optimization of Multistage Distillation Units", *Chem. Eng. Sci.*, **49**(9), 1369-1382 (1994).

Seferlis, P., and A. N. Hrymak, "Sensitivity Analysis for Chemical Process Optimization", submitted to *Comput. Chem. Eng.*, 1995.

Conference Presentations

Seferlis, P., and A. N. Hrymak, "Reduced Order Models for Distillation Optimization", Annual AIChE Meeting, Los Angeles, 1991.

Seferlis, P., and A. N. Hrymak, "Error-based Adaptive Mesh Selection for Collocation Models of Multistage Separation Processes", Annual AIChE Meeting, Miami Beach, 1992.

Seferlis, P., and A. N. Hrymak, "Sensitivity Analysis Methods in Process Optimization", Annual AIChE Meeting, San Francisco, 1994.